CHALMERS
UNIVERSITY OF TECHNOLOGY

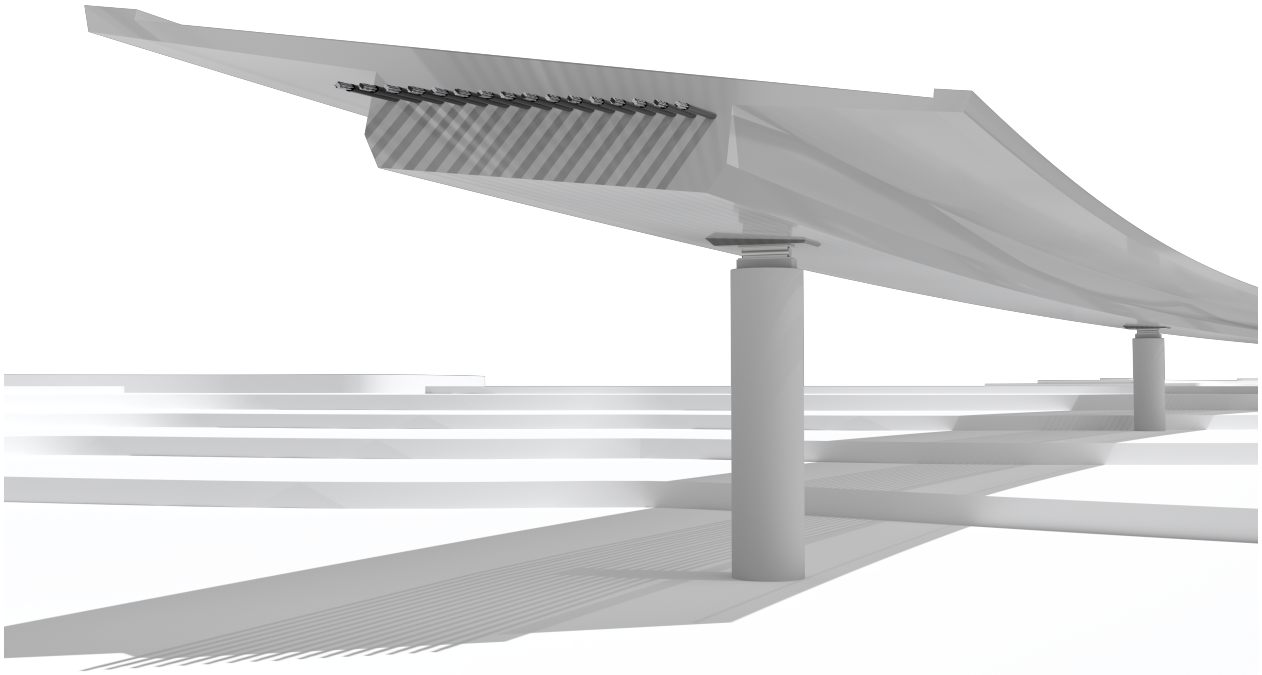

Optimization of Cable Placement in Post-Tensioned Continuous Concrete Bridges

Development of Guidelines using Genetic Algorithms to Reduce Cost and Environmental Impact

Master's Thesis in Master Program Structural Engineering and Building Technology

William Mjörnestål
Benjamin Pettersson

Department of Architecture and Civil Engineering
CHALMERS UNIVERSITY OF TECHNOLOGY
Master's Thesis ACEX30
Gothenburg, Sweden 2022

Master's Thesis
ACEX30

Optimization of Cable Placement in Post-Tensioned Continuous Concrete Bridges

Development of Guidelines using Genetic Algorithms to Reduce Cost and Environmental Impact

William Mjörnestål
Benjamin Pettersson

CHALMERS
UNIVERSITY OF TECHNOLOGY

Department of Architecture and Civil Engineering
Division of Structural Engineering
Concrete Structures
Chalmers University of Technology
Gothenburg, Sweden 2022

Optimization of Cable Placement in Post-Tensioned Continuous Concrete Bridges
Development of Guidelines using Genetic Algorithms to Reduce Cost and Environmental Impact
William Mjörnestål
Benjamin Pettersson

Supervisors: Christoffer Jonsson, Consultant, Bridge Engineering, Ramboll Sweden, Gothenburg
Victor Andersson, Consultant, Bridge Engineering, Ramboll Sweden, Gothenburg

Examiner: Professor/Head of Division Mario Plos, Department of Architecture and Civil Engineering, Concrete Structures

Department of Architecture and Civil Engineering
Division of Structural Engineering
Concrete Structures
Chalmers University of Technology
SE-412 96 Gothenburg
Telephone +46 31 772 10 00

Cover: An illustration of post-tensioning cables in a continuous bridge.

Department of Architecture and Civil Engineering
Gothenburg, Sweden 2022

Optimization of Cable Placement in Post-Tensioned Continuous Concrete Bridges
Development of Guidelines using Genetic Algorithms to Reduce Cost and Environmental Impact
WILLIAM MJÖRNESTÅL
BENJAMIN PETTERSSON
Department of Architecture and Civil Engineering
Chalmers University of Technology

Abstract

Design of prestressed concrete bridges is a complex and iterative process and have a lot of influencing factors to consider and requirements to fulfill. Even though some attempts at recommendations, engineering practices and software exists, either computation time, efficiency in design or availability may be an issue. As there is a desire in the industry to find more cost-efficient and environmentally sustainable solutions, a need for simple and efficient guidelines in bridge design exists. The aim of this study was to compile general guidelines that can be applied to a varying set of continuous post-tensioned bridges to minimize the cost and environmental impact. The guidelines have been generated from optimization of a bridge beam with varying span length using a genetic algorithm solver. For the structural analyses, a finite element solver was implemented into the optimization script.

When comparing bridges designed with both the proposed guidelines and the conventional solution, load balancing, it was found that significant improvements in cost and notable reductions in global warming potential (GWP) could be achieved with the guidelines. On average, the cost was reduced by almost 7% and the GWP by 5% for the examined cross-section. Other sections were also tested and similar trends could be observed though it was noted that the improvements were considerably smaller for bridges with a slightly wider section. A case study of the road bridge, Halvors länk, showed again that the guidelines were able to reduce the cost by 5%. Due to constraints in cross-section geometry, greater improvements could not be achieved. However, reductions of 11% in prestressing steel amount were obtained for both the original cross-section and the case study, suggesting a more efficient layout.

The study also showed that the use of genetic algorithms can be beneficial in structural design. Implementation of genetic algorithms could, however, increase the computational effort to unreasonable levels depending on the complexity of the problem. Therefore, it could be recommended to compile guidelines from the results of several optimizations utilizing genetic algorithms to be used for more generic problems. With this method, results like that of the genetic algorithm optimization could be achieved but the need for long computations is reduced.

Keywords: cable placement, post-tensioning, optimization, genetic algorithm, finite element analyses

Optimering av kabelplaceringen i efterspända, kontinuerliga betongbroar
Utveckling av riktlinjer med genetiska algoritmer för att reducera kostnad och miljöpåverkan
WILLIAM MJÖRNESTÅL
BENJAMIN PETTERSSON
Institutionen för arkitektur och samhällsbyggnadsteknik
Chalmers tekniska högskola

Sammanfattning

Design av förspända betongbroar är en komplicerad och iterativ process med många påverkande faktorer att ta hänsyn till samt flera krav att uppfylla. Även om försök att skapa rekommendationer, praxis och programvaror har gjorts har begränsningar i beräkningstid, kvalitet på lösningar eller tillgänglighet varit begränsande. Då det finns en vilja att skapa kostnadseffektiva och miljövänliga lösningar finns det också ett behov av enkla och effektiva riktlinjer för dimensionering av broar. Målet med denna studie var att sammanställa generella riktlinjer som kan appliceras på olika kontinuerliga efterspända broar för att minimera kostnaden och miljöpåverkan. Riktlinjerna har skapats från optimering av broar med olika spannlängder. Optimeringen gjordes med en genetisk algoritm och strukturella analyser gjordes med finita elementprogram.

Vid jämförelser mellan de föreslagna riktlinjerna och den konventionella lastbalanseringsmetoden uppnåddes tydliga minskningar i kostnad och klimatpåverkan mätt i GWP (Global warming potential). Genomsnittligen minskades kostnaden med nästan 7% och klimatavtrycket med 5% för det undersökta tvärsnittet. För de andra tvärsnitten som testades kunde även liknande trender upptäckas även om de förbättringarna som uppnåddes för ett tvärsnitt med ökad brodäcksbredd var mindre markanta. I en fallstudie av vägbron Halvors länk lyckades kostnaden reduceras med 5% med hjälp av de framställda riktlinjerna. Förbättringar i GWP var däremot svårare att uppnå på grund av den relativt låsta tvärsnittsgeometrin. För både fallstudien och tvärsnittet använt i optimeringen kunde stålmängden minskas med 11%. Detta visar på riktlinjernas effektivitet i brodimensionering.

Studien har också visat att användningen av genetiska algoritmer kan vara gynnsam i dimensioneringstadiet. Implementeringen av genetiska algoritmer kan dock leda till en orimlig ökning av beräkningstiden beroende på komplexiteten av problemet. Det kan därför vara rekommenderat att sammanställa riktlinjer från resultaten av flera optimeringar med genetiska algoritmer som sedan kan användas för mer konventionella problem. På detta vis kan resultat likt det av optimering med genetiska algoritmer nås medan den långa beräkningstiden kan undvikas.

Nyckelord: Kabelplacering, efterspänning, optimering, genetisk algoritm, finita element analyser

Acknowledgements

This study has been carried out in the Master's thesis course ACEX30 during the spring term, 2022, at the Department of Architecture and Civil Engineering of Chalmers University in collaboration with Ramboll Sweden, Gothenburg.

Firstly, we would like to give our gratitude to our Supervisors, Christoffer Jonsson and Victor Andersson at Ramboll Sweden, for providing guidance, support, and expertise in structural engineering continuously throughout the scope of the course.

Secondly, we would like to show our appreciation for Ramboll for giving us the opportunity of working with this project at their office in Gothenburg and supplying both the hardware and software needed in the study. We would also like to add our gratitude to our colleagues for their enthusiasm and for the opportunity of attending several site-visits during the work.

Finally, we would give a big thanks to our examiner Professor Mario Plos for his great ambition in the project and his feedback during the course.

The Authors, Gothenburg, June 2022

Contents

List of Figures

List of Tables

List of Symbols

A_{c}	Area of concrete.
A_{p}	Area of prestressing steel.
A	Area of the cross-section.
C_i	Penalty weight.
$E_{\mathrm{c,ef}}$	Young's modulus for concrete subjected to long term effects.
E_{c}	Young's modulus for concrete.
E	Young's modulus.
F_0	Unpenalized fitness function.
F_{P}	Penalty contribution in the fitness function.
F_{cs}	Creep and shrinkage force.
F	Fitness function.
I	Moment of inertia.
L	Length of the span.
M	Moment.
N	Normal force.
P_0	Prestressing force after stressing.
P_∞	Final prestressing force.
P_{GWP}	Performance in GWP.
P_{cost}	Performance in cost.
P_{i}	Prestressing force after anchorage.
P_{m}	Mean prestressing force along the cable.
P	Prestressing force.
Q_i	Axle load for LM1.
Q	Variable load.
T	Temperature.
W_i	Weight for combining single-objective fitness functions.
$\Delta P_{\mathrm{c,s,r}}$	Loss of prestressing force due to creep, shrinkage and relaxation.
$\Delta\sigma_{\mathrm{c}}$	Change of concrete stress due to deformation during tensioning.
$\Delta\sigma_{\mathrm{pr}}$	Loss of prestressing force due to relaxation.
Δc_{dev}	Deviation tolerance for the cover thickness.
α_{c}	Thermal coefficient for concrete.

α_{ef}	Effective modular ratio.
$\alpha_{\text{Q},i}$	Adjustment factor for the axle load in LM1.
$\alpha_{\text{q}i}$	Adjustment factor for the distributed load in LM1.
$\bar{z}_{\text{NA}}$	Distance from bottom of the beam to neutral axis.
$\bar{z}$	Local z-axis for the beam pointing upwards from the bottom.
$\beta(f_{\text{cm}})$	Factor relating the creep to the concrete strength.
$\beta(t_0)$	Factor relating the creep to the time of load application.
χ_t	Relaxation factor.
δ_i	Penalty distance.
κ_T	Curvature due to internal temperature differences.
κ_∞	Curvature from creep and shrinkage.
μ	Friction coefficient between cable and duct.
μ	Stress ratio for relaxation calculations.
ν	Poissons ratio.
$\overline{P}_{\text{GWP}}$	Reference value for performance in GWP.
$\overline{P}_{\text{cost}}$	Reference value for performance in cost.
ϕ_{duct}	Diameter of ducts.
ϕ_{stirup}	Diameter of stirups.
ϕ_{strand}	Diameter of strand.
ϕ_{s}	Diameter of reinforcement bar.
ρ	Density.
σ_{c}	Stress of the concrete.
σ_{p0}	Stress in the prestressing steel after stressing.
σ_{pi}	Stress in the prestressing steel after anchorage.
σ_{p}	Stress in the prestressing steel.
θ	Support rotation.
Ψ	Reduction factor.
ε_{ca}	Autogenous shrinkage.
ε_{cd}	Drying shrinkage.
ε_{cs}	Creep and shrinkage strain.
φ_0	Notional creep coefficient.
φ_{RH}	Factor that accounts for the relative humidity during creep.
φ	Creep coefficient.
a_{ph}	Minimum horizontal distance between ducts.
a_{pv}	Minimum vertical distance between ducts.
a_{s}	Minimum distance between reinforcement bars.
b_{wb}	Width of the web at the bottom of the beam.
b_{wt}	Width of the web at the top of the beam.

b	Width of the bridge.
c_{l}	Cover thickness to reinforcement.
$c_{\mathrm{lp,Node\ 1}}$	Cover thickness for the prestressing steel at the anchorage point, Node 1.
$c_{\mathrm{lp,b}}$	Bottom cover spacing for duct.
$c_{\mathrm{lp,t}}$	Top cover spacing for duct.
$c_{\mathrm{ls,t}}$	Top cover spacing for reinforcement steel.
$c_{\mathrm{ls,t}}$	Cover spacing for reinforcement steel at the bottom and on the sides.
c_{min}	Minimum cover thickness.
c_{nom}	Nominal cover thickness.
$c_{\mathrm{lp,Node}\ i}$	Cover spacing for the duct in Node i.
d_{center}	Center-to-center distance between the prestressing cables in the anchor.
d_{c}	Distance between the top and surface center of the concrete section.
d_{edge}	Edge distance from the cable attachments in an anchor.
d_{p}	Distance between the top of the beam and surface center of the prestressing steel.
e_i	Eccentricity of the cable in Node i.
$e_{\mathrm{norm},i}$	Normalized eccentricity of the cable in Node i with respect to the maximum and minimum cable eccentricity.
f_{ck}	Characteristic compressive strength of the concrete.
f_{ctk}	Characteristic tensile strength of the concrete.
$f_{\mathrm{p0.1k}}$	0.1%-proof stress of the prestressing steel.
f_{puk}	Ultimate strength of the prestressing steel.
f_j	Single-objective fitness function for objective j.
g	Self-weight.
h_{f}	Height of the flange.
h_{w}	Height of the web.
h	Height of the cross-section.
k	Factor for unintended slope changes in ducts.
m	Number of sub-objectives.
n_{strands}	Number of strands.
n	Number of constraints when optimizing towards a certain objective.
n	Number of cables.
q_i	Distributed load for LM1.
w_{max}	Maximum allowed deflection.
w_i	Width of notional lane i.
w	Width of carriageway.
$x_{\mathrm{f,max}}$	Position of maximum field eccentricity.

List of Acronyms

CSM	Construction Stage Manager.
DOF	Degree of freedom.
FE	Finite element.
GA	Genetic algorithm.
GWP	Global warming potential.
LM	Load model.
NA	Neutral axis.
SLS	Service limit state.
ULS	Ultimate limit state.

1

Introduction

1.1 Background

A common approach when designing concrete bridges with longer spans is to use prestressing to minimize cross-section dimensions and thereby also the self-weight of the structure. By casting ducts threaded with tensioning cables in the beam and tensioning them before the load application, compressive stresses are induced in the beam. By counteracting the tensile stresses from the applied loads, both cracking and deflections of the beam can be reduced. The effectiveness of the prestressing is dependent on the layout of the cables, as noted by Aspegren and Möörk (2021), who also concluded that the optimal cable placement was related on the beam geometry. Finding the optimal cable layout for a prestressed concrete beam could be beneficial in reducing the cross-section dimensions although the complexity makes this difficult. As concrete is commonly considered to have significant environmental impact, this reduction could lead to a more sustainable construction. The material reduction may also lead to a more cost-efficient beam.

Guidelines for designing the cable layout do exist. Magnel diagrams give combinations of eccentricities and prestressing forces that can be used based on the cross-section (Krishnamurthy, 1983). These diagrams have also been expanded upon by Eshani and Russell Blewitt (1986) to describe the valid eccentricities for the cable along a simply supported beam. Their guidelines can be used to find limits for the cable placements but does not suggest any optimal placement. This means that the engineer is tasked with finding the best layout, and due to time or other restrains might have to settle for an adequate solution. Several optimization software for prestressed beams and slabs have therefore been developed and show that both economic and environmental gain can be achieved (Ahsan et al., 2011; Khan et al., 2010; Kuyucular, 1991). These software are however either not applicable for continuous prestressed beams, do not follow Eurocode or Swedish regulations, or are unavailable to the common engineer. As efficient cable layouts are desirable in terms of sustainability and cost, guidelines for a more optimized cable placement that are widely applicable and available would be a valuable tool for the engineer.

1.2 Aim and Objective

The aim of this thesis is to develop guidelines to aid the design of continuous prestressed concrete bridges by suggesting optimal cable placement for reduced cost and environmental impact for a range of span lengths. The guidelines are to be based on finite element analyses. The objectives in the project are the following:

- Investigate current design approaches.
- Optimize the cable layout using genetic algorithm optimization and finite element analysis.
- Analyze the optimized cable layouts and establish general guidelines.
- Apply the generated guidelines and a conventional design approach for a set of chosen bridge beam geometries, including a case study of the Halvors länk road bridge, and compare the results.

1.3 Limitations

The project is limited to incompletely fully prestressed post-tensioned continuous beams for bridge structures with span lengths between 25 and 40 m. The analysis of each beam was based on Eurocode 2 (SIS, 2008) and requirements from the Swedish Transport Administration (Trafikverket) (2019a) and the Swedish Transport Agency (Transportstyrelsen) (2018). The beam models were verified in serviceability limit state (SLS) with regards to long-term effects for service life class L100. As prestressing mainly affects the behavior of the bridge in SLS, no verification was done in the ultimate limit state (ULS). Hence, stiffness changes due to crack formation and yielding are irrelevant and the study was performed with linear finite element analysis. The bridges were also not verified with respect to shear forces which can be counteracted by increasing the amount of shear reinforcement in the elements. Crack widths were also not considered as the bridge was fully prestressed, meaning that no cracks were allowed.

1.4 Method

The project began with a literature study investigating the design of prestressed concrete beams in bridges to identify the relevant actions, load cases and verifications relevant for this study. Furthermore, previous research in optimization of prestressed beams and cable placements were investigated. With the information about actions and load cases from the literature study, a general parametric model describing prestressed concrete bridge beams was established.

The next step was to define a beam model to be analyzed. The model should be a good representation of the sizes regularly used in prestressed bridges and allow for the analysis results to be applied to different beam geometries.

To describe the beam geometry and cable profiles parametrically, the design tool Grasshopper 3D was used (Robert McNeel & Associates, n.d.-b). The tool enables

the geometry as well as the parametrization algorithm to be presented visually to more effectively prevent any parameter combinations that would result in an incompatible geometry. To find the most optimal cable layout, the Grasshopper native evolutionary optimization tool Galapagos (Robert McNeel & Associates, n.d.-a) was used to iteratively update the cable profile until the most efficient solution had been found for each beam geometry. Each solution was analyzed with the finite element software SOFiSTiK (n.d.-e) to find cross-sectional load effects and capacities in each iteration. The efficiency of the cable layout have been defined by its cost and environmental impact together with the utilization in SLS. By performing tests on different geometries, the parameters describing the cable layout was related to the beam geometry and compiled into guidelines.

The guidelines established were then applied to study a small set of different geometries to analyze if the optimized cable layout had a considerable impact on the efficiency compared to the conventional approach, load balancing. Finally, a case study of the road bridge Halvors länk was performed to evaluate which benefits could have been gained by using the guidelines.

2

Prestressed Concrete

Prestressing of concrete is a technique used in beams and slabs when designing for longer spans or slender cross-sections. The main concept of prestressed concrete is to introduce compressive stresses into the concrete to counteract the tensile stresses created by the load. As concrete is a brittle material and cannot handle any larger tensile stresses, it is prone to cracking. In normal concrete structures, it is solved by placing reinforcement bars in the tensile zones in order to absorb the force. However, for the reinforcement bars to contribute, the concrete first needs to crack so that the forces can be transferred into the reinforcement. When the concrete cracks the cross-section area is reduced and stiffness is lost. The use of prestressed concrete results in a delayed cracking and the retained stiffness leads to a more effective cross-section and smaller deflections. The final strength of the structure is however not remarkably increased (Dolan & Hamilton, 2019).

A beam can be designed to be either fully or partially prestressed. If a beam is designed to be fully prestressed, there cannot be any cracks in service state. Smaller tensile stresses are, however, still allowed in fully prestressed structures, a concept known as incomplete prestressing (Engström, 2011). When a beam is partially prestressed, cracks are allowed to form in service state. This still result in higher stiffness of the beam compared to one that is regularly reinforced since the cracking is both delayed and reduced (Engström, 2011).

2.1 Production Methods

Prestressing is achieved by constructing the concrete element with a cable that is tensioned before bonding with the concrete. The strain difference between the materials results in a compressive force in the concrete. The two techniques of tensioning a cable are called pretensioning and post-tensioning.

2.1.1 Pretensioning

Pretensioning means that the cable is tensioned in a tensioning bed before the concrete is cast. After the concrete has cured and a bond has formed between the cable and concrete, the cable is released from the tensioning bed and the compressive force begins acting on the concrete. Pretensioning works well for prefabricated elements as the tensioning bed can be reused. It is also possible to cast multiple elements within the same bed by stacking them length-wise and cutting the cable between each element after curing (Bhatt, 2011). With the cables under tension, placing them with varying eccentricities induces large forces in the tensioning bed, thus, straight profiles are often used (Libby, 2012). The need for a tensioning bed

and the difficulties to create varying cable layouts make this production method less relevant for continuous beams.

2.1.2 Post-Tensioning

In post-tensioned structures, ducts threaded with tensioning cables are cast into the beam. When the concrete is cured to an acceptable level of strength, usually 70% of the final strength, the cables are tensioned by jacks at either one or both ends and then anchored to the sides of the beam to induce compression (Engström, 2011). The ducts are thereafter grouted which bonds the cable to the duct and provides protection from corrosion (Bhatt, 2011). Post-tensioning allows for cable layouts with varying eccentricities since the placement of the ducts can be relatively freely chosen. This quality makes post-tensioning a more relevant choice for the scope of this study since it allows for more flexibility in the cable placement.

2.2 Loss of Prestressing Force

The force from the cables acting on the concrete beam and compressing it is called the prestressing force. This force is measured by the jacks when the cable is tensioned. The prestressing steel is however subjected to several losses of prestressing force during its life span. These losses are presented in Eurocode 2 and are divided into instantaneous and time-dependent losses, see Table 2.1 (SIS, 2008).

Table 2.1: Prestressing losses for a post-tensioned beam.

Instantaneous	Time-dependent
• Deformation of concrete	• Shrinkage and creep of concrete
• Friction losses	• Relaxation in the cable
• Anchoring losses	

To ensure that the design works as intended, the loss of prestressing force needs to be relatively small compared to the initial force. This can commonly be solved by increasing the initial force (Libby, 2012). If the loss is larger in relation to the initial force, the function of prestressing would fade and the beam would act more as an ordinary reinforced beam.

2.2.1 Deformation of Concrete

When a design requires multiple prestressing cables, some loss of prestressing force will occur when the cables are tensioned successively. As the cables are tensioned, the compressive stresses in the concrete will increase leading to the beam being elastically shortened. As a result, the previously tensioned cables will lose some strain and prestressing force (Engström, 2011). This loss can, according to Eurocode 2, be calculated with (2.1)-(2.2) (SIS, 2008). Here, ΔP_{el} is the mean loss of the prestressing force in each cable which is dependent on the difference in concrete stress at the center of each cable (Engström, 2011).

$$\Delta P_{\mathrm{el}} = A_{\mathrm{p}}\, E_{\mathrm{p}} \cdot \sum \left[\frac{j \cdot \Delta\sigma_{\mathrm{c}}(t)}{E_{\mathrm{cm}}(t)} \right] \tag{2.1}$$

$$j = (n-1)/2n \approx \frac{1}{2} \tag{2.2}$$

2.2.2 Friction Losses

Friction losses in post-tensioned beams occur between the cables and the ducts and results in varying prestressing forces along the beam (Engström, 2015). The losses are calculated starting at the active end, i.e., the end where the jack is placed, and accumulates with the length of the beam. Figure 2.1 shows an example of how the prestressing force decreases in a beam due to friction.

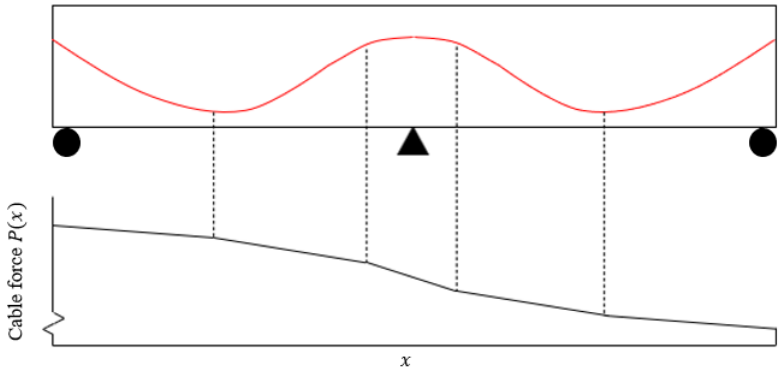

Figure 2.1: Loss of cable force due to friction for a beam with an active end and a passive end, based on Engström (2015)

The loss of prestressing force is based on the change of slope and is calculated with (2.3) (Engström, 2015). Here, $P_0(s)$ is the prestressing force at the duct length, s, after stressing and $P_{\mathrm{i}}(0)$ represents the force at the active end. The friction is described by the friction coefficient between the cable and the duct, μ, and the factor for unintended changes in slope of the duct, k. The nominal change in slope from the active end to the position s is represented by α given in (2.4) (Engström, 2015).

$$P_0(s) = P_0(0) \cdot e^{-\mu(\alpha + k \cdot s)} \tag{2.3}$$

$$\alpha = \alpha(0) - \alpha(s) \tag{2.4}$$

2.2.3 Anchoring Losses

When the cable is released from the jack, it will contract to some extent. This action is, however, prevented by the friction along the cable (Engström, 2011). The contraction results in a reduction of the cable force near the active end, see Figure 2.2.

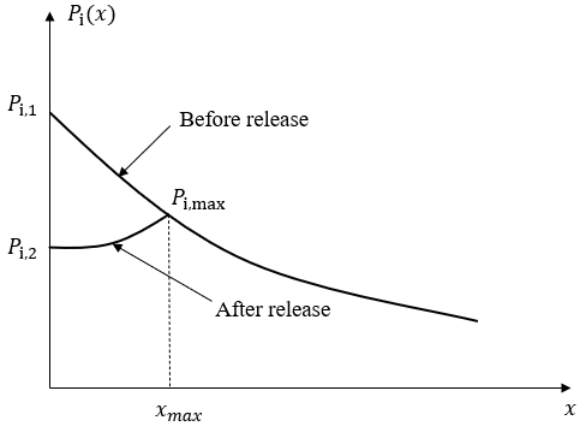

Figure 2.2: Loss of cable force during release from tensioning jack, based on Engström (2011).

After detensioning, it is therefore necessary to calculate the maximum cable force and its position. The maximum cable force, $P_{\mathrm{i,max}}$, can be calculated by measuring the cable force in the active end, before and after detensioning, and then using (2.5) (Engström, 2011). The position of the maximum cable force along the cable $x_{\max}$ is given by (2.6) (Engström, 2011).

$$P_{\mathrm{i,max}} = \sqrt{P_{\mathrm{i,1}} \cdot P_{\mathrm{i,2}}} \tag{2.5}$$

$$x_{\max} = \frac{1}{k}\left[\frac{1}{2\,\mu}\ln\left(\frac{P_{\mathrm{i,1}}}{P_{\mathrm{i,2}}}\right) - \alpha\right] \tag{2.6}$$

When anchoring the cable, anchorage slip can occur. If this happens, the maximum cable force can no longer be calculated by (2.5) (Engström, 2011). Instead, the maximum cable force is decided by (2.3) where s is replaced by the distance x_{s}, representing the length of cable affected by the anchorage slip, see Figure 2.3 (Engström, 2011). The length x_{s} can be calculated with (2.7). Here, Δs is the distance of the anchor slip and R is the radius of the cable curvature (Engström, 2011).

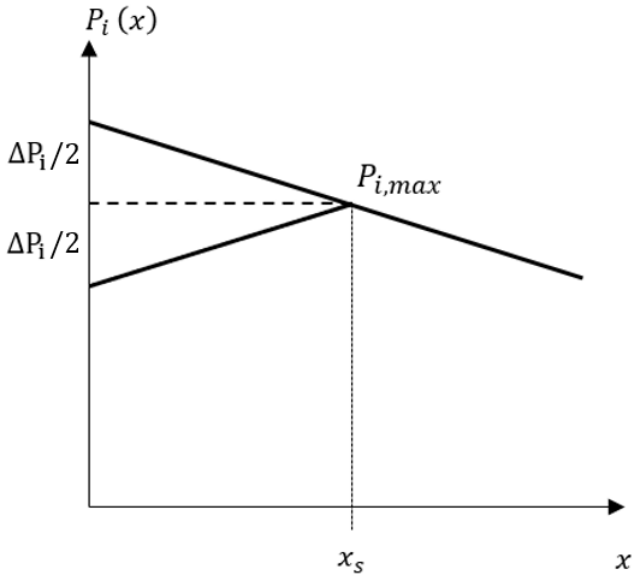

Figure 2.3: Loss of prestressing force due to anchor slip, based on Engström (2011).

$$x_s = \sqrt{\frac{\Delta s\, E_p\, A_p}{P_{\mathrm{i}}(0)\,\mu\left(\frac{1}{R}+k\right)}} \tag{2.7}$$

2.2.4 Time-Dependent Losses

In Eurocode 2 the losses from creep, shrinkage and relaxation can all be described by (2.8) (Engström, 2011; SIS, 2008). The initial cable and concrete stresses after anchorage, σ_{pi} and σ_{cpi}, respectively should be calculated for the quasi-permanent load (SIS, 2008). In (2.8), the stresses and strains are defined as positive in tension, this is an alteration from the equation in Eurocode 2 made by Engström (2011).

$$\Delta P_{\mathrm{c,s,r}} = A_{\mathrm{p}} \frac{\varepsilon_{\mathrm{cs}}\, E_{\mathrm{p}} + 0.8\,\chi_t\,\sigma_{\mathrm{pi}} - \dfrac{E_{\mathrm{p}}}{E_{\mathrm{cm}}}\varphi(t,t_0)\,\sigma_{\mathrm{cpi}}}{1+\dfrac{E_{\mathrm{p}}}{E_{\mathrm{cm}}}\dfrac{A_{\mathrm{p}}}{A_{\mathrm{c}}}\left(1+\dfrac{A_{\mathrm{c}}}{I_{\mathrm{c}}}(d_p-d_c)^2\right)[1+0.8\,\varphi(t,t_0)]} \tag{2.8}$$

In (2.8), the variables $\varepsilon_{\mathrm{cs}}$, $\varphi(t,t_0)$ and χ_t describe time-dependent material properties for the concrete and the prestressing steel. The stress independent strain caused by both drying and autogenous shrinkage is defined as $\varepsilon_{\mathrm{cs}}$. The creep of the concrete is accounted for by the creep coefficient $\varphi(t,t0)$ while the relaxation of the prestressing cable is represented by χ_t (Engström, 2011).

2.3 Cable Layout

The choice of cable layout is important as it will affect the structural response of the beam (Aspegren & Möörk, 2021; Khan et al., 2010; Nusrath et al., 2015). Despite

this, the cable layout is commonly decided by the engineer based on experience and intuition (Aalami & Jurgens, 2003). A general assumption when designing continuous prestressed beams is that the cable will follow an idealized parabolic shape with the largest eccentricity in the middle of the span, see Figure 2.4a. This assumption is made to simplify the calculations of the response (Dolan & Hamilton, 2019). It is, however, not practically feasible to construct such a beam since the cable must have a sharp bend over the mid-support. A more representative way to model the eccentricities in the cable is to use a series of parabolas instead, see Figure 2.4b (Dolan & Hamilton, 2019).

When restraining statically indeterminate beams, moments due to eccentricities of the restraining force can have a noticeable influence on the structural response. In sectional moment analysis, it can, therefore, be meaningful to distinguish between two different types of contributions, the upwards bending action from the prestressing and the restraining action from the mid-support. The prior, referred to as the primary moment M_{P}, is the product of the cable force and the eccentricity and is therefore highly dependent on the cable placement (Dolan & Hamilton, 2019). The latter, referred to as the secondary moment M_{S}, is caused by the moment from the reaction force of the mid-support since it is preventing the deformations caused by the primary moment (Dolan & Hamilton, 2019). Hence, the secondary moment is the product of the primary moments influence. The total sectional moment will thereby be the sum of the two contributions, i.e., $M_{\mathrm{P}} + M_{\mathrm{S}}$, see Figure 2.5. The secondary moment must be taken into account both for service and ultimate state according to Eurocode 2 (SIS, 2005). In design, an iterative design process needs to be adopted for finding an appropriate layout as the moment both is dependent on and influences the cable layout. This includes estimating the initial restraint moment (Engström, 2015).

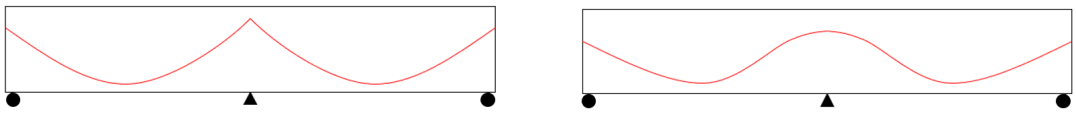

(a) Simplified cable eccentricity **(b)** Actual cable eccentricity

Figure 2.4: Schematic illustration of the cable eccentricity (a) Simplified as a parabolic shape and (b) The actual cable layout, based on Dolan and Hamilton (2019).

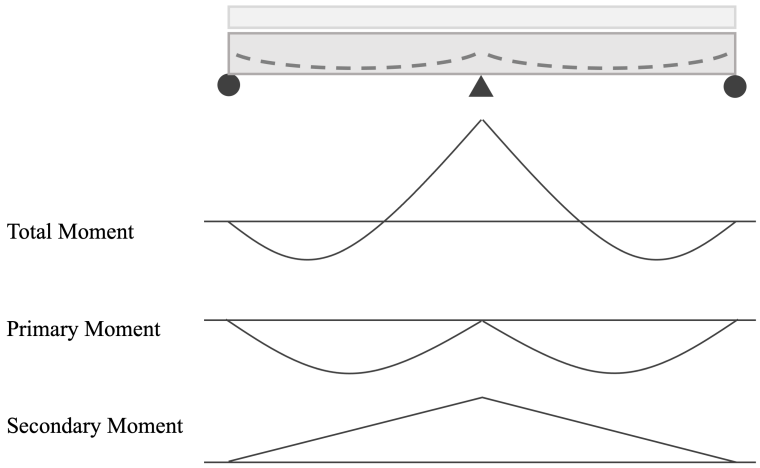

Figure 2.5: Sectional moment in a prestressed beam caused by a primary and a secondary moment, based on Dolan and Hamilton (2019).

The placement of the cables in the beam is limited by the capacity in both compression and tension. In order to use the prestressing steel in the most efficient manner, the cable eccentricity should be maximized in the critical sections. Too high eccentricity can, on the other hand, also be a limiting factor if the cross-section is to remain uncracked before applying the service load. When placing the cable within the cross-section core, i.e., the zone where compression forces only results in compressive stresses, tensile stresses can be avoided (Dolan & Hamilton, 2019). If the self-weight is applied simultaneously as the prestressing force, the tensile stresses from the prestressing can be counteracted, allowing the cable to be placed outside the core (Dolan & Hamilton, 2019).

3

General Design Approaches

In this chapter, normal bridge designs and geometries will be discussed and the standards relevant for the theory will be presented. Previous work in optimization of prestressed beams and slabs will also be investigated.

3.1 Common Dimensions

Bridges can be defined partly based on their primary structural members. The effectiveness of each bridge type vary with the span length and load as well as the limitations of deflection. The most common bridge in Sweden is the slab frame bridge where the main supporting slab is fixed to each support (Trafikverket, 2020). This type of bridge can be constructed with regular reinforcement or prestressed cables and reach spans of 25 and 35 m, respectively (Trafikverket, 2020). For design of slightly longer spans, beam bridges are usually chosen. Beam bridges have higher cross-sections compared to slab bridges, resulting in stiffer constructions. This study is focusing on beam bridges as the effect of prestressing can be larger due to the increased height of the cross-section and thus there are more potential in material reductions based on the cable placement.

Beam bridges can be constructed with one or multiple beams as the primary structural members but it is preferred to minimize the number of beams in the structure (Vägverket, 1996). Higher beams are, according to the Swedish Road Administration (1996), often more cost efficient but due to limitations in clearance and length of the deck extensions, it is in practice hard to achieve. It is not unusual for beam bridges to have varying height to further maximize the efficiency. However, this is not considered in this study. The height of the beam can be estimated based on the span lengths of the bridge. Engström (2011) suggests that for prestressed simply supported beams, the height should be $L/48$ (2.1%) while the Swedish Road Administration (1996) states that the height usually is 4-7% of the bridge span. For very large spans, box girders are often used as they reduce the self-weight of the beam while still providing great strength (Trafikverket, 2020; Vägverket, 1996). Similar to this, single beam bridges of smaller spans may also have voids built into them (Trafikverket, 2020). As the placement of the cable is the main focus for the project, single beam bridges with solid cross-sections are studied. A solid cross-section allows for unhindered placement of the cable while using a single beam reduces the complexity.

Beam bridges with regular reinforcement are usually constructed with spans larger than 15 m. When the spans have reached 25 m, it is possible that it would be more economical to use prestressing cables and for spans longer than 30 m prestressed

beams should be used (Vägverket, 1996). Beam bridges can be built with spans that are 200 m long. For these structures, a box girder cross-section should be used (Vägverket, 1996). In this study, spans in the range 25-40 m are of interest in order to represent a wide range of prestressed concrete beam bridges while still being able to maintain a solid, single beam cross-section.

The Swedish Transport Administration (2022) provides requirements for bridge widths. Depending on number of lanes and speed limit, the bridge widths ranges between 6 to 23 m. Here, the lower limit corresponds to a single-lane bridge while the upper limit represents a four-lane bridge. Since the number of beams in a bridge may vary with the width and only a single-beam bridge will be studied, the geometry will be set to represent a double-lane bridge. Following the requirements from the Swedish Transport Administration (2022), a double-lane bridge should have a section width of 7.5 m, excluding the widths for edge barriers and possible shoulder bicycle lanes. As a simplification, the total bridge deck width is rounded up to 8 m to compensate for eventual barriers, road shoulders, or similar. In addition, the bridges are also assumed to only carry vehicle traffic and no pedestrian nor bicycle traffic is regarded.

3.2 Standards

The project is based on the Eurocode standards. When designing bridges in Sweden, it is also required to fulfill the criteria presented by the Swedish Transport Administration (Trafikverket) and the Swedish Transport Agency (Transportstyrelsen) for service life class L100, corresponding to a service life of 120 years (Trafikverket, 2019a). The following sections include criterion that must be fulfilled for prestressed concrete bridges.

3.2.1 Geometric Requirements

In order to ensure a good reinforcement bond, prevent spalling, protect against environmental exposure and ease the construction process, it is necessary to verify the reinforcement geometry, i.e., the cover thickness as well as the minimum and maximum distances (Al-Emrani et al., 2013).

Eurocode 2 specifies that the cover thickness must be greater than the nominal cover thickness (SIS, 2008). This thickness can in turn be expressed to include two terms, one generally accounting for environmental durability, fire-safety and reinforcement bond, and the other accounting for deviations. The nominal cover thickness is expressed as in (3.1). The Swedish Transport Agency (2018) specifies that the cover thickness due to deviation tolerance, Δc_{dev}, should be included and Eurocode recommends setting this term to 10 mm (SIS, 2008). The minimum cover thickness c_{min} can be expressed as in (3.2) in accordance with the recommendations in Eurocode (SIS, 2008).

$$c_{\text{nom}} = c_{\text{min}} + \Delta c_{\text{dev}} \tag{3.1}$$

$$c_{\min} = \max \begin{cases} c_{\min,\mathrm{b}} \\ c_{\min,\mathrm{dur}} \\ 10\,\mathrm{mm} \end{cases} \tag{3.2}$$

The spacing related to bond, $c_{\min,\mathrm{b}}$, is in Eurocode set to the diameter of the reinforcement bars and the post-tensioning ducts. The spacing related to durability, $c_{\min,\mathrm{dur}}$, should be set in accordance with the Swedish Transport Agency (Transportstyrelsen, 2018) since these are stricter than the requirements from Swedish Transport Administration (Trafikverket, 2019a).

Following the guidelines from the Swedish Transport Agency (2018), the minimum cover thickness $c_{\min,\mathrm{dur}}$ can be set based on the exposure class and water-cement ratio of the concrete. For bridge surfaces directly exposed to road salts, the agency recommends the exposure classes XD3 and XF4 to be used. When using concrete with a water-cement ratio of 0.40, the minimum cover thickness can be set to 45 mm (Transportstyrelsen, 2018). For the sides that are not directly subjected to road salts, XD1 may be chosen when following the recommendations in Eurocode (SIS, 2008). For the same water-cement ratio, a minimum cover thickness of 25 mm is given from the Swedish Transport Agency (2018). When applying the requirements to a post-tensioned beam, an additional 10 mm of cover thickness should be added. The concrete cover is also measured to the duct instead of the cable. When including the deviation term, the requirements can be expressed as in (3.3)–(3.4) following the notation scheme in Figure 3.1.

$$c_1 - \phi_{\mathrm{stirrups}} \geq \begin{cases} 35\ \mathrm{mm} & \text{for reinforcement steel} \\ 45\ \mathrm{mm} & \text{for post-tension ducts} \end{cases} \tag{3.3}$$

$$c_{1\mathrm{top}} - \phi_{\mathrm{stirrups}} \geq \begin{cases} 55\,\mathrm{mm} & \text{for reinforcement steel} \\ 65\,\mathrm{mm} & \text{for post-tension ducts} \end{cases} \tag{3.4}$$

In addition to the cover thickness, Eurocode 2 also requires the spacing between the reinforcement bars to fulfill (3.5) in both horizontal and vertical direction (SIS, 2008). For the prestressing steel in post-tensioned systems, the horizontal and vertical spacing between the ducts is instead required to fulfill (3.6)-(3.7), respectively, (SIS, 2008). For reference, see Figure 3.1. In cross-sections where the ducts are not fully vertically aligned, the aggregate diameter can be neglected. Bundling of post-tension ducts is not allowed except for when two ducts are stacked vertically. The design of stacked ducts is, however, in practice inconvenient as the ducts must be separated in the anchoring region. As a consequence, there will be regions where the ducts are not stacked and do not fulfill the requirement of minimum spacing in (3.7).

$$a_{\mathrm{s}} \geq \max \begin{cases} \phi_{\mathrm{s}} \\ d_{\mathrm{agg}} + 5\,\mathrm{mm} \\ 20\,\mathrm{mm} \end{cases} \tag{3.5}$$

$$a_{\mathrm{ph}} \geq \max \begin{cases} d_{\mathrm{agg}} + 5\,\mathrm{mm} \\ \phi_{\mathrm{duct}} \\ 50\,\mathrm{mm} \end{cases} \tag{3.6}$$

$$a_{\mathrm{pv}} \geq \max \begin{cases} d_{\mathrm{agg}} & \text{Only if the ducts are fully aligned} \\ \phi_{\mathrm{duct}} \\ 40\,\mathrm{mm} \end{cases} \tag{3.7}$$

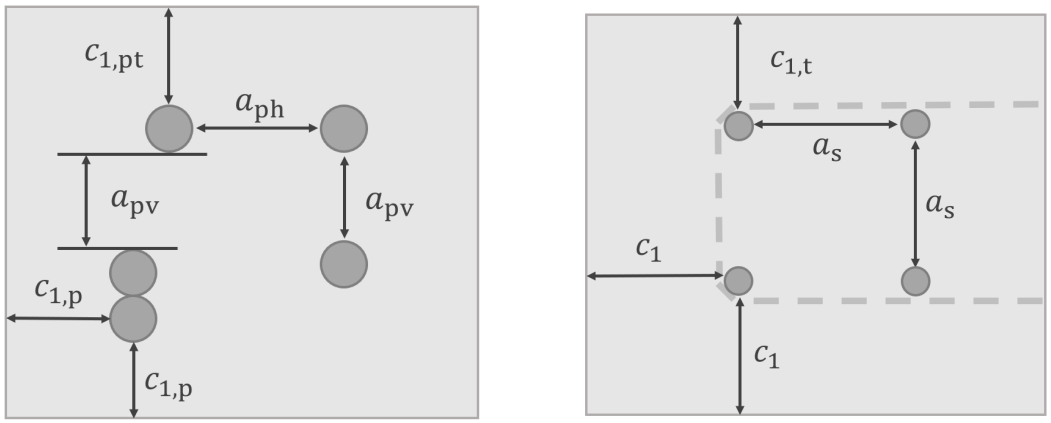

(a) Post-tensioning ducts **(b)** Reinforcement bars

Figure 3.1: Schematic illustration of the notations used for reinforcement spacings of a fictional cross-section for (a) Post-tensioning ducts and (b) Reinforcement bars, based on Eurocode 2 (SIS, 2008).

3.2.2 Actions

When designing bridges, there are a number of different actions that needs to be taken into account. Depending on bridge type, geometry, and function, different actions must be designed for. In the scope of this project, vertical loads have been identified as the relevant actions since the main purpose of the prestressing steel is to counteract the bending from these. The actions that influences the main bending are:

- Self-weight

- Traffic loads
- Prestressing force
- Thermal constraints
- Creep and shrinkage
- Relaxation

3.2.2.1 Self-Weight

Normal prestressed concrete can be assumed to have a self-weight of 25 kN/m^3, including the weight of the reinforcement (SIS, 2002b). In addition, the self-weight from pavement and traffic barriers should also be added. For mastic asphalt pavement, the self-weight is 24 kN/m^3 (Trafikverket, 2019a). A reasonable self-weight per barriers is 0.5 kN/m (C. Jonsson & V. Andersson, personal communication, Mars 3, 2022).

3.2.2.2 Traffic Loads

Traffic loads are accounted for in Eurocode 2 by the use of load models, denoted LM1–4 (SIS, 2010). These load models are based on European traffic patterns from the year 2000 and are valid for bridges shorter than 200 meters. Both LM3 and LM4 can be disregarded in this study as LM3 only should be used if the developer specifies it while LM4 should be neglected for all road bridges (Trafikverket, 2019a). Furthermore, LM2 is often only governing in smaller structural members in the range 3-7 m, thus it too can be disregarded in this study (SIS, 2010). LM1 is then the only traffic load from Eurocode 2 that will be used. The load model consists of both point loads and distributed loads. The point loads are positioned in a tandem system in order to represent two axles, see Figure 3.2 (SIS, 2010).

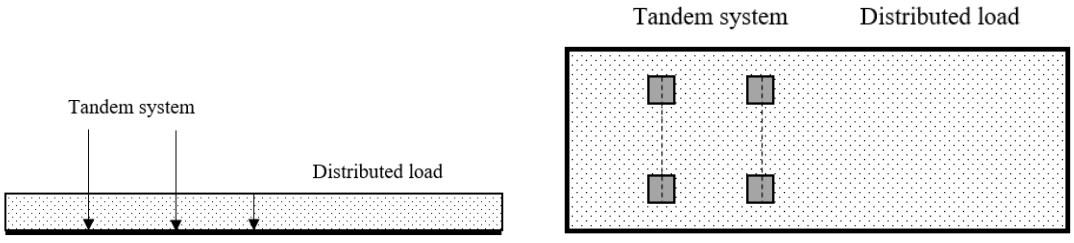

(a) Seen from the side **(b)** Seen from above

Figure 3.2: General model for LM1 as seen from (a) The side, and (b) Above.

When applying traffic load to the structure, it should be done using notional lanes, see Figure 3.3. The carriageway is divided into a number of notional lanes based on its width and the division is defined by the expressions in Table 3.1 (SIS, 2010).

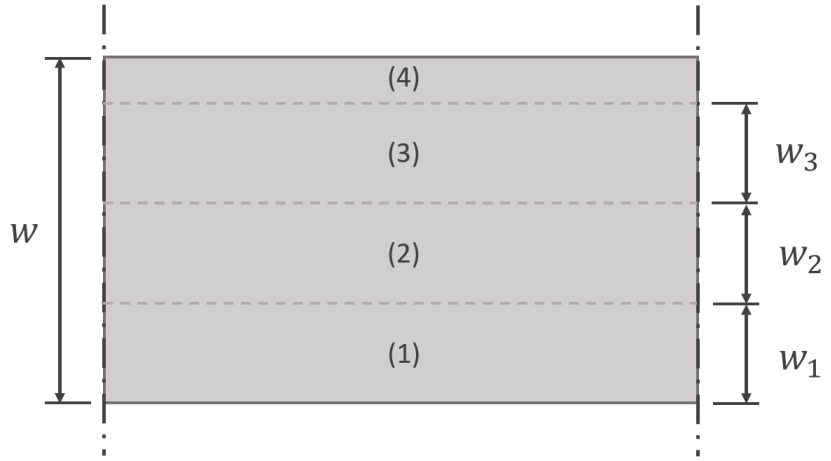

Figure 3.3: Schematic illustration of possible notional lane numbering.

Table 3.1: Lane division in Eurocode 1 (SIS, 2010).

Carriageway width w	**No. of notional lanes**	**Notional lane width w_i**
$\leq 5.4\,\mathrm{m}$	1	$3\,\mathrm{m}$
5.4–6 m	2	$\frac{w}{2}$
$> 6\,\mathrm{m}$	$\mathrm{floor}\left(\frac{w}{3}\right)$	$3\,\mathrm{m}$

The numbering of the notional lanes in Figure 3.3 represent how unfavourable a load placed in each lane is with 1 being the most unfavourable lane. When applying the load models onto the notional lanes, point loads and distributed loads should be placed in the most unfavourable positions. This means that the distributed load does not have to be placed along the whole length and that the distributed loads also are free to overlap the point loads (SIS, 2010).

The characteristic point loads and the distributed load in LM1 are defined in Eurocode 2 and presented in Table 3.2 (SIS, 2010). Note that Q_i is the total load for each axle. These loads should also be multiplied by an adjustment factor α_{Q_i} or α_{q_i} depending on load type and notional lane, see Table 3.3 (Transportstyrelsen, 2018).

Table 3.2: Load magnitudes for LM1 according to Eurocode 1 (SIS, 2010).

Notional lane	**Axle load Q_i [kN]**	**Distributed load q_i [kN/m^2]**
1	300	9
2	200	2.5
3	100	2.5
>3	0	2.5
Remaining area	0	2.5

Table 3.3: Adjustment factors for LM1 (Transportstyrelsen, 2018).

Adjustment factor	**Value**
α_{Q1}	0.9
α_{Q2}	0.9
α_{Q3}	0
α_{q1}	0.8
α_{qi} $(i > 1)$	1
α_{qr}	1

By Swedish regulations, it is not sufficient to only take the load models in Eurocode 2 into account. In addition, The Swedish Transport Agency have also defined 14 different vehicle models, denoted a-n, that should be included in bridge design (Transportstyrelsen, 2018). These vehicle models will not be accounted for in this study in order to reduce the complexity of the task. However, their application will still be explained. The vehicle models consists of point loads and distributed loads q with defined distances. An example of a vehicle model is shown in Figure 3.4 for reference. The magnitude of the point loads are defined differently for each vehicle model but the distributed load is always either 0 or 5 kN/m (Transportstyrelsen, 2018). One model is placed in each notional lane up to a maximum of two lanes after which a distributed load of either 0 or 5 kN/m is placed in the subsequent lanes (Transportstyrelsen, 2018). The vehicle models in the two notional lanes are multiplied by 0.8 and 1.0, respectively. Similar to the placement of the load models in Eurocode 2 the vehicle models should be placed in the most unfavorable positions (Transportstyrelsen, 2018). Point loads in both LM1 and the vehicle models should be amplified by adding a dynamic impact factor of 25% (Trafikverket, 2019a).

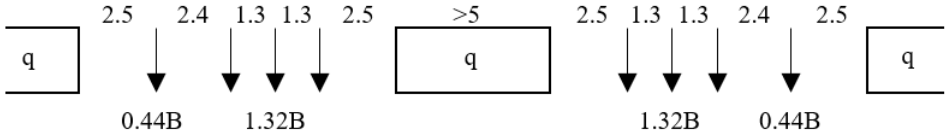

Figure 3.4: Example of a vehicle model (model g) according to the Swedish Transport Administration (2018) where B is set to 300 kN.

3.2.2.3 Prestressing Force

The prestressing force will be a permanent force acting on the beam. The maximum force that a cable can be tensioned to by the jack is decided by (3.8), where the prestressing stress σ_{p} is set by (3.22). The stress in the cable should however not exceed the limit in (3.24) after anchorage, which limits the initial prestressing force (Engström, 2011). In service state, the upper and lower characteristic prestressing forces can be expressed with (3.9)-(3.10) where P_{m} is the mean prestressing force along the beam.

$$P_{\mathrm{max}} = A_{\mathrm{p}} \cdot \sigma_{\mathrm{p}} \tag{3.8}$$

$$P_{\mathrm{k,sup}} = 1.1\, P_{\mathrm{m}} \tag{3.9}$$

$$P_{\mathrm{k,inf}} = 0.9\, P_{\mathrm{m}} \tag{3.10}$$

In Section 2.2, the different types of loss of prestressing force are presented and explained. For this study, only the friction losses and the time-depended losses are deemed relevant and included in the model. Anchoring losses are excluded as they are judged to not vary significantly with different cable layouts. Deformation losses were also excluded as it was assumed, as a simplification, that all cables would be tensioned simultaneously.

3.2.2.4 Thermal Constraints

The thermal load consists of two parts, uniform temperature change and internal temperature gradients (SIS, 2003). However, strains from uniform temperature change will not affect the construction as free movement is allowed in the horizontal direction in this study, see Section 4.6. The internal temperature gradient in the beam will, due to a difference in expansion or contraction, induce curvature in the beam, see (3.11) (Al-Emrani et al., 2014). The temperature difference between the top and bottom of the beam, ΔT, is set to 15°C if the top side is warmer and 8°C if it is cooler (SIS, 2003). In accordance with Eurocode 2, the thermal coefficient for concrete, α_{c}, can be set to $10 \cdot 10^{-6}$ K^{-1} (Al-Emrani et al., 2014). As a simplification, the prestressing cable is said to have the same thermal coefficient as the concrete.

$$\kappa_T = \pm \frac{\alpha_{\mathrm{c}}\, \Delta T}{h} \tag{3.11}$$

3.2.2.5 Creep and Shrinkage

Long-term application of load induces additional deformations in the concrete, in addition to shrinkage, referred to as creep. Whereas the shrinkage is independent from the loading, the creep is not (Al-Emrani et al., 2014). The strain from each of the contributions are often denoted $\varepsilon_{\mathrm{cs}}$ and ε_{c}, respectively. The shrinkage strain

further consists of two components, drying shrinkage and autogenous shrinkage, and can therefore be expressed as in (3.12) (Al-Emrani et al., 2014). Since the shrinkage is restrained internally by both the reinforcement and the prestressing steel, it is of interest to relate the induced strains in the materials to the internal shrinkage force in (3.13) (Al-Emrani et al., 2014).

$$\varepsilon_{\mathrm{cs}}(t) = \varepsilon_{\mathrm{cd}}(t) + \varepsilon_{\mathrm{ca}}(t) \tag{3.12}$$

$$F_{\mathrm{cs}}(t) = E_{\mathrm{s}}\, A_{\mathrm{s}}\, \varepsilon_{\mathrm{cs}}(t) \tag{3.13}$$

To quantify the final creep contribution, the notional creep factor $\varphi(t, t_0)$ is used. In Eurocode the creep coefficient is expressed using different factors considering the relative humidity, concrete strength, and time of load application, respectively, as in (3.14) (Al-Emrani et al., 2013). The final strain can be calculated using the effective Young's modulus in (3.31) from Section 3.2.5.

$$\varphi(\infty, t_0) = \varphi_{\mathrm{RH}} \cdot \beta(f_{\mathrm{cm}}) \cdot \beta(f(t_0)) \tag{3.14}$$

3.2.2.6 Relaxation

When steel is being put under strain for a longer time, relaxation losses will occur, leading to decrease in material stresses. This is a relevant phenomenon for prestressed structures as the larger initial forces will lead to more relaxation compared to a regularly reinforced structure where relaxation can be neglected (Engström, 2011). The loss of stress due to relaxation can be described by (3.15)-(3.16) where $\Delta\sigma_{\mathrm{pr}}(t)$ is the loss of prestressing force at the time t in hours (Engström, 2011).

$$\sigma_{\mathrm{p}}(t) = \sigma_{\mathrm{p0}} - \Delta\sigma_{\mathrm{pr}}(t) \tag{3.15}$$

$$\chi_t = \frac{\Delta\sigma_{\mathrm{pr}}(t)}{\sigma_{\mathrm{p0}}} \tag{3.16}$$

The relaxation factor, χ_t, can be calculated with (3.17)-(3.18) according to Eurocode 2 for steel in relaxation class 2, i.e., wires and strands with low relaxation (Engström, 2011; SIS, 2008). Here, the relaxation factor for steel stressed to 70% of the characteristic strength for 1000 hours at a mean ambient temperature of 20°C, denoted χ_{1000}, can be set to 2.5% (SIS, 2008). Final relaxation should according to Eurocode be derived for a 500,000 hour period after tensioning (SIS, 2008).

$$\chi_t = 0.66 \cdot \chi_{1000} \cdot e^{9.1\mu} \left(\frac{t}{1000\,\mathrm{h}}\right)^{0.75(1-\mu)} \cdot 10^{-3} \tag{3.17}$$

$$\mu = \frac{\sigma_{\mathrm{p0}}}{f_{\mathrm{puk}}} \tag{3.18}$$

3.2.3 Load Combinations

EN 1990 (SIS, 2002a; Transportstyrelsen, 2018) defines the following load combinations in (3.19)-(3.21) for serviceability limit state, referred to as the characteristic, frequent and quasi-permanent load combination. The reduction factors Ψ_0-Ψ_2 are presented in Table 3.4 based on the values given in Eurocode (SIS, 2002a). All favorable permanent loads are to be considered while all favorable variable loads should be ignored in the combinations.

Characteristic

$$\sum_{j=1}^{m} G_{\mathrm{k},j} + P_{\mathrm{s}} + Q_{\mathrm{k},1} + \sum_{i=2}^{n} \Psi_{0,i} Q_{\mathrm{k},i} \tag{3.19}$$

Frequent

$$\sum_{j=1}^{m} G_{\mathrm{k},j} + P_{\mathrm{s}} + \Psi_{1,1} Q_{\mathrm{k},1} + \sum_{i=2}^{n} \Psi_{2,i} Q_{\mathrm{k},i} \tag{3.20}$$

Quasi-permanet

$$\sum_{j=1}^{m} G_{\mathrm{k},j} + P_{\mathrm{s}} + \sum_{i=1}^{n} \Psi_{2,i} Q_{\mathrm{k},i} \tag{3.21}$$

Table 3.4: Reduction factors for variable actions in Eurocode.

Action	$\boldsymbol{\Psi_0}$	$\boldsymbol{\Psi_1}$	$\boldsymbol{\Psi_2}$
Tandem system	0.75	0.75	0
Distributed traffic loads	0.40	0.40	0
Thermal	0.6	0.6	0.5

3.2.4 Stress Limits

Post-tensioned beams are exposed to several risks during their construction and lifetime concerning fracture in the prestressing steel, unintended concrete cracking as well as long-term and environmental effects. In order to protect the structure, there are several requirements and recommendations in Eurocode. In the following sections, it is described how the stress should be limited in accordance with Eurocode and the Swedish Transport Agency under different load combinations.

3.2.4.1 Construction Stage

In the construction stage, i.e., before the service load is applied, the structure is analysed using a quasi-permanent load combination with self-weight and thermal effects. Verification are performed at two stages, before and after anchorage.

After stressing (i.e., before anchorage) there are two verifications that should be performed. When tensioning the cables, there is a risk that the steel fractures after stressing the element (Engström, 2011). In order to prevent fracturing as well as the

potential injuries it might lead to, the steel stress after tensioning should be limited according to (3.22).

$$\sigma_{\mathrm{p0}} \leq \begin{cases} 0.90 f_{\mathrm{p0.1k}} \\ 0.80 f_{\mathrm{puk}} \end{cases} \tag{3.22}$$

Right after tensioning the element, the structure will be subjected to no service load. Since the prestressing force is meant to counteract the service load, the prestressing will at this stage have a negative influence on the risk for cracking. The reason is that the bending of the element is inverted at this stage compared to in service state. Hence, tensile stresses will occur at the side that in service state will be compressed (Engström, 2011). To prevent cracking at this side, the criterion in (3.23) should be fulfilled where $f_{\mathrm{ctk}}(t_{\mathrm{i}})$ is the tensile strength at tensioning (Engström, 2011).

$$\sigma_{\mathrm{cti}} \leq \begin{cases} 0 & \text{for complete prestressing} \\ f_{\mathrm{ctk}}(t_{\mathrm{i}}) & \text{for incomplete prestressing} \end{cases} \tag{3.23}$$

After anchorage, it is relevant to limit the steel stresses in order to reduce the relaxation losses which is done using (3.24) from Eurocode (Engström, 2011).

$$\sigma_{\mathrm{pi}} \leq \begin{cases} 0.85 f_{\mathrm{p0.1k}} \\ 0.75 f_{\mathrm{puk}} \end{cases} \tag{3.24}$$

3.2.4.2 Quasi-Permanent Loading

Too high steel stresses should also be avoided after applying the long term loading. This is done using (3.25) (Engström, 2011).

$$\sigma_{\mathrm{p}\infty} \leq \begin{cases} 0.85 f_{\mathrm{p0.1k}} \\ 0.75 f_{\mathrm{puk}} \end{cases} \tag{3.25}$$

When treating creep for long term loading as linear, (3.26) must also be fulfilled (Engström, 2011).

$$\mid \sigma_{\mathrm{cc}\infty} \mid \leq 0.45 f_{\mathrm{ck}} \tag{3.26}$$

3.2.4.3 Frequent Loading

If the structure is exposed to a corrosion risk from chlorides (either seawater, road salts or other causes) or if there is a risk of freeze-thaw attacks, corresponding to Exposure Class XD, XS, and XF, an additional criterion, (3.27), must be verified. This is referred to as a decompression check and is verified for the frequent load case.

$$\sigma_{\mathrm{cp}\infty} \leq 0 \tag{3.27}$$

The Swedish Transport Agency (2018) also demand that the requirement (3.27) should be valid for a radius of 100 mm around the duct.

3.2.4.4 Characteristic Loading

If the bridge is subjected to the exposures mentioned in Section 3.2.4.3, the long term compressive concrete stress should also be limited by (3.28) in order to prevent micro cracking (Engström, 2011).

$$\mid \sigma_{\mathrm{cc}\infty} \mid \leq 0.6 f_{ck} \tag{3.28}$$

In order for a fully prestressed element to remain fully prestressed, the tensile stress should also by definition fulfill (3.29) for the entire cross-section (Engström, 2011).

$$\sigma_{\mathrm{ct}\infty} \leq \begin{cases} 0 & \text{for complete prestressing} \\ f_{\mathrm{ctk}} & \text{for incomplete prestressing} \end{cases} \tag{3.29}$$

3.2.5 Deflection

In serviceability limit state, deflection should be limited to ensure comfortability and prevent damages of adjacent structural members (Al-Emrani et al., 2014). The Swedish Transport Administration (2019a) limits the span deflection to $L/400$ as given in (3.30). In Eurocode, the deflection is limited under frequent loading (Trafikverket, 2019a). In order to accommodate for long-term effects, creep, shrinkage, and relaxation is accounted for (Engström, 2011). To include the creep, Eurocode provides (3.31)–(3.32) (SIS, 2008). Since sections in a fully prestressed element can be regarded as uncracked in the service state, a constant State I flexural stiffness can be used along the beam.

$$w_{\mathrm{max},\infty} \leq \frac{L}{400} \tag{3.30}$$

$$E_{\mathrm{c,ef}} = \frac{E_{\mathrm{cm}}}{1 + \varphi(\infty, t_0)} \tag{3.31}$$

$$\alpha_{\mathrm{ef}} = \frac{E_{\mathrm{s}}}{E_{\mathrm{c,ef}}} \tag{3.32}$$

The modular ratio, can in turn, be divided into two factors, $\alpha_{\mathrm{p,ef}}$ and $\alpha_{\mathrm{s,ef}}$, for the prestressing and reinforcement steel, respectively (Engström, 2011). Since the relaxation occurs in the prestressing steel only, (3.33) can be used (Engström, 2011).

$$\alpha_{\mathrm{p,ef}} = \frac{E_{\mathrm{p}}\,(1-\chi_{\infty})}{E_{\mathrm{c,ef}}} \tag{3.33}$$

The curvature contribution from the relaxation and the shrinkage in the prestressing steel can be expressed as in (3.34) where M_{quasi} is the moment from quasi-permanent loading and F_{cp} is the shrinkage force given by (3.35) (Engström, 2011).

$$\kappa_{\infty} = -\frac{-(1-\chi_{\infty})(P_{0\mathrm{i}} - F_{\mathrm{cp}})e_{\mathrm{f}} + M_{\mathrm{quasi}}}{E_{c,ef}\cdot I_{\mathrm{I,ef}}} \tag{3.34}$$

$$F_{\mathrm{cp}} = E_{\mathrm{p}}\,\varepsilon_{\mathrm{cp}}\,A_{\mathrm{p}} \tag{3.35}$$

3.3 Support Moment

The moment at the mid-support for continuous symmetric beams (with symmetric loading) can be evaluated by setting the support rotation equal to zero and solving the unknown restraint moment for all known contributions (Engström, 2015). This can be fulfilled by superposing all contributions to the support rotations on each side from Table 3.5 and setting the combined rotation to zero as expressed in (3.36). Note how all contributions except the restraint moment are given for a simply supported beam which is consistent with the restraint moment corresponding to the additional restraint from the mid-support (Engström, 2015). The curvature distribution for the prestressing may vary due to differences in eccentricity and cable force, making it unique for each bridge.

$$\sum \theta_i = 0 \tag{3.36}$$

Table 3.5: Rotations at the mid-supports for different actions (Engström, 2015).

Action	**Curvature distribution**	**Mid-support rotation**
Self-weight	Parabolic	$\frac{ql^3}{24\,EI}$
Restraint moment	Triangular	$\frac{M_{\mathrm{r}}l}{3\,EI}$
Thermal	Constant	$-\frac{1}{2}\frac{\alpha_{\mathrm{c}}\Delta T l}{h}$
Prestressing	Case specific	$\frac{1}{l}\int_0^l -\frac{P_{\mathrm{m}}\,e(x)}{EI}\cdot x\,dx$

3.4 Optimization of Prestressed Beams

When designing a prestressed concrete beam, the engineer is required to make several choices including cable layout and prestressing force before a solution can be found (Aalami & Jurgens, 2003). As stated in Section 2.3, the choice of cable layout will impact the efficiency of the beam and thereby also affect the cost and sustainability of the structure. The engineers will often have to rely on their experience and intuition when choosing a cable layout. This might lead to the most optimal design not being found, resulting in potential savings regarding cost and environmental impact being lost.

The possibility of optimizing the design of prestressed concrete beams have been investigated in several studies. Lounis and Cohn (1993) produced design charts from where the most cost-efficient cross-section can be chosen based on the number of spans and span lengths of the bridge. Their study was of pretensioned precast beams and, thus, they did not investigate different cable layouts. They also concluded that their study focused on optimizing the cost of the components of the bridge separately and more cost efficient solutions could be possible if the complete structure was optimized.

An optimization algorithm created by Kuyucular (1991) showed savings up to 50% could be achieved by varying the cable layout in two-way slabs. Of these, up to 35 percentage points (p.p.) were accredited to using a non-uniform distribution of cables. Kuyucular (1991) also established that the cable profile most often is assumed to be parabolic between the beam end and the mid span. The variation in cable placement is instead usually between the mid span and the intermediate support, where different profiles can be chosen (Kuyucular, 1991).

A previous master thesis conducted by Aspegren and Möörk (2021) found that in order to reduce both the environmental impact and the cost of the bridge, a more slender cross-section with a larger number of prestressing cables should be used. They also found that the length of the spans will impact how the cable layout should be designed. For spans shorter than 32 m, the secondary moment should be minimized as the self-weight of the bridge is too small to properly balance the forces. Likewise, for longer spans, the secondary moment should instead be increased.

A study by Utrilla and Samartín (1997) examined the effect of the cable profile. The profile of the cables in continuous beams were optimized to minimize the necessary prestressing force. Only the longitudinal stresses in the service state were considered as requirements for their designs. Friction losses were included in the study and the cables were assumed to be actively tensioned from both sides. The cable was represented by four points, end of the beam, position of maximum eccentricity, inflection point and position over support. Each point had three degrees of freedom, position in x and y as well as the inclination. Between the points the cable was approximated by a cubic hermitian polynomial. Utrilla and Samartín (1997) concluded that the position of maximum eccentricity in the span should be placed at 0.4 of the span length and the inflection point at 0.9 of the span length. Furthermore, both the point of maximum eccentricity and the point over the support should be placed as

close as possible to the edge.

Through optimization of simply supported I-girders, it was found that cost could be reduced by 35% (Ahsan et al., 2011). In this study, both the girder cross-section and cable layout were included in the optimization. For the cables, a correlation between cost of steel and eccentricity could be found where higher prices led to larger eccentricities. It was also discovered that cables consisting of eight and nine strands were the most effective for concrete with strengths of 40 and 50 MPa, respectively (Ahsan et al., 2011).

4

Finite Element Analysis

The structural analyses for the beam optimization was carried out using linear finite element (FE) analysis in SOFiSTiK 2020, version 14.0.1948 (SOFiSTiK AG, n.d.-e). Since the scope of the study only covers behavior in service state and the analysis was confined to only fully prestressed beams, nonlinear behavior such as stiffness redistributions due to cracking and yielding is irrelevant. As nonlinear analysis also is more time consuming, linear analysis was deemed to be most suitable for this study.

4.1 Beam Geometry

The bridge beams that will be studied as well as corresponding geometric notations are presented in Figure 4.1. As explained in Section 3.1, the bridge deck width b was set to 8 m, and the span length L was set to range between 25 and 40 m. As a consequence, reliability class 3 can be used in accordance with The Swedish Transport Agency (2018). The total beam height, h, was set to 5% of the span length L based on common heights among prestressed concrete beam bridges (Vägverket, 1996). In addition, the slab height, h_{f}, is limited to at least 170 mm (Trafikverket, 2019b), but due to the cantilevers commonly being tapered, a constant slab height of 300 mm was instead used for all investigated beam geometries. Consequently, the web height h_{w} is given by (4.1).

The bottom web width, b_{wb}, was set to the smallest width possible in order to fit the chosen number of prestressing cables based on the requirements for cover thickness and spacing between ducts and reinforcement bars in Section 3.2.1. Additionally, a minimum width of 1 m was used to maintain more realistic dimensions with respect to conventional support executions. In addition, the side-extensions of the deck are, by the Swedish Road Administration (Vägverket) (1996), not recommended to exceed 3 m, resulting in a top web width, b_{wt}, of at least 2 m. If the bottom web width, b_{wb}, should exceed 2 m, the top width, b_{wt}, was set according to (4.3) in order to keep the web inclined. As stated in Section 3.2.1, the cables are limited in placement due to requirements in cable spacing and cover thickness. For determining the horizontal spacing of the ducts, (3.6) was used. When using ducts with outer diameters larger than the maximum aggregate size, the web with should be limited by (4.2) where n is the number of cables and the cover thickness, c_1, is taken from (3.3). The bridge dimensions are compiled into Table 4.1 with reference to the notations in Figure 4.1.

In accordance with the requirements from the Swedish Transport Administration (2019a), the outermost 100 mm of the slab width on each side of the beam should

be neglected when calculating the capacity. The slab width b is therefore decreased by 200 mm in the effective cross-section.

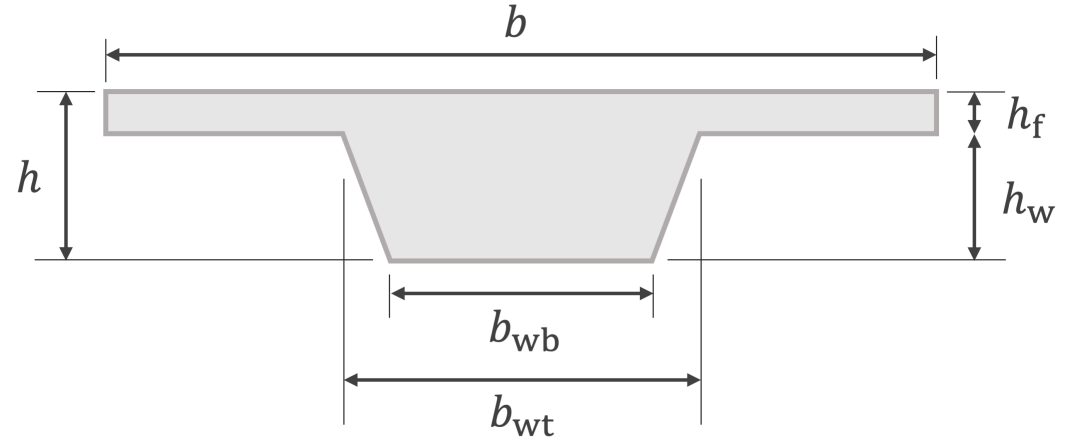

(a) Cross-section view

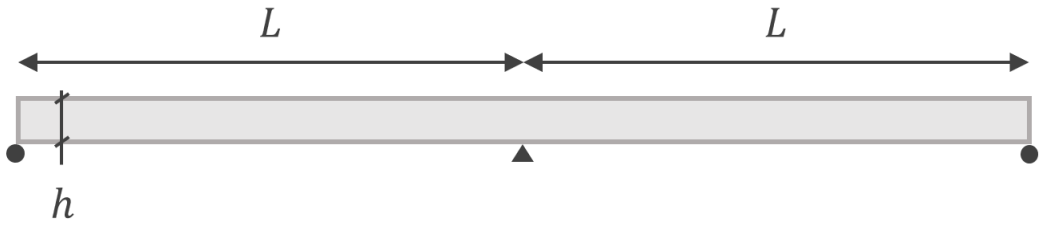

(b) Longitudinal view

Figure 4.1: Geometry and notation from (a) Cross-section view and (b) Longitudinal view of the beam model.

$$h_{\mathrm{w}} = h - h_{\mathrm{f}} \tag{4.1}$$

$$b_{\mathrm{wb}} \geq \begin{cases} n \cdot \phi_{\mathrm{duct}} + (n-1) \cdot a_{\mathrm{s}} + 2 \cdot c_1 \\ 1\,\mathrm{m} \end{cases} \tag{4.2}$$

$$b_{\mathrm{wt}} \geq \begin{cases} 2\,\mathrm{m} \\ b_{\mathrm{wb}} + 1\,\mathrm{m} \end{cases} \tag{4.3}$$

Table 4.1: Bridge dimensions.

L	h	b	b_{wb}	b_{wt}	h_{f}	h_{w}
25-40 m	$L/20$	8 m	See (4.2)	See (4.3)	300 mm	$h - h_{\mathrm{f}}$

4.2 Cable Geometry

For this study, strands with a diameter of 15.7 mm were chosen. A wide range of cables consisting of 5-27 strands was considered, available from DYWIDAG (n.d.) or similar supplier. Following the recommendations from DYWIDAG (n.d.), corresponding ducts in corrugated steel for each cable were also selected, ranging between 60-117 mm in diameter. Since the minimum radius of the cable depends on the number of strands in the cable, it could be determined using the product page from DYWIDAG (2021).

The chosen cables were placed in the cross-section with respect to the dimensions of the ducts, reinforcement bars and stirrups. For the regular reinforcement, 20 mm bars were chosen combined with 16 mm stirrups although the configuration of the regular reinforcement, in practice, will depend on the ULS behavior. As the ULS verification seldom is critical for the design of the prestressing reinforcement, it was not included in this study. Consequently, the prestressing cables were placed such that one layer of main reinforcement could be inserted both at the bottom and the top of the bridge, enclosing the prestressing steel. This was considered a reasonable design choice as the web thicknesses were regarded as sufficient for all bridge geometries. Since duct sizes of 60-117 mm were used, it was concluded that the duct dimensions will be governing for the design rather than the aggregate size as presented in previous section. Hence, the required cable spacing, a_{ph}, could be set to the duct size whereas the web width was calculated using (4.2). The total cover thicknesses at the bottom and top of the beam for the prestressing steel, denoted $c_{\mathrm{1p,b}}$ and $c_{\mathrm{1s,t}}$, were calculated using (4.4)-(4.5). For the top cover, an additional reinforcement layer was added for transverse reinforcement. As an assumption, the same bar diameter was used as for the main reinforcement. Consistent with Section 3.2.1, c_{1s} corresponds to the general cover thickness for the reinforcement steel whereas $c_{\mathrm{1s,t}}$ represents the special case where the cover thickness is taken from the top. The cable spacing for the prestressing steel in the vertical direction, is denoted a_{pv}. This can be considered as a conservative choice as the spacing between the ducts and the reinforcement bars instead can be limited to the spacing of the bars, a_{s}.

$$c_{\mathrm{1p,b}} = c_{\mathrm{1s}} + \phi_{\mathrm{stirrups}} + \phi_{\mathrm{s}} + a_{\mathrm{pv}} \tag{4.4}$$

$$c_{\mathrm{1p,t}} = c_{\mathrm{1s,t}} + 2\,\phi_{\mathrm{s}} + a_{\mathrm{pv}} \tag{4.5}$$

In order to achieve as much flexibility in the cable placement as possible using only a small number of degrees of freedom (DOFs), some compromises were made. While a model defined with a greater number of DOFs may increase the flexibility of the layout, it is also limited by the additional computational expenses of optimizing with respect to additional variables. The cable placement was therefore defined by using fifteen nodes, six in each span and one over each support. Between the nodes, the cable was interpolated with a spline curve, i.e., a series of polynomials. Possible

movements of the cable within the duct was set to zero in order to make the cable definition consistent with the FE model. By setting the tangent of the cable to zero at the nodes of maximum eccentricity in the span and over the supports, Node 1, 5 and 8 in Figure 4.2 becomes local extrema. At the ends of the beam, the duct should be straight to reduce the amount of friction during the tensioning of the cable. To achieve this in the model the cable was defined as linear between Node 1 and 2. The tangents are defined according to the spline methods presented by SOFiSTiK AG (n.d.-a) and presented for each node in Table 4.2.

Table 4.2: Spline type in each cable node along the span. "$*$" refers to a spline with zero-valued tangent, "/" to a spline without any tangent constraints and "#" to linear interpolation. (SOFiSTiK AG, n.d.-a)

Node	1	2	3	4	5	6	7	8
Spline type	#	/	/	/	$*$	/	/	$*$

In order to reduce the number of DOFs, the x-position of Node 3, 4, 6 and 7 was set to be dependent on the location of maximum eccentricity, Node 5, see Figure 4.2. By defining the intermediate nodes at relative distances from Node 5, the cable definition will be relatively consistent between different beams with different lengths. Node 2 was set at a distance of 1.0 m from the end and used to regulate the cable inclination at the anchoring point since the cable there is defined to be straight.

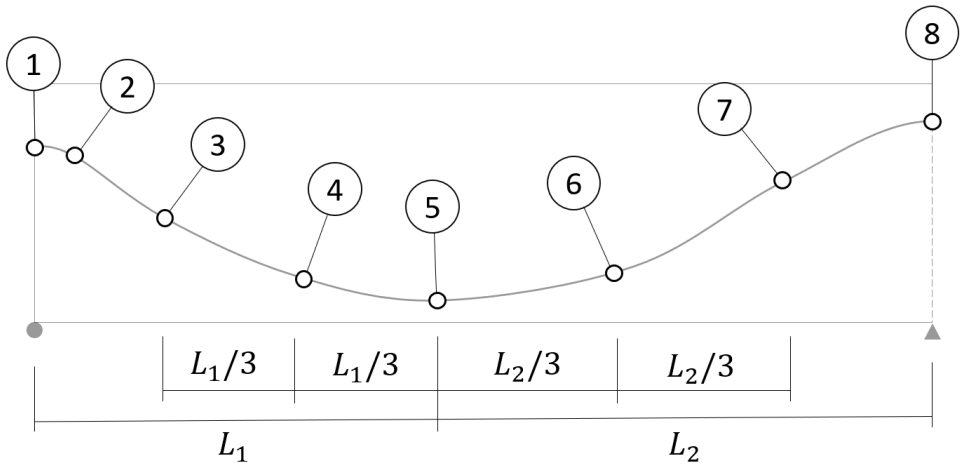

Figure 4.2: Distances for Node 3, 4, 6 and 7 in relation to the node of maximum eccentricity, Node 5.

Node 8 over mid-support is placed as close to the edge as allowed by the cover thickness. This is in order to maximize the effect of the prestressing cable since the moment in this section will be the most critical. This is also beneficial since the system can be described with one less DOF. With symmetry over the mid-support, the cable placement can be defined using only eight DOFs, see Figure 4.3.

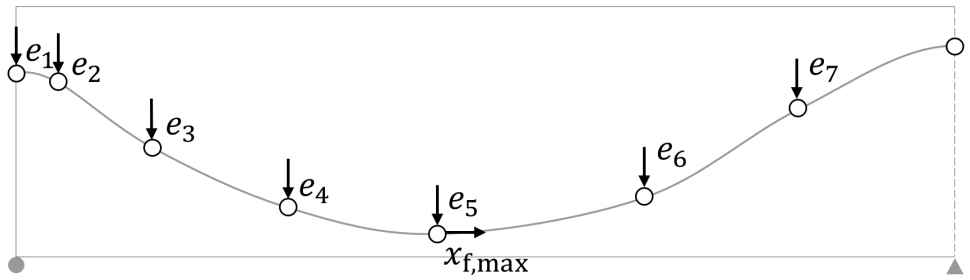

Figure 4.3: Numbering of degrees of freedom for the prestressing cable.

The position of Node 1 was also restricted due to the space required for anchorage. It was assumed that the anchors would be placed in two rows and that Node 1 will represent the average position of the two rows. The space required at the top and bottom of the beam, $c_{1p,\text{Node 1}}$ could then be calculated with (4.6). The center and edge distances, d_{center} and d_{edge}, were based on the product page from DYWIDAG (n.d.).

$$c_{1p,\text{Node 1}} = \frac{d_{\text{center}}}{2} + d_{\text{edge}} \tag{4.6}$$

The intermediate nodes (Node 3-4 and 6-7) were added to the cable in order to provide more flexibility in the cable placement. The use of both one and two intermediate nodes on each side of the maximum field eccentricity was considered when establishing the definition of the cable layout. A schematic illustration of the flexibility in cable eccentricity between two fix nodes is shown in Figure 4.4. By using two intermediate nodes instead of one, the region of maximum field eccentricity can either be expanded or contracted. In both cases, there is, however, a risk that the cable may overshoot the intended point of maximum field eccentricity, resulting in a cable layout with higher maximum eccentricity than intended. Consequently, the point of maximum field eccentricity will not necessarily coincide with Node 5 for neither the cable nor the duct. Thus, the cable geometry will not be fully consistent between the cable definition and the FE model. More specifically, overshooting can be problematic if a larger region of high eccentricity is desired as it can lead to the geometric requirements not being fulfilled. By using two intermediate nodes, the problem cannot be fully solved but rather avoided for a wider set of layouts. Hence, the use of two intermediate nodes were chosen instead of one.

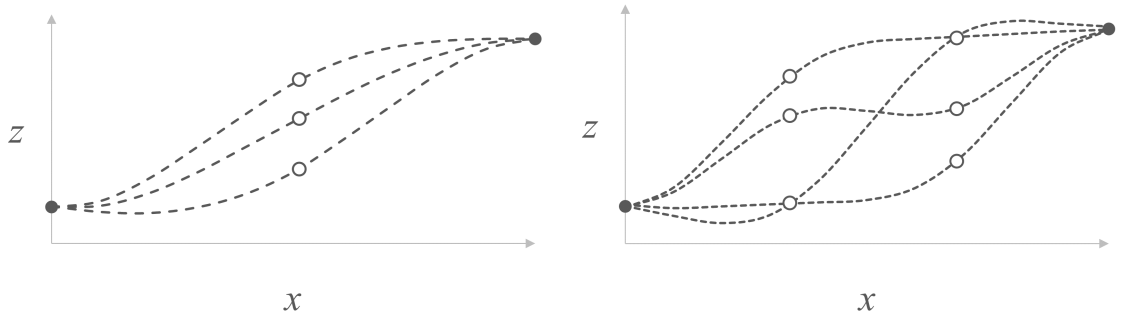

(a) One intermediate node **(b)** Two intermediate nodes

Figure 4.4: Example illustrating the flexibility in cable placement when using (a) One and (b) Two intermediate nodes, evenly distributed along the x-axis.

4.3 Material Properties

For prestressed concrete structures, higher strength concrete is commonly used in order to compensate for higher material stresses and to reduce the prestressing loss from creep (Gilbert et al., 2017). According to Gilbert et al. (2017), the characteristic strength in design of prestressed bridges usually ranges between 40-65 MPa. However, in order to decrease cost, streamline the construction process, and account for the available selection provided by suppliers, lower strengths are in practice often preferred, e.g., C40/50 (C. Jonsson & V. Andersson, personal communication, March 3, 2022; Gilbert et al., 2017). Hence, C40/50 was chosen for this study. For reference, see Table 4.3 for the material properties.

Table 4.3: Predefined material properties for concrete class C40/50 computed in SOFiSTiK based on Eurocode 2 (SOFiSTiK AG., 2020b)

Material properties	**Magnitude**	**Unit**
Compressive strength, f_{ck}	40.00	MPa
Mean strength, f_{cm}	48.00	MPa
Tensile strength, f_{ctk}	2.46	MPa
Density, ρ	25.0	kN/m^3
Young's modulus, E_{cm}	35,220	MPa
Poisson's ratio, ν	0.2	-

Regular reinforcement steel, e.g., K500C-T, cannot be used for prestressing and higher strength steel is therefore used instead. In accordance with Section 2.2, the prestressing force needs to be large in order to accommodate for the large prestressing losses that will occur. A common choice of prestressing steel, Y1860 from DYWIDAG (n.d.) or similar, was chosen for the analysis (C. Jonsson, personal communication, March 3, 2022). The corresponding properties were computed in SOFiSTiK and are presented in Table 4.4.

Table 4.4: Predefined material properties for steel grade Y1860 computed in SOFiSTiK based on Eurocode 2 (SOFiSTiK AG., 2020b)

Material properties	Magnitude	Unit
Yield strength, $f_{\mathrm{p0.1k}}$	1,600	MPa
Ultimate strength, f_{puk}	1,860	MPa
Density, ρ	78.5	kN/m^3
Young's modulus, E_{p}	195,000	MPa
Poisson's ratio, ν	0.3	-

4.4 Loads

The loads and actions implemented in the FE-model were the ones specified in Section 3.2.2, namely the loads from self-weight of the beam, pavement, and rails, prestressing force as well as traffic loads. Furthermore, the actions of creep and shrinkage of the concrete, relaxation and friction losses in the prestressing steel together with curvature from internal temperature differences were added to the model.

4.4.1 Self-Weight

The self-weight of the beam, pavement, and rails were added to the model as line loads since the model consists of beam elements (see Section 4.5), making the transverse distribution of the vertical loads irrelevant for this study. The self-weight from the beam is calculated in SOFiSTiK by the use of the cross-section area and the weight of the material that was set to 25 kN/m^3. The load from the pavement is calculated separately. By assuming a thickness of 0.1 m, a deck width of 8 m, and a weight of 24 kN/m^3, the line load was calculated to 19.2 kN/m. This load was then implemented into the SOFiSTiK model. The loads from the two rails were set to 1 kN/m and could be added to the model directly.

4.4.2 Prestressing Force

The prestressing force was added to the model trough the use of *Prestressing System* in SOFiSTiK (SOFiSTiK AG, n.d.-d). In the system, the number of strands per cable, area per strand and strand diameter were defined. The latter two parameters were set to 193.6 mm^2 and 15.7 mm, respectively. The program also computes the maximum permissible force in the cables with respect to (3.22) and applies it as the prestressing force. Consequently, the requirement in (3.22) was always automatically fulfilled and was thereby not verified. The losses from friction and anchorage slip were also computed and applied within the system. As stated in Section 3.2.2, anchorage losses were not accounted for in this study and the slip at the anchor was therefore set to zero. The friction coefficient, μ, and the factor for unintended inclination, k, have each been set to 0.19 and 0.005, respectively, in accordance with Eurocode 2 (SIS, 2008). To make the model more physically accurate for prestressed bridges, the implemented cables were divided equally into two different groups, each having both an active and a passive end. Consequently, half of the cables was

assumed to be tensioned from the left and the other half from the right side. For a model with an odd number of cables, the group of cables tensioned from the left was assumed to include one more cable than the group tensioned from the right. When defining the load cases, both cable groups where implemented into the same load case to ease the load combination.

4.4.3 Traffic Load

The traffic loads were added to the model through the SOFiSTiK module *Traffic Loader* (SOFiSTiK AG, n.d.-g). For the analysis, the full deck width b was, as a simplification, set as the loaded area. The deck was then partitioned into notional lanes by the module in accordance with Eurocode 2 (SOFiSTiK AG, n.d.-g), see Figure 4.5. For a 8 m wide deck, two notional lanes were then defined. Load trains where then added to the module. Two load trains were added, one for each lane, with the loads taken from Eurocode 2, see Table 3.2 in Section 3.2.2.2 (SOFiSTiK AG, n.d.-g). The module also takes the adjustment factors from the Swedish Transport Agency (2018) into account, see Table 3.3. Two load groups were then defined in the module, one containing the axle loads and the other containing the uniformly distributed loads. Consequently, the relevant load coefficients could be placed on each group in the final load combinations. For the axle load, a dynamic amplification factor of 1.25 was included, see Section 3.2.2.2. The loads were subsequently iteratively repositioned in the span to generate the maximum and minimum values for the following quantities:

- Normal force
- Shear force
- Bending moment
- Deflection along the x-axis
- Deflection along the z-axis

4.4.4 Thermal Actions

The thermal actions were defined as two load cases, one for heating and the other for cooling of the top side. The temperature differences were set to 15°C and 8°C for heating and cooling, respectively, as described in Section 3.2.2. These temperature differences were then applied to all the beam elements in the model.

4.4.5 Creep, Shrinkage and Relaxation

The long term effects in the model were handled by the SOFiSTiK program *Construction Stage Manager* (CSM) (SOFiSTiK AG., 2020d). First, the different construction stages were defined (see Table 4.5) where each stage corresponds to an added action. The long term effects were computed in Stage 35 and 45 whereas the others corresponds to actions related to load application or addition of self-weight. In the two final stages, the long term effects of creep, shrinkage, and relaxation were

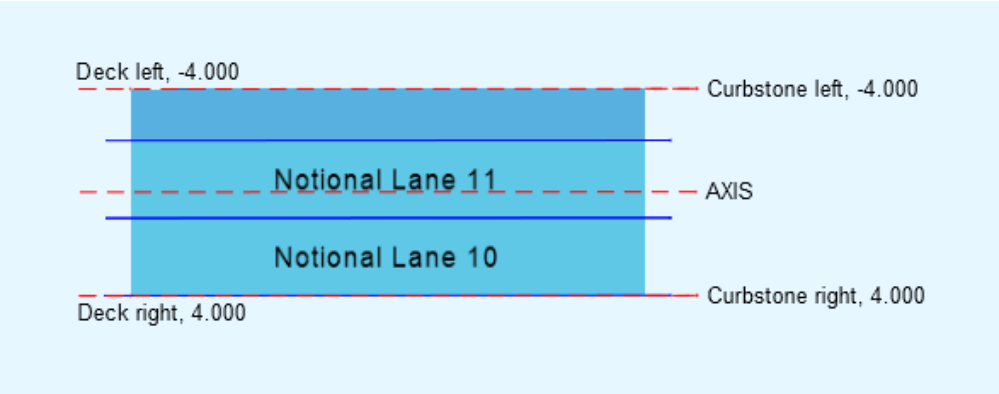

(a) Right-aligned

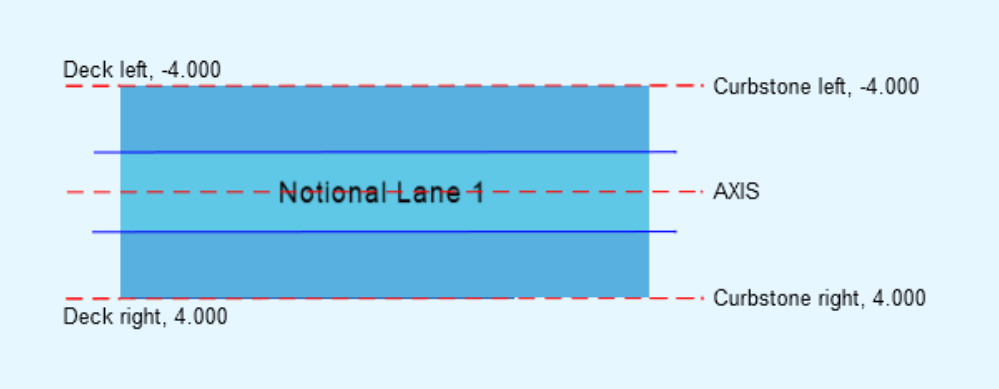

(b) Center-aligned

Figure 4.5: Notional lanes for (a) Right- and (b) Center-aligned configurations from SOFiSTiK based on Eurocode.

considered. The time of Stage 35 was set to 28 days as this is the time it takes for the concrete to develop the strength defined in Eurocode 2 and, thus, it is appropriate to add the traffic load in this stage (Al-Emrani et al., 2013). Stage 45 was given a time of 44,000 days corresponding to service life class L100, see Section 3.2. Due to its length, Stage 45 was divided into three creep steps to more accurately estimate the long term effects. For both Stage 35 and 45, it was assumed that the relative humidity would be at 80% (Engström, 2015). The temperature for Stage 35 and 45 was set to 10°C as is common practice.

Table 4.5: Defined construction stages in *Construction Stage Manager*.

Stage	Action	Duration [days]	Creep Steps
20	Self-weight Beam		
21	Prestressing and grouting		
23	Pavement		
24	Railing		
35	Time effects until service	28	1
45	Long term effects	44,000	3

4.4.6 Superimposition

The loads and actions were then superimposed according to the combinations stated in Section 3.2.3. This was done with the SOFiSTiK program *Maxima*. The program is further explained in the manual provided by SOFiSTiK AG (n.d.-b). *Maxima* multiplies the loads with the relevant factors for the different load combinations and combines the loads and actions in order to maximize and minimize different results, e.g. bending, normal force, shear force, or deflections. The combinations that yield the maximum and minimum results are then saved as different load cases for that specific load combination. During the combinations some loads are set as permanent, i.e., the self-weight, prestressing force and time-dependent actions, and are present in all combinations. Even though the thermal actions are variable, they are also present in all combinations although cooling and heating cannot occur simultaneously. For this project, seven different load combinations were necessary in order to verify the requirements in Section 3.2.4. The load combinations and corresponding verifications are presented in Table 4.6.

Table 4.6: Load combinations and corresponding construction stages and verifications.

State	Stage	Load combination	Verifications
Construction	21	Quasi-permanent	(3.23)
	24	Quasi-permanent	(3.23), (3.24)
Service	35	Quasi-permanent	(3.24)
		Frequent	(3.27), (3.30)
		Characteristic	(3.28), (3.29)
	45	Quasi-permanent	(3.26)
		Frequent	(3.27), (3.30)
		Characteristic	(3.28), (3.29)

4.5 Element Types

There are multiple ways of modelling T-beams. Depending on the level of accuracy needed in the analysis, geometry of the element, and the response of interest, different element types are more suitable (Rombach, 2011). When studying T-beams with thin slabs and webs, shell elements may be a relevant choice. Rombach (2011) also suggests that a combination of shell elements and beam elements is an alternative. Since the focus in the study lies on optimizing the cable layout, which in turn is related to the flexural bending action, the beam was chosen to be represented solely by beam elements.

When defining the tendons with the *Tendon Geometry Standard* component, the prestressed elements can be chosen to either be quadrilateral or beam elements (SOFiSTiK AG, n.d.-f). Since the concrete elements were already modelled as beam elements, the same choice was made for the prestressing steel.

4.6 Boundary Conditions

The boundary conditions for the model have been selected in order to represent the global response of the beam when subjected to flexural bending actions. The system was therefore interpreted as a two-dimensional system. Roller supports were placed at each end and a pin connection at the mid-support. Note that this is consistent with the use of beam elements subjected to in-plane action. Since the mentioned boundary conditions only describes the constraints within xz-plane, see Figure 4.6, additional constraints were also added in order to make the model representation valid in a three-dimensional space. The beam will therefore also be fixed at mid-support in both translation along the y-axis, and rotation around the x- and z-axes.

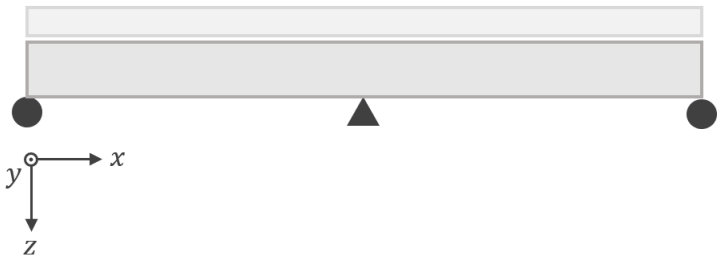

Figure 4.6: Boundary conditions in the beam model.

4.7 Mesh and Convergence Analysis

Each span was divided into structural lines between Node 1-8 to ensure that the cable eccentricities in these nodes will be transferred to the model correctly. Each structural line was then divided evenly into beam elements where a maximum element size dictated the number of elements. In order to find a sufficient maximum element size for the model, a convergence analysis was performed. The mesh convergence was performed with element sizes ranging from 4 to 0.5 m. Both internal

forces and deflections were included in the convergence analysis and the model for the analysis was implemented using the input parameters presented in Table 4.7. For reference, see Figure 4.7. The cable layout was chosen with the load balancing method described in Section 5.2. For the solver, the default option in SOFiSTiK, *Direct Sparse*, was used throughout the study (SOFiSTiK AG., 2020c).

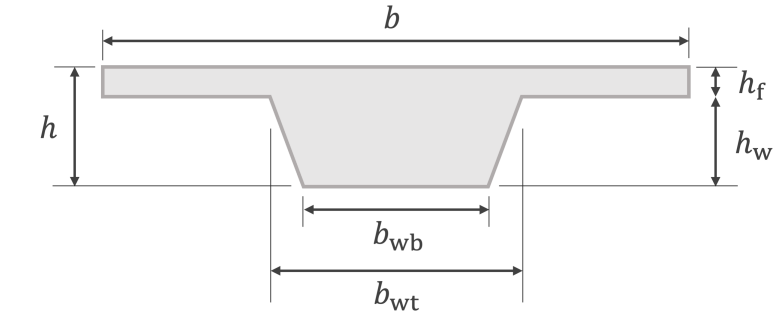

(a) Cross-section view

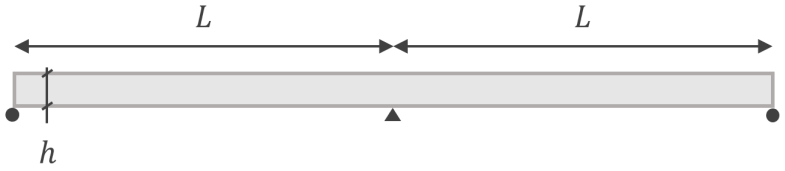

(b) Longitudinal view

Figure 4.7: Geometry and notation from (a) Cross-section view and (b) Longitudinal view of the beam model.

Table 4.7: Input data for the model used in the convergence study and the analytical verification.

Parameter	**Magnitude**	**Unit**
Length, L	30	m
Top web width, b_{wt}	2,990	mm
Bottom web width, b_{wt}	1,990	mm
No. of cables, n	10	-
No. of strands per cable, n_{strands}	19	-

The results from the convergence study is presented in Figure 4.8-4.9 for both deflection and internal forces. For two of the series, the magnitudes together with corresponding number of elements are presented in Table 4.8. As can be seen, even the coarser meshes have relatively small deviations from the converged results, never exceeding 1.4% deviation for any of the tested quantities or load cases. Due to larger deviations for the coarsest mesh size of 4 m in the analytical verification, a mesh size

of 2 m was chosen instead. As time-consumption is a crucial factor in optimization problems, an even finer mesh size was not considered.

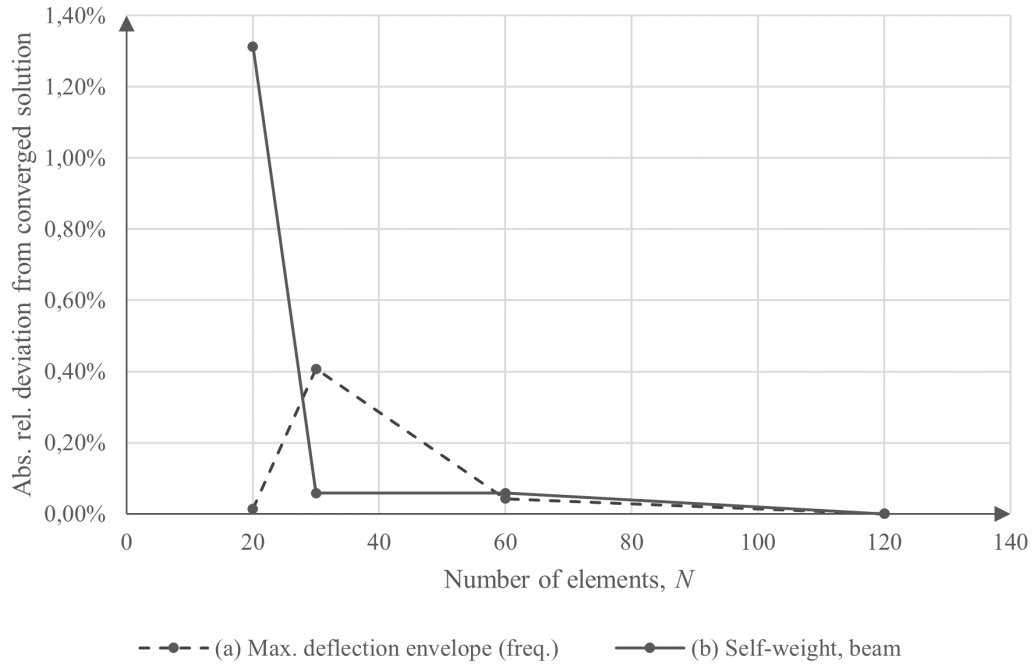

Figure 4.8: Convergence analysis of deflections for (a) Maximum deflection envelope under frequent loading and (b) Self-weight of the beam.

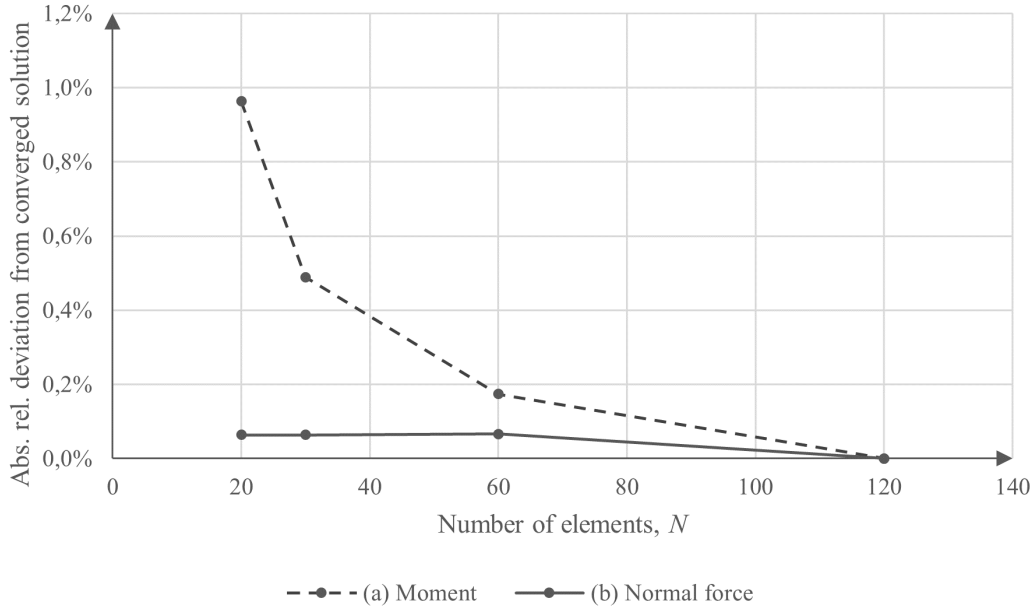

Figure 4.9: Convergence analysis of internal forces at the mid-support for (a) Maximum moment in the maximum moment envelope under characteristic loading and (b) Normal force when subjected to pure prestressing.

Table 4.8: Results for tested element sizes and corresponding number of elements for two cases, (a) Deflection for maximum deflection envelope under frequent loading and (b) Support moment for maximum negative moment envelope under characteristic loading.

Elem. size [m]	**No. of elem.**	**(a) Deflection,** w **[mm]**	**(b) Moment,** $M_{y,\mathbf{s}}$ **[kNm]**
4.0	20	21.142	-12,551
2.0	30	21.053	-12,611
1.0	60	21.130	-12,651
0.5	120	21.139	-12,673

4.8 Analytical Verification

The FE model was verified by performing analytical calculations for a conventional beam and then comparing it to the results of the finite element analysis. The calculations were performed using Mathcad Prime, version 7.0.0.0 (PTC Inc., 2022) for the same model as was used for the convergence study. For the FE model, a mesh size of 2 m was used as the 4 m mesh from the convergence analysis was judged to be too course in the verification. The main theory of the approach used is described in Section 3.3 and the verification was performed for short term behavior for all individual actions in the model except the traffic load, i.e., self-weight, thermal effects and prestressing. In addition, the characteristic load combination was also studied. Since neglecting the traffic load also resulted in the thermal loading being the only variable load, no reduction factors were used in the combination. The prestressing force, however, have both an upper and a lower characteristic value given by (3.9)-(3.10) whereby the lower value was chosen. As a simplification, the friction losses and creep effects until service have both been neglected in the analytical and the FE model for the verification.

The script used for the verification is presented in Appendix A.1 for the characteristic load combination and the moments corresponding to each individual load case is presented in Table 4.9. Both the fundamental and restraint-induced contributions are presented in Appendix A.2. In Table 4.9, a comparison between the moments under previously described loads can be seen. The FE model correlated well with the analytical results with a maximum difference of around 2% and can thereby be considered valid based on the verification.

Table 4.9: Comparison of the short term support moment between the analytical and the FE model.

Actions	**Analytical [kNm]**	**FE Model [kNm]**	**Difference [%]**
Self-weight, $g_{\mathrm{d}} = 25$ kN/m	-17,426	-17,240	-1.07
Thermal loading, $\Delta T = -8°\mathrm{C}$	-2,977	-2,914	-2.12
Prestressing, $P_{0\mathrm{m}}$	15,522	15,356	-1.07
Characteristic combination, $\gamma_{\mathrm{p}} = 0.9$	-6,406	-6,386	-0.31

4.9 Post-Processing

To be able to perform verifications presented in Section 3.2.4 and 4.4.6, the stresses in the beam had to be calculated. This was done with a Python script. The internal moment and normal force for the relevant load cases were exported from SOFiSTiK together with the cross-section area, moment of inertia and neutral axis for bending. Using Navier's formula for stresses presented in (4.7), the concrete stress at the top and bottom of the beam could be calculated and verified.

$$\sigma = \frac{N}{A} + \frac{M_y \cdot z}{I_y} \tag{4.7}$$

To verify that the concrete around the duct remains in compression, as is required by (3.27), the stresses were linearly interpolated between the top and bottom of the beam, see Figure 4.10. This could be done as it was assumed that the beam would be uncracked and thus remain in Stage I. The stresses in the cables were computed in SOFiSTiK with the program *AQB* and then exported for verification (SOFiSTiK AG., 2020a).

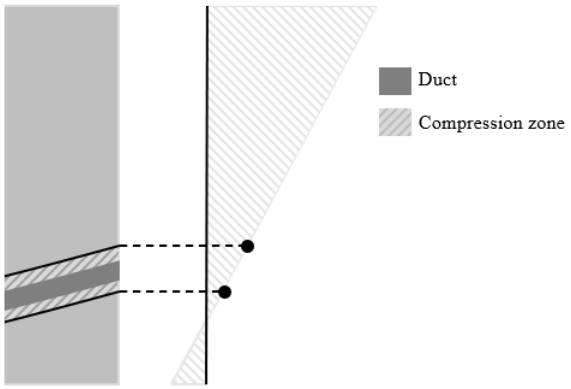

Figure 4.10: Linear interpolation of the stresses in the concrete in order to determine if the area around the duct is in compression

5

Optimization

The cable layout optimization was performed using the genetic algorithm (GA) solver in the built-in plugin *Galapagos* in Grasshopper 3D, version 1.0.0007 (Robert McNeel & Associates, n.d.-a). The tool allows systems with many input variables to be optimized by exploring a diverse set of solutions and then converges through a process based on the theory of evolution.

Although the tool is very powerful, it has its limitations. Firstly, the user must formulate a clear objective that the solution can converge towards which can be difficult if the problem contains multiple constraints or sub-objectives. In GAs, the main objectives are represented by fitness functions. Another problem is that convergence may be hard to achieve in a short time, limiting the possibilities in problems where each solution has a significant computation time. The implementation of the algorithm in this study has, as a result of time-constraints, required some techniques to be tested and implemented.

Due to the large number of variables in the problem, the domain of each variable have been reduced in order to avoid an excessive runtime. This has partly been achieved by limiting the cable placement in the bridge to remove trivially ineffective solutions but also by subdividing the optimization process into two steps. In the first step, the number of cables and strands in the bridge were optimized for a conventional cable layout, and the in second, the cable layout with respect to additional parameters describing the cable layout was optimized. Using the results from the first step, the domain could be reduced for the second step. The optimization procedure is shown in Figure 5.1 where the first subprocess have been denoted Process 1, and the second, Process 2.

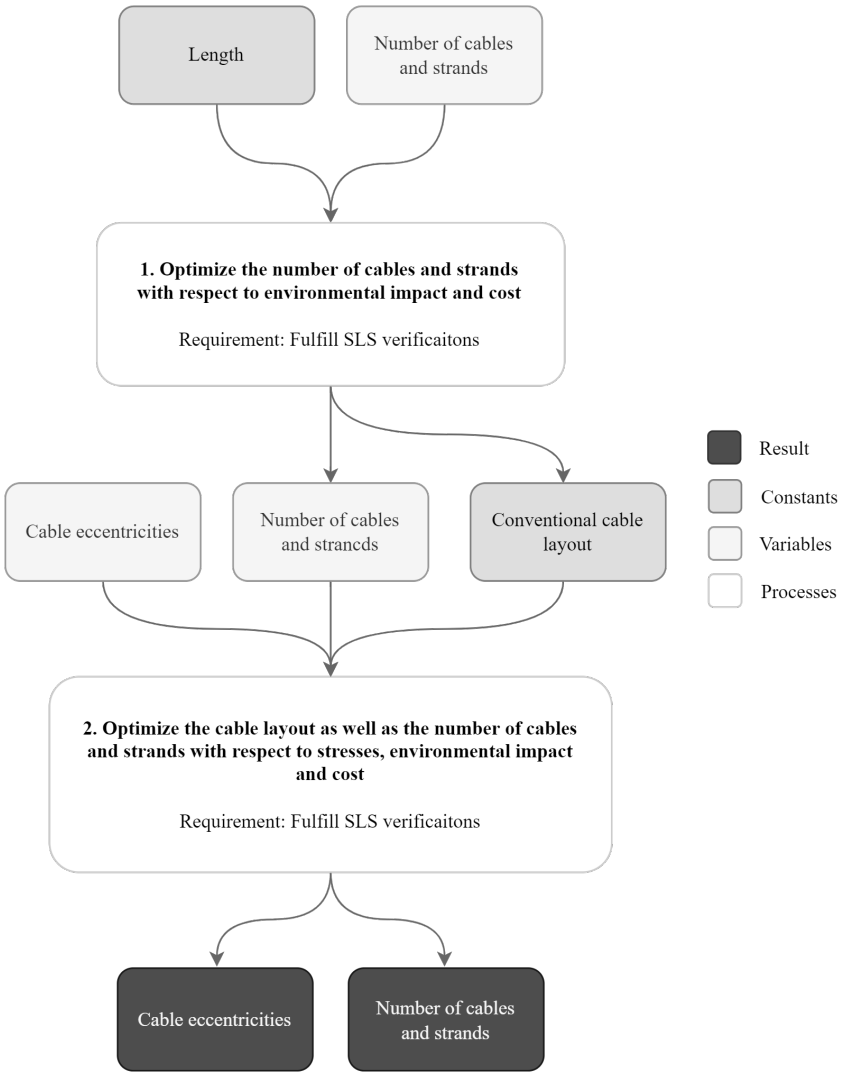

Figure 5.1: Flowchart of the optimization process. Process 1 represents the optimization of the number of cables and strands while Process 2 represents the optimization of the cable layout as well as further optimization of the number of cables and strands.

5.1 Parametrization

To generate the SOFiSTiK model used in Chapter 4, the process shown in the flowchart in Appendix B was used. As means of communication between the Grashopper model and the SOFiSTiK program, a SOFiSTiK plugin for Grasshopper was installed (SOFiSTiK AG, n.d.-c). The plugin adds components into Grasshopper to generate cross-section geometries, structural elements, boundary conditions, as well as, to convert these into text files for SOFiSTiK to run. In addition, it also contains a component that can run FE analyses, allowing the optimization process to be fully automatic. By complementing the Grasshopper model with additional

scripts created within the text editor inside the SOFiSTiK Structural Desktop environment, a complete model containing instructions for load combinations, analysis settings and exportation of results could be created.

The model was parameterized as explained in Section 4.2 to achieve relative scalability with respect to beam length and to allow for optimization. Since the optimization is implemented in Galapagos using sliders, the same elements have been used in Figure 5.2 to represent the parametrization. For the optimization, four types of parameters are studied, the eccentricities in Node 1-7, the location of maximum eccentricity and the number of prestressing cables as well as strands. For each optimization, the beam length have been fixed, making it a constant within this context. The cable eccentricity at Node 8, i.e., the support eccentricity, is however not fixed but instead depends on the number of strands which is related to the duct size that, in turn, is governing for the cover spacing.

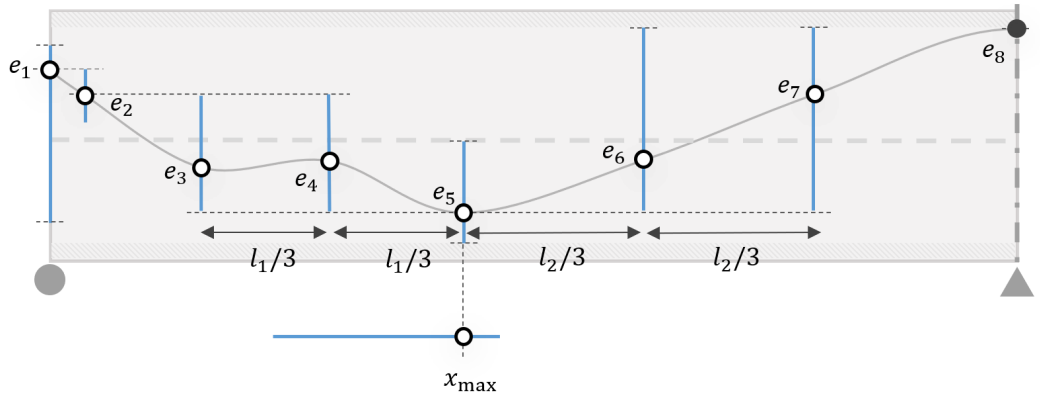

Figure 5.2: Schematic illustration of the slider definitions in Grasshopper for eccentricities and location of maximum eccentricity, their relations, and their constraints.

Another important objective of the parametrization was to eliminate trivially unfit and unfeasible solutions. This was achieved by reducing the domain of each variable without any excessive compromises on flexibility, see Figure 5.2. To make the sliders scalable with the cross-section, all sliders have been set to range between 0 and 1. In order to achieve a relatively consistent accuracy throughout the model, different sliders have also been given different precisions. Whereas the eccentricities for Node 6-7 are limited by the cover thickness and eccentricity of Node 5, the eccentricity for Node 1-5 is much more limited. The eccentricities for Node 1 and 3-5 are, generally speaking, close to being twice as constrained in movement as Node 6-7. As a consequence, the former has been given an accuracy of 0.02 while the latter has been given an accuracy of 0.01. As for Node 2, its primary function is to describe the inclination and its accuracy have therefore been set to 0.1 with a maximum inclination of 5%. Concerning the location of maximum eccentricity, an accuracy of 0.01 has been chosen to represent a wide array of cable layouts although it still corresponds to the largest physical step size of all sliders. All variables, constants and dependent variables together with corresponding ranges are presented in

Table 5.1-5.2 for each process.

Table 5.1: Variables, constants and independent variables in Process 1.

Variable type	Parameter	Notation	Range	Step size
Free	No. of cables	n	7-20	1
	No. of strands	n_{strands}	5-27	*
Dependent	Beam length	L	25-40 m	
	Location of max. ecc.	$x_{\max}$		
	Eccentricities	e_1-e_8		
		e_8		

* Following the available cables from DYWIDAG (DYWIDAG-Systems International, n.d.).

Table 5.2: Variables, constants and independent variables in Process 2.

Variable type	Parameter	Notation	Range	Step size
Free	Eccentricities	e_1, e_3-e_5	0-1	0.02
		e_2	0-1	0.1
		e_6-e_7	0-1	0.01
	No. of cables	n	± 3*	1
	No. of strands	n_{strands}	± 2*	1
	Location of max. ecc.	$x_{\max}$	0.30 L-0.50 L	0.01
Dependent	Beam length	L	25-40 m	
	Support ecc.	e_8		

* The range is based on the results from Process 1. When the range exceeds the upper or lower limit, the range is shifted in order to keep the number of possible cable and strand configurations the same.

5.2 Preliminary Optimization

The purpose of the preliminary optimization was to reduce the domain for the final optimization by finding the relevant range for the number of cables and strands for the specific span length. Furthermore, the preliminary optimization will act as a benchmark by providing cost and environmental impact for the fitness function used in the final optimization. The cable layout will also be included in the first generation for the final optimization in order to initiate the process with a verified and valid design. This initiation was used with the intention to decrease the convergence time.

The cable layout used in the preliminary optimization was based on the load balancing method. When designing with load balancing, the cable is placed in the beam in such way that the primary moment from the cables balances the moment generated by a chosen load case (Dolan & Hamilton, 2019). For this study, the frequent load combination was chosen as the load case to be balanced. Both the upper and lower bound moments were calculated and the mean moment was balanced. For simplicity, the axle loads from the traffic load as well as the temperature loads were

disregarded. Furthermore, no long term effects were considered. By assuming a constant prestressing force P_i, it was possible to determine a reasonable eccentricity of the cable from the moment distribution with (5.1). An example of this design is shown in Figure 5.3 where the correlation between the moment distribution to be balanced and the cable placement is apparent.

$$e(x) = \frac{M(x)}{P_\mathrm{i}} \tag{5.1}$$

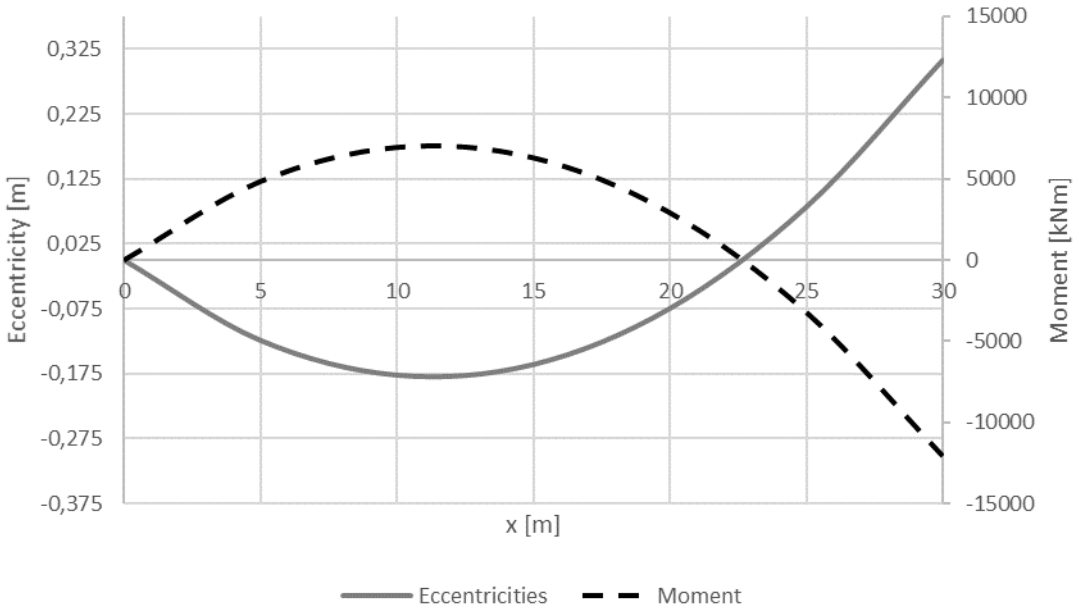

Figure 5.3: Example of a cable layout designed with load balancing together with its corresponding moment distribution

By manually optimizing the number of cables and strands for the conventional solutions for different span lengths, reference values for the cost and the environmental impact could be derived. The expressions and the relations are shown in Figure 5.4.

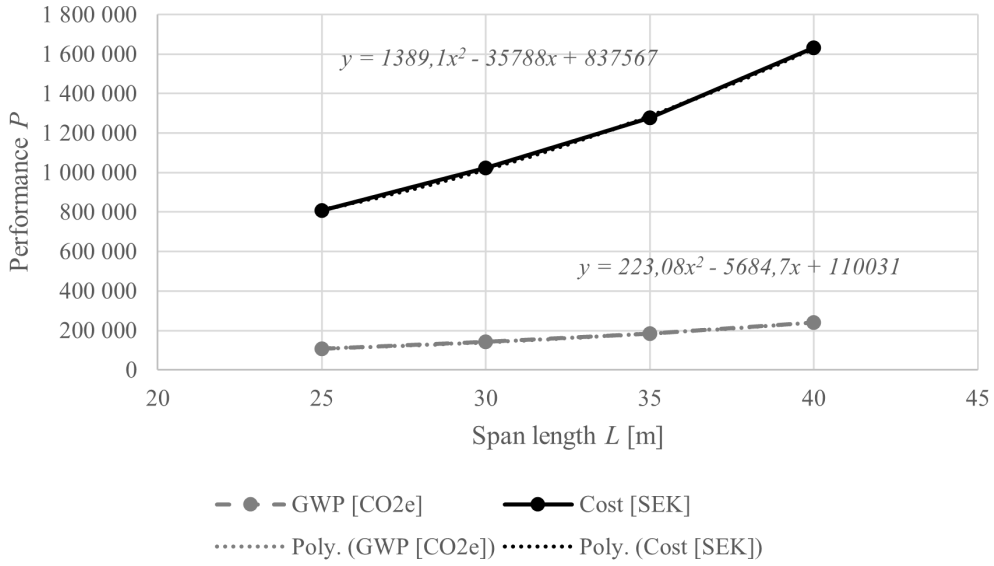

Figure 5.4: Reference performances in cost and GWP in relation to the bridge span.

The cost and environmental impact of the bridge, P_{cost} and P_{GWP}, were based on the thesis work of Aspegren & Möörk (2021), see Table 5.3. Consistent with the data presented in their research, the environmental impact has been measured by its global warming potentional (GWP). From their data, the expressions in (5.2)-(5.3) for cost and GWP was derived as functions of the span length L and the cross-sectional area A together with the number of prestressing cables n and strands n_{strands}.

$$\begin{aligned} P_{\text{cost}} = {} & (6,500\,\text{SEK} + (30\,\text{SEK/m} \cdot n_{\text{strands}} + 75\,\text{SEK/m}) \cdot 2L) \cdot n \\ & + 1,800\,\text{SEK/m}^3 \cdot 2L\,A \end{aligned} \tag{5.2}$$

$$P_{\text{GWP}} = (388\,\text{CO}_2\,\text{e/m}^3 \cdot A + 8,580\,\text{CO}_2\,\text{e/m}^3 \cdot A_{\text{p}}) \cdot 2L \tag{5.3}$$

Table 5.3: Material costs and GWPs for the concrete and the prestressing steel, based on data from Aspegren and Möörk (2021).

Material	**Component**	**Cost**		**GWP** $[\mathbf{CO_2\,e/m^3}]$
Concrete		1,800	SEK/m^3	388
Prestressing steel	Strands			
	• Material	30	SEK/m	8,580
	• Labor	75	SEK/m	
	Anchors	6,500	SEK	

5.3 Final Optimization

The aim of the final optimization was to find values for e_1-e_7 and $x_{\max}$ that minimizes the environmental impact and cost, and enhances the bridge's performance with respect to the requirements presented in Table 4.6 in Section 4.4.6. The number of cables and strands were also subject to optimization but only within a reduced range, see Table 5.2. This stage was conducted with the use of the evolutionary optimization tool *Galapagos* which contains two types of generic solvers, genetic algorithm and simulated annealing (SA). For this project the GA solver was chosen because of its ability to find better solutions faster than SA and since the fitness function was deemed smooth enough that the increased exploration capabilities of SA were not needed (Rutten, 2013).

5.3.1 Genetic Algorithms

GAs are population-based solvers that search for the solution through evaluation of the populations fitness (Mirjalili, 2019). The first step is to define the phase space for the population. The phase space is the domain that contains all possible solutions and its dimension is equal to the number of variables in the problem (Rutten, 2013). GAs begin by randomly assigning genes (values) to each chromosome (solution) in the population within the defined phase space. Each chromosome is then evaluated based on a fitness (objective) function that should either be minimized or maximized. The result from the fitness function decides how likely it is that the chromosome gets selected for generating the next population. This type of weighted selection of chromosomes, where not only the most fit population can be selected, is beneficial to reduce the risk of the solution converging to a local solution (Mirjalili, 2019). Once the chromosomes have been selected, new child chromosomes for the next generation are created by combining the genes of two parent chromosomes from the selection. This is called crossover and the most common types are single- and double-point, see Figure 5.5 for examples (Mirjalili, 2019). In Galapagos, single-point crossover is used (Rutten, 2010b).

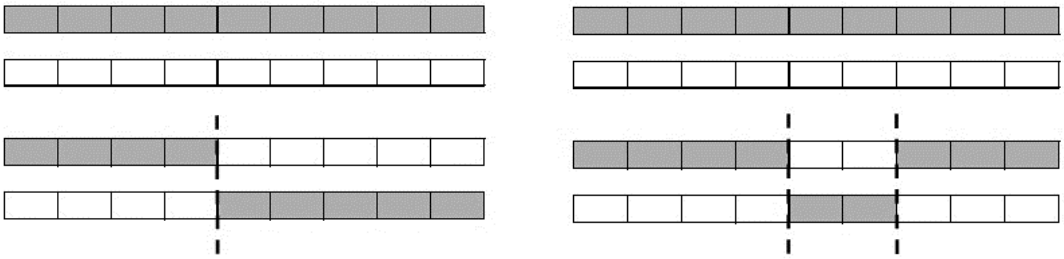

(a) Single-point crossover **(b)** Double-point crossover

Figure 5.5: Schematic illustration of (a) Single- and (b) Double-point crossover for generating new chromosomes, based on (Mirjalili, 2019)

The last step in creating a new population is to include some form of gene mutation where a set of genes are altered randomly in the chromosomes. This is done to increase the diversity of the population and, again, to avoid local solutions (Mirjalili, 2019). However, the mutation should not be excessive as it can lead to the algorithm becoming a random search function and losing the advantages a GA have (Mirjalili, 2019).

5.3.2 Fitness Function

To measure the quality of a specific solution, a fitness function that reflect the goal of the optimization is used. Since the goal of this study was to find a cable layout that is more efficient than a conventional solution, the fitness function was designed to reduce the environmental impact and the cost of the bridge. In addition, the function also aimed at improving the performance with regards to the requirements from Table 4.6. To reflect the aim of reducing the aforementioned quantities, the fitness function was designed to be minimized. As it also is important that the optimal design fulfills all the requirements, the problem can more generally be described as a multi-objective optimization with several constraints.

Although there exist no optimum way of measuring the fitness of a solution for multi-objective optimization, some guidelines have been presented in various research. Amouzgar (2012) describes that multi-objective optimization commonly is reduced to single-objective optimization in research. In order to reduce a multi-objective into a single-objective optimization problem, the expression in (5.4) is, among others, a common choice (Marler & Arora, 2004). The expression describes the global fitness $F(\mathbf{x})$ as a weighted exponential sum of the fitnesses for each individual objective $f_j(\mathbf{x})$ with the weights w_j for each objective j up to m. A common simplification of the expression can be achieved by setting the exponent p to 1 (Marler & Arora, 2004).

$$F(\mathbf{x}) = \sum_{j=1}^{m} W_i \left[f_j(\mathbf{x})\right]^p \tag{5.4}$$

When several constraints are of interest, a simple method is to deconstruct the fitness function into two terms, one unpenalized function corresponding to the overall fitness of the design without any regards to the constraints and another containing the penalty for not satisfying the constraint (Smith & Coit, 1996). The fitness $F(\mathbf{x})$ can then be expressed as in (5.5) where $F_0(\mathbf{x})$ and $F_\mathrm{p}(\mathbf{x})$ are the unpenalized fitness and the penalty contributions.

$$F(\mathbf{x}) = F_0(\mathbf{x}) + F_\mathrm{p}(\mathbf{x}) \tag{5.5}$$

Smith and Coit (1996) presents a few penalty functions and describes the use of a *distance-based static penalty function*, expressed in (5.6), as both being a simple and relatively effective choice. The term *static* refers to the penalty being constant throughout the optimization process. Here, d_i and C_i represents the distance to the feasible region and the weight for corresponding constraint i whereas the exponent κ commonly is set to either 1 or 2. In this study, it was decided to set κ to 1. The number of constraints are here denoted n and the coefficient δ_i was either set to 0 or 1 depending on if the solution $\mathbf{x}$ lies within the feasible domain or not. Following the recommendations from Bäck et al. (2000), the penalty should neither be to severe nor to lenient. Whereas as a stricter penalty may favor the convergence rate at the cost of the solution quality, a weaker penalty may cause the algorithm to extensively explore infeasible solutions (Bäck et al., 2000).

$$F_\mathrm{p}(\mathbf{x}) = \sum_{i=1}^{n} C_i \, \delta_i \, d_i^{\kappa} \tag{5.6}$$

The fitness function for this study is presented in (5.7) and is primarily weighted in terms of performance in production and material cost, P_cost, and environmental impact, P_GWP. The function was also weighted with respect to the material stresses, σ_j, in relation to corresponding limits, $\sigma_{j,\max}$ as well as the deflection and the decompression limits that both were implemented in a similar manner. The fitness function also includes distance based static penalties for the performance with respect to requirements in material stresses, deflection and decompression. The distance, d_i, was computed with (5.8) and the weighting coefficient, C_i was set to 20 for all requirements. In order to properly scale each performance in relation to the other, reference values for performance in cost and environmental impact were derived, denoted $\overline{P}_\mathrm{cost}$ and $\overline{P}_\mathrm{GWP}$. These were taken for the conventional solution and are presented as a function of the bridge length in Figure 5.4. The cost and environmental impact each have a weight of 40% of the fitness value while the rest of the requirements only account for 20%. The choice of equal weights for environmental impact and cost was done in order to remain neutral towards both objectives and stay within the scope of the study. By not only optimizing towards minimizing the environmental impact and cost, reduced material stresses may be beneficial for the convergence. By incrementally improving the solution reductions in steel could be encouraged. The parameters chosen for the fitness function are presented in Table 5.4 for each sub-objective.

$$F(\mathbf{x}) = 0.4 \left[\frac{P_{\text{GWP}}}{\overline{P}_{\text{GWP}}} + \frac{P_{\text{cost}}}{\overline{P}_{\text{cost}}} \right] + \frac{0.2}{n-1} \left[\sum_{j=1}^{n-2} \frac{\sigma_j}{\sigma_{j,\max}} + \frac{w}{w_{\max}} \right] + \sum_{i=1}^{n} 20\, \delta_i\, d_i \tag{5.7}$$

$$d_i = \begin{cases} \dfrac{\sigma_j}{\sigma_{j,\max}} - 1 & \text{for stresses} \\ \dfrac{w}{w_{\max}} - 1 & \text{for deflection} \\ 1 & \text{for decompression} \end{cases} \tag{5.8}$$

Table 5.4: Parameters for the fitness function for each individual objective and their constraints.

Objective, j	$f_0(\mathbf{x})$	C_i	W_i
GWP	$\dfrac{P_{\text{GWP}}}{\overline{P}_{GWP}}$	-	0.4
Cost	$\dfrac{P_{\text{cost}}}{\overline{P}_{cost}}$	-	0.4
Stresses, σ_j	$\dfrac{\sigma_j}{\sigma_{j,\max}}$	20	$\dfrac{0.2}{n-1}$
Deflection	$\dfrac{w}{w_{\max}}$	20	$\dfrac{0.2}{n-1}$
Decompression	$\begin{cases} 1 & \text{if true} \\ 0 & \text{else} \end{cases}$	20	0

5.3.3 Optimization Settings

Due to the great number of variables in the optimization process, improving the performance was deemed of high importance for the analysis. Each solution in Galapagos may take between 70-120 sec., stressing the need for decreasing the number of analyzed solutions as much as possible. In Galapagos, there are several input parameters that can be tweaked, all of which can be important to achieve fast convergence and avoid local extrema. The choice of the different parameters are presented and motivated in the following sections and a summary is compiled in Table 5.5.

Table 5.5: Parameter settings in *Galapagos*.

Optimization setting	Magnitude
Population size	25
Initial boost	4
Remaining population	10%
Inbreeding radius	75%
Maximum stagnant	7
Maximum time limit	16 hr

5.3.3.1 Population Size

Population is the measure of the number of solutions studied at a certain generation. Since the objective is to improve the overall fitness in the population over each generation, the population size is a critical parameter for the study. Whereas a larger population increases the opportunity for exploring new solutions and representing a wider range of possible solutions, the overall number of unfeasible or unfit studied solutions may increase if the parameter is not chosen carefully. A too small population may, however, result in convergence towards a less fit solution since local extrema may be hard to avoid (Mirjalili, 2019). In time-critical problems, Johansson and Evertsson (2003) found that 16-26 is the most efficient for relatively continuous fitness functions. For irregular fitness functions, however, the number may range between 9-142, stressing the need for a smooth fitness function. They also presented previous research on the topic, suggesting a population size of 60-200 where alternative implementations had been used, e.g., concerning remaining population size. The population size can thereby be assumed to be fairly case-specific. For this analysis, a population size of 25 was chosen as the fitness landscape was deemed to be relatively smooth in accordance with Johansson and Evertsson (2003).

5.3.3.2 Initial Boost

An optimization process using GAs, can according to Johansson and Evertsson (2003) intuitively be described as a two-phase process, the exploration and the exploitation phase. The first reflects an objective of exploring the fitness landscape to find where potential fit solutions may be found whereas the second refers to improving these solutions. Although no clear shift between these phases exists, a more gradual transition may be noticed. The initial boost in Galapagos is an additional set of solutions added to first generation to accelerate the exploration phase in order to more quickly reach the exploitation phase. In time-critical problems, Johansson and Evertsson (2003) found that their maximum population size of 34-143 was the most efficient as the initial population depending on, e.g., the dimensions and smoothness of the fitness function. For this problem, an initial boost of 400% was chosen, resulting in 100 solutions in the first generation.

5.3.3.3 Remaining Population

In some optimization problems, it can be of interest to retain a small set of the population into the next generation, a phenomenon known as generation gap (Johansson & Evertsson, 2003). The set is often referred to as the remaining population and serves the function of preserving fit solutions in order to allow a higher mutation rate. The result is that the population may be prevented from acting as a collective representation of the optimal solutions and instead be more diverse while still maintaining fit solutions. Bäck et al. (2000) presents research suggesting a generation gap of 90-100% as the best choice. In this study, a remaining population of 10% was selected corresponding to a generation gap of 90%.

5.3.3.4 Inbreeding

When a chromosome has been chosen to generate the next generation in Galapagos, it selects its mate based on the genomic distance between them (Rutten, 2010a). The genomic distance describes how different the two chromosomes are based on their genes. This is however only a rough representation as the exact distance cannot be accurately calculated due to the high dimension of the phase space (Rutten, 2010a). The inbreeding value in Galapagos, ranging from -100% to 100%, describes at what distance the chromosome looks for its mate with 100% being in its immediate genomic vicinity (Rutten, 2010a). An excessive inbreeding value is, however, not recommended. With a large value, the GA is at risk of being incestuous which reduces diversity quickly and increases the probability of the solution converging to a local solution (Rutten, 2010a). A too small value instead means that the chromosomes that might be striving towards different maxima gets combined. Consequently, the resulting chromosomes will not be striving towards either solution (Rutten, 2010a). For this study 75% was chosen as it is the default value and no other recommendations could be found.

5.3.3.5 Maximum Stagnant and Time Limit

Maximum stagnant defines how many generations are run without any improvements before Galapagos terminates the optimization process. For this study, this setting was deemed less relevant since it is more useful in analyses with greater number of generations. As a too small number of generations results in premature convergence while a too large number results in long runtimes, the parameter was set to seven generations corresponding to 10 hours of runtime. The optimization was given also a time limit of 16 hours due to time constraints in the study.

6

Results

6.1 Conventional Cable Layout

Results were fist studied for the conventional cable layout according to the load balancing method presented in Section 5.2. To compare the eccentricities between different span lengths, ranging from 25 to 40 m, normalized cable eccentricities were used. These were normalized with respect to span length and distance between maximum and minimum eccentricity. The normalized cable eccentricity is shown in Figure 6.1 and has its x-axis located in the neutral axis of the beam in order to more accurately represent the effect in bending. From the graph, it is clear that the shape has remained relatively unchanged between the different span lengths. It can be seen that for all span lengths except 25 m, the anchors are placed at the level of the neutral axis. This is consistent with the load balancing method as there is no moment to be balanced at the edges. For the bridge with 25 m long spans, the cable placement at the anchorage point has instead been limited by the spacing needed for the anchors as this bridge has the smallest cross-section height. From Figure C.1 in Appendix C.1, there are also indications that a longer span results in a somewhat larger field eccentricity although both the differences and the data set are very small, making it hard to draw any conclusions. For the actual eccentricities given in millimeters, see Table C.1 in Appendix C.1.

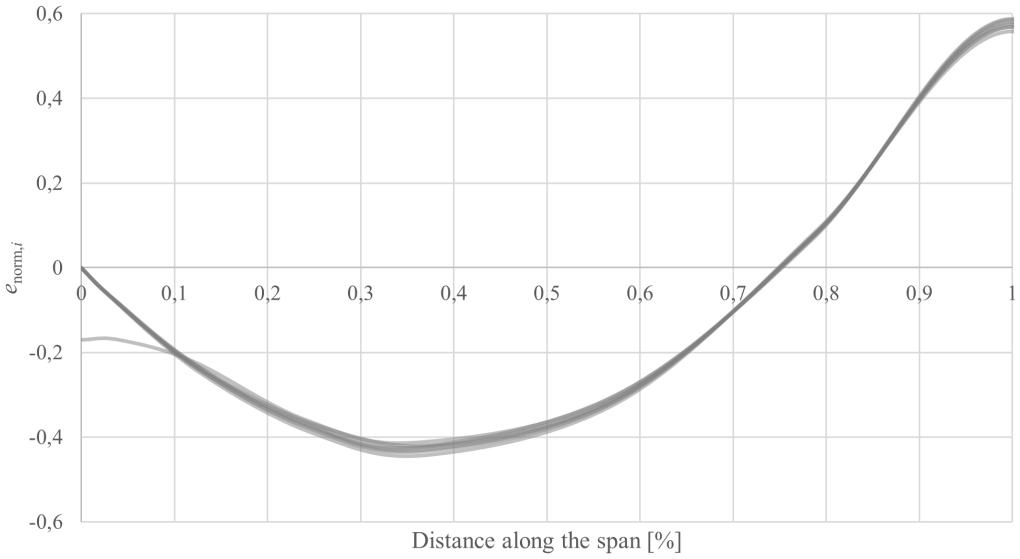

Figure 6.1: Normalized cable eccentricities for conventional layouts with respect to both span length and distance between maximum and minimum eccentricity. The data is compiled for seven different span lengths ranging from 25 to 40 m.

The cost, environmental impact and fitness for the conventional layout for the different span lengths are presented in Table 6.1. Following the definition in Section 5.3.2, a lower fitness value will represent a better solution. From the fitness values, it can be seen that the conventional layout has a similar performance across all the tested span lengths. Fitness values close to 1 was expected as 80% of the value, i.e., the cost and GWP, is based on reference values from the conventional solution. The margin of 5-8% in fitness primarily corresponds to the performance with respect to the requirements although some deviation from the interpolated reference cost and GWP also is expected. In Table 6.1, the optimum number of cables for each examined span length is also presented. It can be seen that 9 or 10 cables with 22 strands is the most common configuration for the conventional layouts with two exceptions.

Table 6.1: Cost, environmental impact and fitness values for bridges with conventional cable layouts for different span lengths.

Span length *L* [m]	**Cables**	**Strands**	**Cost** [SEK]	**GWP** [CO_2e]	**Fitness *F***
25	9	22	808,300	106,800	0.9273
28	9	22	934,200	127,300	0.9412
30	9	22	1,022,400	142,000	0.9427
33	8	27	1,180,500	166,200	0.9398
35	8	27	1,278,400	182,700	0.9432
38	10	22	1,517,700	220,500	0.9508
40	10	22	1,631,400	240,100	0.9411

6.2 Optimized Cable Layout

The optimized layouts were normalized with regards to length and maximum and minimum eccentricities in the same manner as the conventional ones and are presented in Figure 6.2. It can be seen that the shape of all the layouts are relatively similar although the variation is larger compared to the conventional layout. The variation is most prominent in the span between the point of anchoring and maximum eccentricity. In contrast to the conventional layout, Node 1 is, with one exception, always placed slightly below the neutral axis. For a more detailed graph and the actual eccentricities in millimeter, see Figure C.3 and Table C.2 in Appendix C.2.

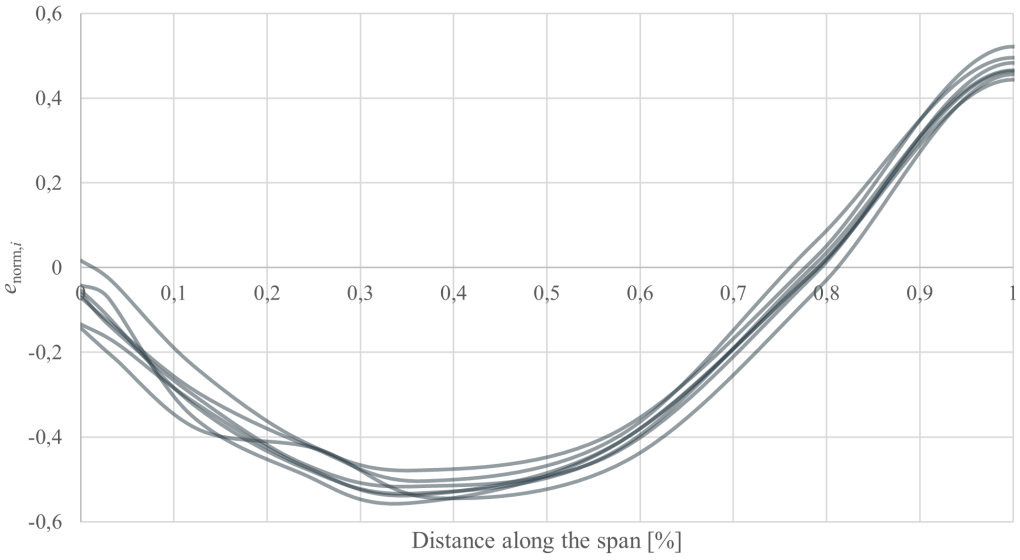

Figure 6.2: Normalized cable eccentricities for optimized layouts with respect to both span length and distance between maximum and minimum eccentricity. The data is compiled for seven different span lengths ranging from 25 to 40 m.

The cost, GWP and fitness of the optimized layout are presented in Table 6.2. It can be seen that nine cables is the most optimum number for all tested span lengths, with one exception. The total number of strands for each span has all decreased compared to the conventional layout. This is also reflected in a reduction in cost and GWP. The fitness of the optimized layouts are on average 0.90 which is a notable improvement.

Table 6.2: Cost, environmental impact and fitness values for bridges with optimized cable layouts for different span lengths.

Span length *L* [m]	**Cables**	**Strands**	**Cost** [SEK]	**GWP** [CO_2e]	**Fitness *F***
25	9	19	760,500	103,000	0.8840
28	9	19	879,400	122,800	0.8939
30	9	19	962,800	136,900	0.9024
33	9	22	1,161,100	165,300	0.9194
35	9	22	1,257,900	181,700	0.9012
38	10	19	1,428,500	212,200	0.9070
40	9	22	1,514,700	226,100	0.8767

6.3 Comparison

When comparing the eccentricities between the optimized and conventional solutions for different span lengths, the normalized cable eccentricities were analyzed and are presented in Figure 6.3 with the x-axis defined in level with the neutral axis. From the results, one can conclude that the shape is relatively similar between the optimized and conventional layouts although the former is slightly shifted downwards.

In Table 6.3, the cost, GWP, and fitness of the optimized and conventional solutions are compared and it can be seen that the optimized solution performs better in all these aspects. Whereas the average cost is reduced by 4.8%, the GWP is 3.1% lower, and the fitness value decreased by an average of 4.4%. For some span lengths, however, the optimization did not result in a significant improvement. For example, the optimized solutions for the 33 and 35 m spans only gave a 1.6% decrease in cost, virtually no change in GWP and only a small decrease of the fitness value. The cable and strand configurations are presented in Figure 6.4. As can be seen, the number of cables and strands stays relatively consistent for the different span lengths. For the optimized solution, 9 cables together with 19 or 22 strands each was the most common configuration. Table 6.4 shows the material reductions in the cross-section for the optimized solution compared to the conventional. The optimized bridges have on average 11.6% less prestressing steel. The reduction in concrete area was not as noticeable at an average of only 1.7% with exception for the bridges with 33 and 35 m long spans that even had a slight increase.

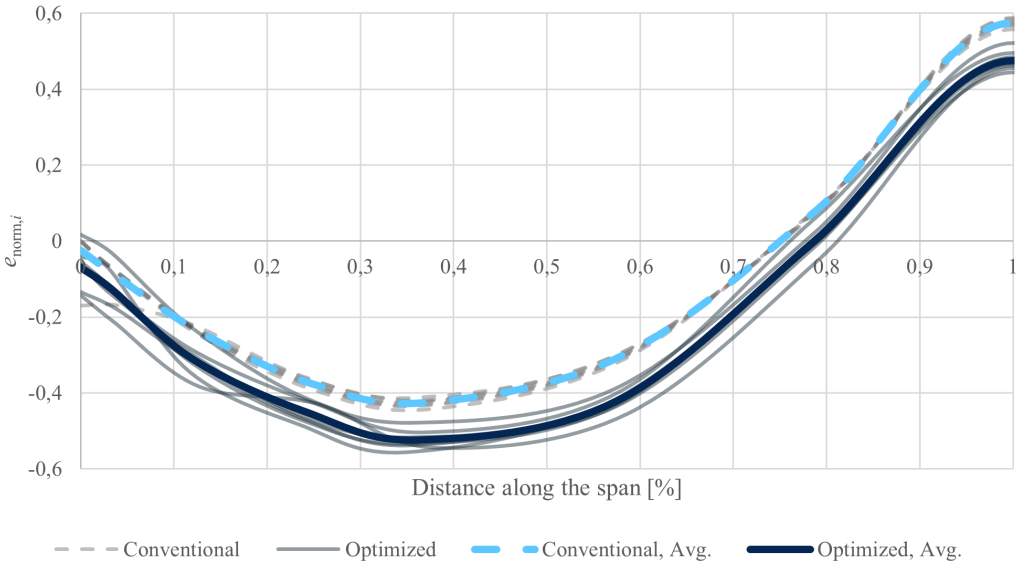

Figure 6.3: Normalized cable eccentricities for the conventional and optimized layouts with respect to both span length and distance between maximum and minimum eccentricity. The data is analyzed and compiled for seven different span lengths ranging from 25 to 40 m.

Table 6.3: Changes in cost, GWP and fitness values for the optimized compared to the conventional layout.

Span length *L* [m]	**Cost** [%]	**GWP** [%]	**Fitness *F*** [%]
25	-5.91	-3.57	-4.67
28	-5.86	-3.57	-5.02
30	-5.83	-3.57	-4.28
33	-1.64	-0.56	-2.17
35	-1.60	-0.50	-3.43
38	-5.88	-3.75	-4.60
40	-7.15	-5.83	-6.84
Avg.	**-4.84**	**-3.05**	**-4.43**

Table 6.4: Changes in material usage concerning steel and concrete in the cross-sectional area for the optimized solution.

Span length L [m]	**Steel area** [%]	**Concrete area** [%]
25	-13.6	-1.7
28	-13.6	-1.9
30	-13.6	-1.9
33	-8.3	0.7
35	-8.3	0.8
38	-13.6	-2.3
40	-10.0	-5.3
Avg.	**-11.6**	**-1.7**

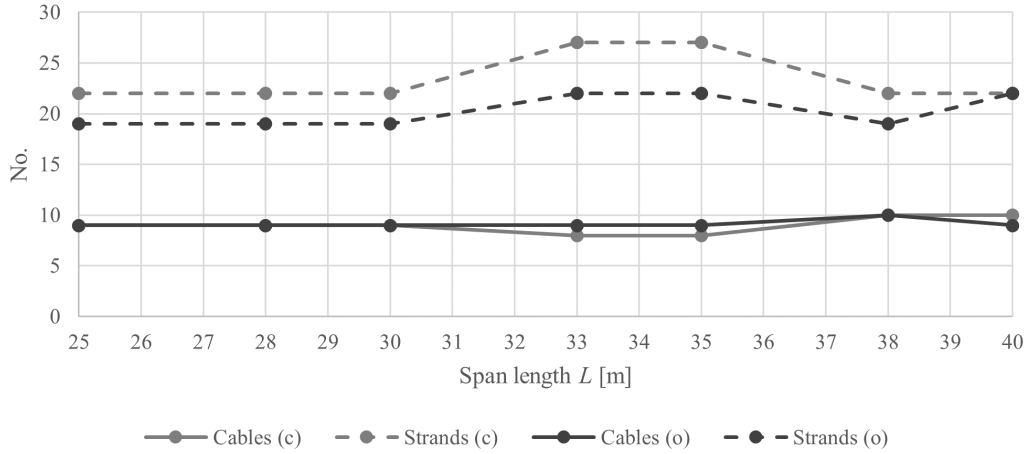

Figure 6.4: Optimum cable and strand configuration for optimized and conventional solutions.

A geometric comparison of the cable eccentricities between the optimized and conventional layouts is shown in Figure 6.5 and, from the graphs, it can be concluded that the optimized solutions tends to have more field eccentricity whereas the support eccentricity remains unchanged, consistent with the definition of Node 8. The shift in neutral axis, although not very pronounced, is a result of changes in the number of cables or strands as these are decisive for the web width. For the bridge width 25 m long spans, the cable layout was interpolated differently in Appendix C.1 compared to Figure 6.5. Whereas Figure 6.5a shows a smooth cable curvature, Figure C.2 in Appendix C.1, obtained from SOFiSTiK, shows a plateau at 3-5 m from the end-supports.

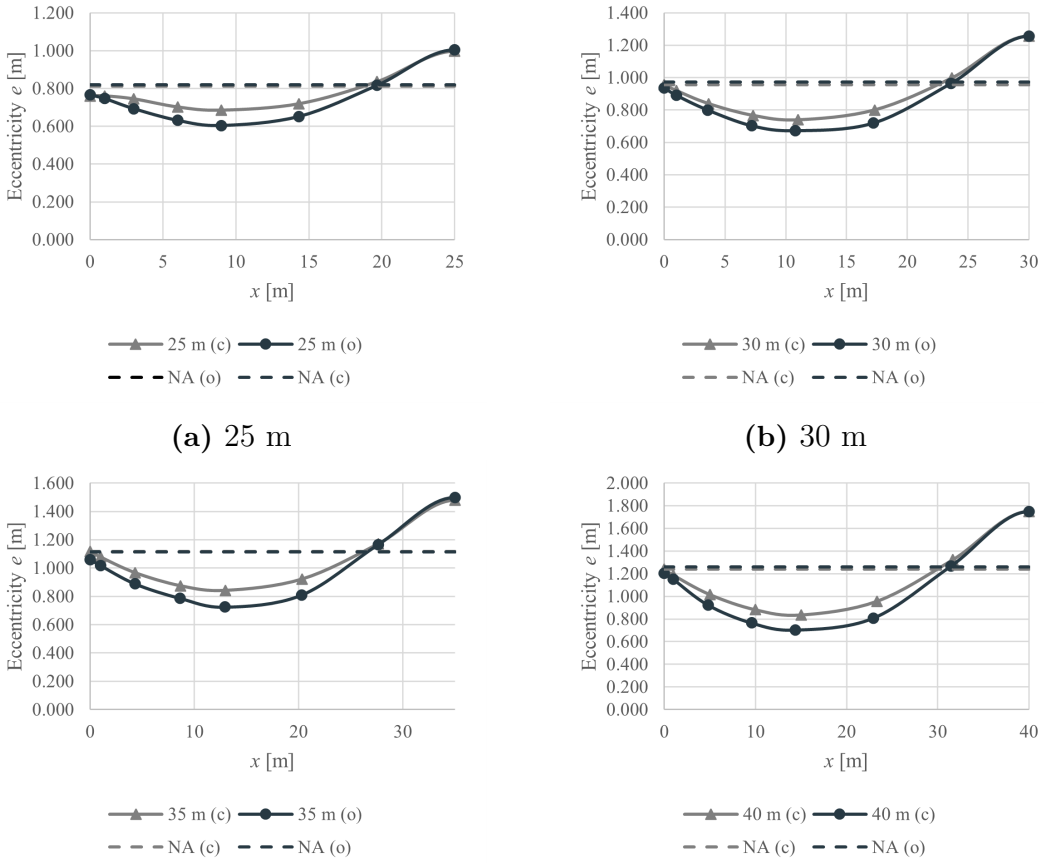

(a) 25 m **(b)** 30 m

(c) 35 m **(d)** 40 m

Figure 6.5: Cable eccentricities for (o) Optimized and (c) Conventional layout for span lengths between 25-40 m in (a)-(d).

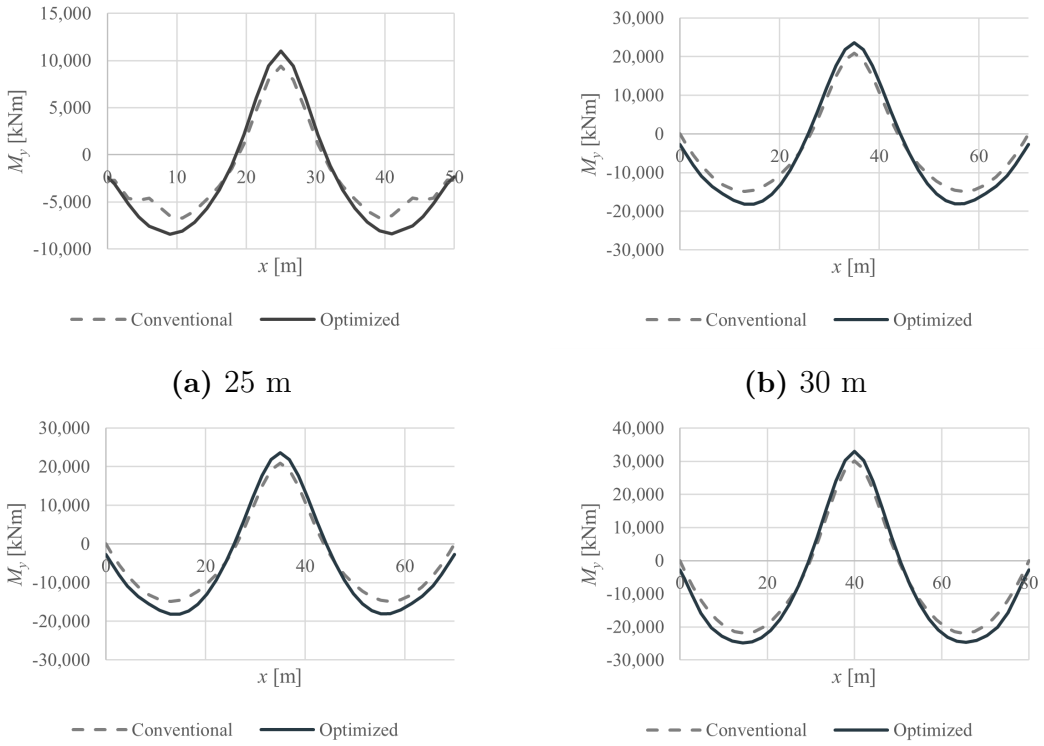

(a) 25 m **(b)** 30 m

(c) 35 m **(d)** 40 m

Figure 6.6: Prestressing moment for optimized and conventional layout for span lengths between 25-40 m in (a)-(d).

The total prestressing moment for both the conventional and optimized solutions for four selected span lengths is shown in Figure 6.6. From the figure it can be seen that the optimized cable layout produce a higher moment both in the span and over the support even though the total prestressing force has been reduced in all cases. The increased span moment can be attributed to the larger cable eccentricity, as can be seen in Figure 6.5, resulting in a larger primary moment. For reference, see Figure C.4 in Appendix C.3. Over the supports, however, the eccentricity has remained relatively unchanged as it is only dependent on the cover thickness. The increased moment instead comes from the secondary moment. Figure 6.7 shows that the optimized solution generate substantially more secondary moment. Between 18-26% of the total support moment comes from the secondary moment for the optimized layouts, compared to 1-5% for the conventional layouts. For the bridge with 25 m long spans with the conventional layout, the moment distribution in Figure 6.6a had a sharp bend. This is caused by the plateaued eccentricity of the cable in this area, see Figure C.2 from Appendix C.1.

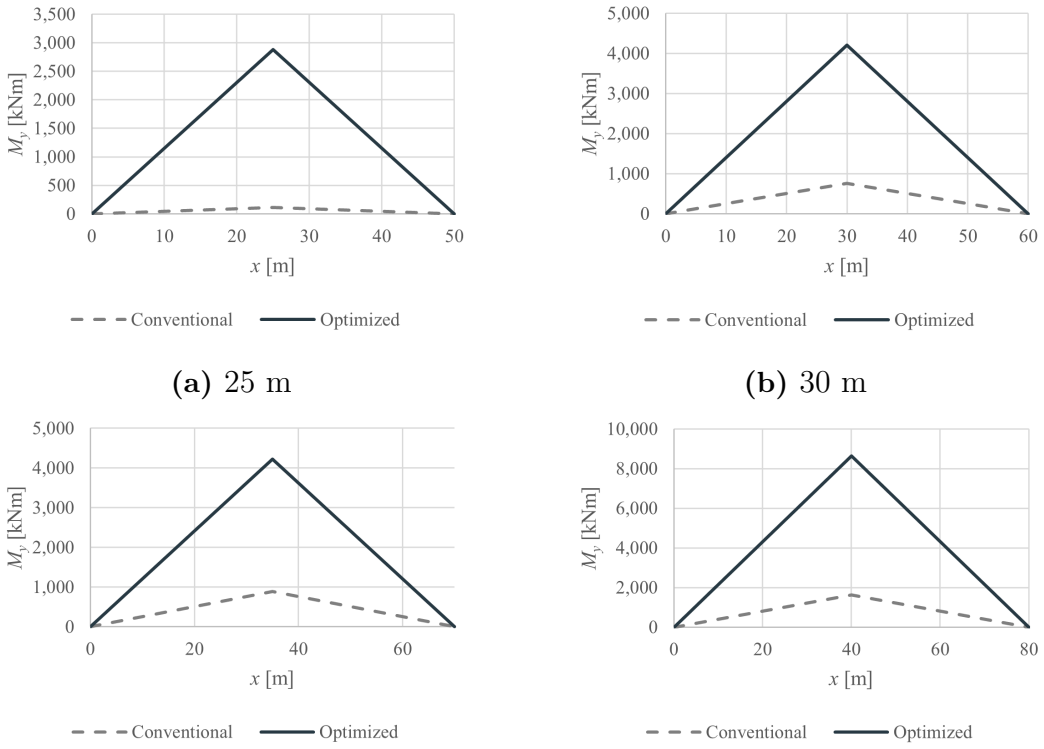

(a) 25 m **(b)** 30 m

(c) 35 m **(d)** 40 m

Figure 6.7: Secondary prestressing moment for optimized and conventional layouts for span lengths between 25-40 m in (a)-(d).

6.4 Guidelines

By averaging the contributions in the optimized cable eccentricity, a suggested cable layout for use in early design state could be compiled for the studied cross-section. In order to make the guidelines less dependent of the cross-section dimensions and span length, the normalized curves have been used to characterize the suggested layout. Hence, the suggested layout was created from the normalized node eccentricities, linearly interpolated, and presented in Figure 6.8a. From these, a linear regression was performed to more accurately analyze how dependent each eccentricity is on the span length, see Figure 6.8b. As the eccentricities in Node 1 and 2 seemed be dependent on the span length, the expressions for the trend lines are presented in (6.1)-(6.2). The other normalized eccentricities were instead found to be relatively constant and are consequently compiled into Table 6.5 as average values. For the point of maximum eccentricity, the data presented in the graph from Figure 6.9 was used to estimate where Node 5 should be placed. From the test data, the node position ranges between 35-38% of the span length. As there were no strong indications of the node placement being dependent on the length, the location of maximum eccentricity was chosen empirically as 37% although the average is 36%. The choice is further motivated in Section 6.4.1. The normalized eccentricities with reference to the neutral axis for suggested cable placement is presented in Figure 6.10 with the highlighted area representing the possible variation in eccentricity in Node

1-2.

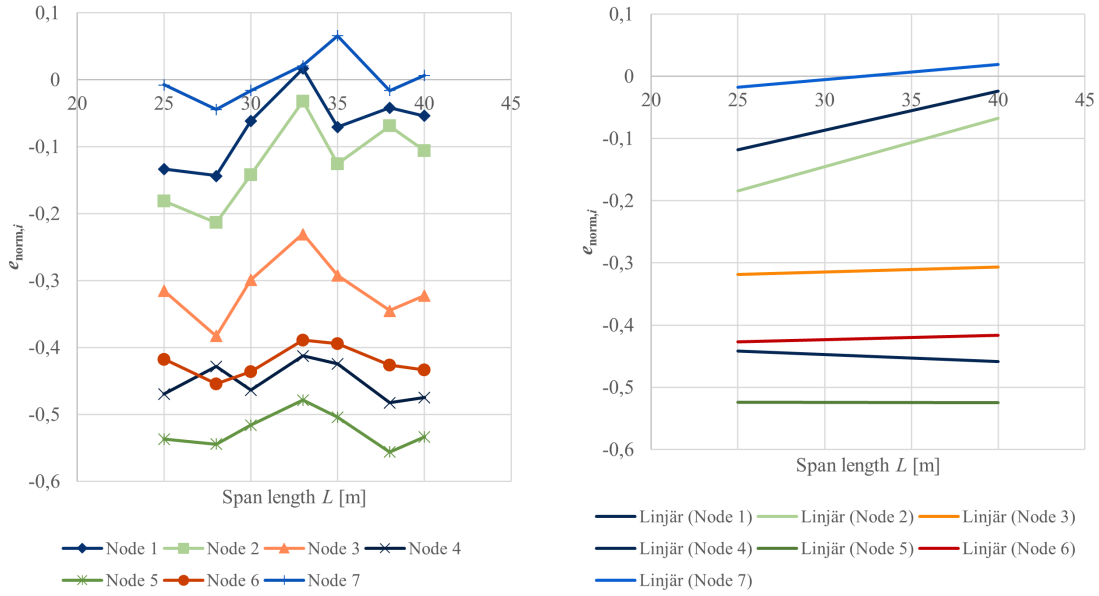

(a) Linearly interpolated **(b)** Linear regression

Figure 6.8: Node eccentricities (a) Linearly interpolated from the results and (b) Corresponding linear trend line.

$$e_{\text{norm},1} = 0.0063\,\text{m}^{-1} \cdot L - 0.275 \tag{6.1}$$

$$e_{\text{norm},2} = 0.0077\,\text{m}^{-1} \cdot L - 0.378 \tag{6.2}$$

Table 6.5: Suggested cable placement in Node 1-7 for general T-section based on the average of the normalized eccentricities $e_{\text{norm},i}$ compared to conventional layout.

Normalized ecc.	**Node**								
	1	**2**	**3**	**4**	**5**	**6**	**7**	**8**	
Layout									
• Suggested	*	**	-31.2	-45.1	-52.4	-42.1	0.1	47.6	%
• Conventional	-	-	-23.3	-37.5	-42.5	-30.2	8.4	57.5	%
Difference	-	-	-7.9	-7.6	-9.9	-11.9	-8.3	-9.9	%

* See (6.1). ** See (6.2).

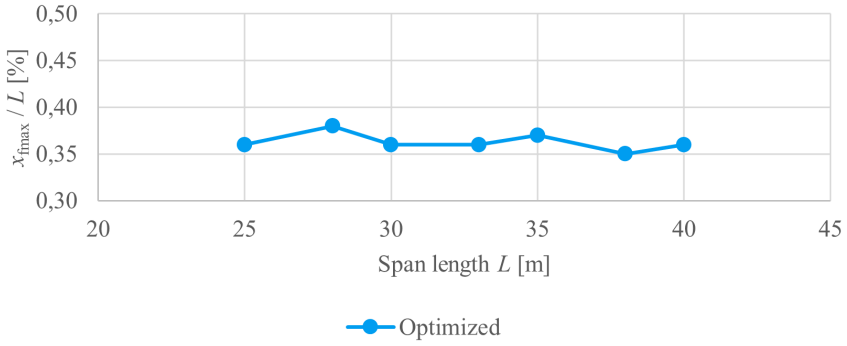

Figure 6.9: Relative position of the node with maximum eccentricity, interpolated for different span lengths for the optimized layout.

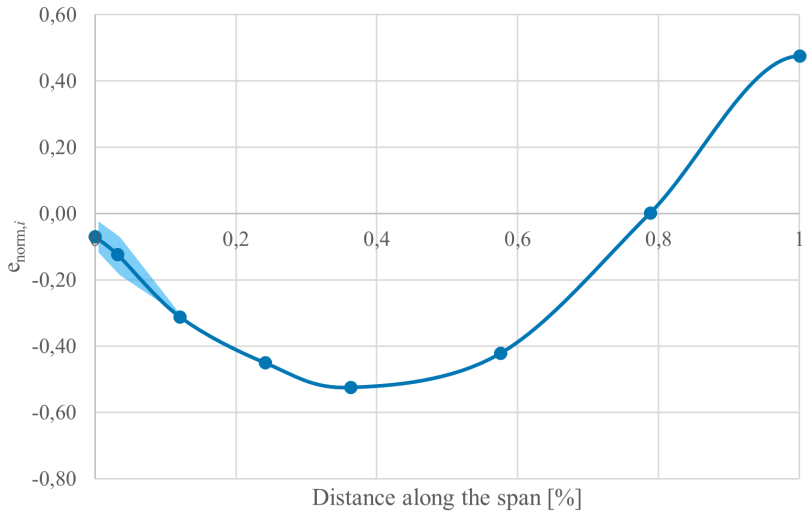

Figure 6.10: Normalized cable eccentricity for the suggested cable layout based on averages of the normalized eccentricities $e_{\text{norm},i}$ for the optimized layout.

To implement the suggested layout, the expression in (6.3) can be used where $\bar{e}_i$ describes the distance of each node from the bottom of the beam. As inputs, the position of Node 8 and the neutral axis, $\bar{e}_8$ and $\bar{z}_{\text{NA}}$, have been defined. The cable eccentricity for each node, denoted $\bar{e}_i$ for Node i, can thereby be evaluated by using the normalized eccentricities $e_{\text{norm},i}$ from Table 6.5.

$$\bar{e}_i = \frac{\bar{e}_8 - \bar{z}_{\text{NA}}}{e_{\text{norm},8}} \cdot e_{\text{norm},i} + \bar{z}_{\text{NA}} \tag{6.3}$$

6.4.1 Verification

To verify that the guidelines correspond to the results of the optimization, the guidelines were used to design cable layouts for each of the span lengths that has been optimized. The designs from the guidelines were then compared to the optimized

solutions in terms of cost, GWP, and fitness. As can be seen in Table 6.6, the guidelines perform very similarly to the optimized solutions. In the case of a span length of 33 m, the guidelines even outperformed the optimized solution by a noticeable margin. When comparing to the conventional solution, an average reduction of 6.8% in cost and 5.0% in GWP can be seen, see Table 6.7. For the material usage, a reduction of 10.6% in steel area and 4.14% in concrete volume was achieved where the latter shows a notable improvement over the optimized layouts.

Even though the position of the maximum eccentricity was found to be at 36% for the average normalized curve used to create the guidelines, it was discovered during the verification that using a value of 37% gave better results in terms of fitness values and was thus chosen as the value for the guidelines.

Table 6.6: Changes in cost, GWP and fitness values for the designs based on the guidelines compared to the optimized layout.

Span length *L* [m]	**Cost** [%]	**GWP** [%]	**Fitness *F*** [%]
25	-1.77	-1.83	-0.53
28	-1.84	-2.05	-0.62
30	-1.89	-2.19	-1.48
33	-7.15	-6.12	-4.04
35	0.00	0.00	0.90
38	-1.34	-2.08	-1.90
40	0.00	0.00	0.72
Avg.	**-2.00**	**-2.04**	**-0.99**

Table 6.7: Average changes in cost, GWP, fitness, and material usage compared to the conventional layout.

Solution	**Cost** [%]	**GWP** [%]	**Fitness *F*** [%]	**Steel Area** [%]	**Concrete Area** [%]
Optimized	-4.84	-3.05	-4.43	-11.6	-1.7
Guidelines	-6.76	-5.04	-5.39	-10.6	-4.14

6.4.2 Application on Other Sections

To further evaluate the performance of the proposed guidelines and their limitations, they were applied to two other cross-sections as well as in a case study of the road bridge Halvors länk. Following, they were then compared to the conventional layout. For the conventional layout, the load balancing method described in Section 5.2 was used.

6.4.2.1 T-section with Constant Web Width

The suggested cable placement was first applied to a T-section with a constant web width b_w as presented in Figure 6.11. The parameters defining the section are the same as the parameters presented in Section 4.1 with the exception of the web width. The web width b_w is instead constant over the height and was calculated with (6.4). The loads and actions were left unchanged from the ones presented in Section 4.4.

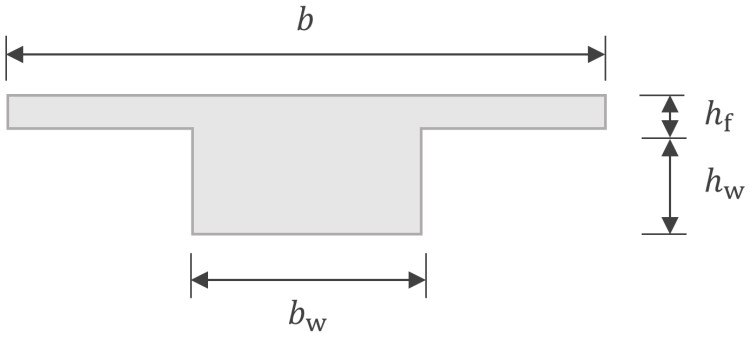

Figure 6.11: Cross-section geometry for T-section with box-shaped web.

$$b_w \geq \begin{cases} n \cdot \phi_{duct} + (n-1) \cdot a_s + 2 \cdot c_1 \\ 2\,\text{m} \end{cases} \tag{6.4}$$

The comparison between the proposed guidelines and the load balancing method, with regard to cost, GWP, and fitness, are shown in Table 6.8. It can be seen that the design based on the guidelines on average outperform the conventional solution with the cost reduced by 6.3% and the fitness value by 3.9%. The average GWP is however not improved notably. In terms of material, using the guidelines reduced the steel area by 19% and increased the concrete area by 1.8%. This is however skewed by the result for the bridge with 40 m long span length where the guidelines performed significantly worse in cost and GWP but still had a 26% reduction in steel area. When excluding this result, the average reduction in steel area was instead 17%.

Table 6.8: Changes in cost, GWP, fitness, and material usage for the designs based on the guidelines compared to the conventional layout.

Span length *L* [m]	**Cost** [%]	**GWP** [%]	**Fitness *F*** [%]	**Steel area** [%]	**Concrete area** [%]
25	-11.3	-6.38	-7.02	-18.2	-4.03
30	-7.23	-2.99	-5.09	-18.5	0.00
35	-9.17	-4.02	-6.18	-14.1	-2.27
40	2.61	7.74	2.72	-25.9	13.6
Avg.	**-6.28**	**-1.42**	**-3.89**	**-19.2**	**1.83**

6.4.2.2 T-section with Extended Deck Slab

Another variant of the T-section can be generated by retaining the same general shape of the cross-section but setting the slab width to 10 m instead, see Figure 6.12. Apart from the possibility of adding a third notional lane, resulting in additional traffic load, the structure is also subjected to additional self-weight from both the concrete and the pavement. For the asphalt pavement, a line load of 24 kN/m was used. The parameters for defining the carriageway are presented in Table 6.9 while the notional lanes are shown in Figure 6.13.

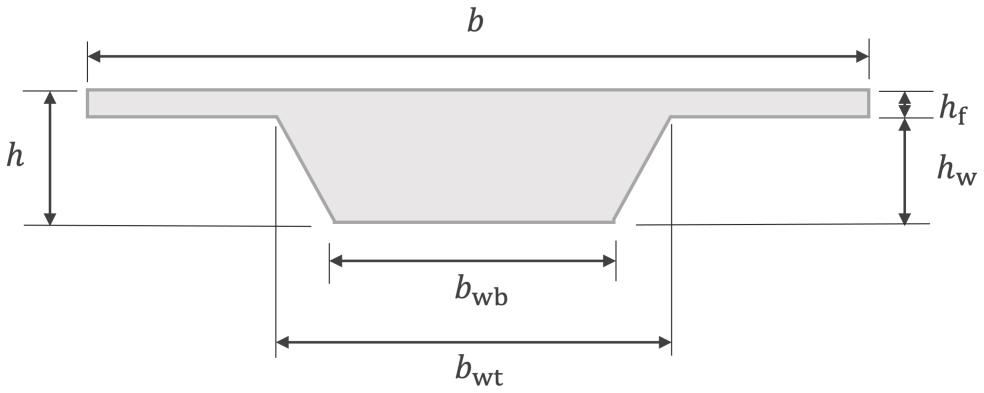

Figure 6.12: Cross-section geometry for T-section with tapered web and extended slab.

Table 6.9: Carriageway geometry for T-section with wider deck slab.

Object	Position [m]
Left deck end	-4.5
Left curbstone	-4.5
Right curbstone	4.5
Right deck end	4.5

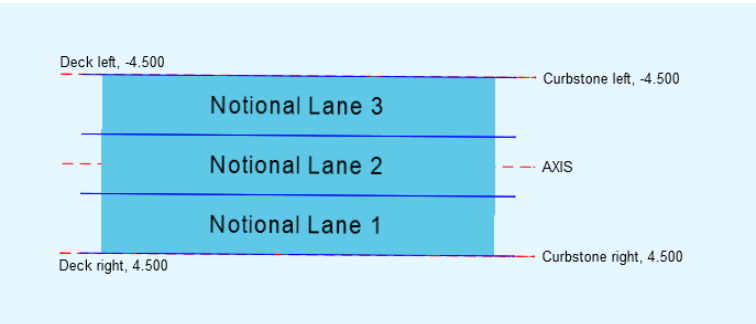

Figure 6.13: Center-aligned notional lanes for bridge with extended slab from SOFiSTiK based on Eurocode.

Compared to the section with constant web width, the guidelines did not give any significant improvements when compared to the conventional load balancing method for the section with the extended slab, see Table 6.10. Both the cost and GWP were on average reduced by less than 1% while the fitness value was 1.4% lower for the guidelines compared to the conventional solution. Whereas the steel area could be reduced with almost 7%, the concrete area was marginally increased similar to the bridge with a constant web.

Table 6.10: Changes in cost, GWP, fitness, and material usage for the designs based on the guidelines compared to the conventional layout.

Span length *L* [m]	**Cost** [%]	**GWP** [%]	**Fitness *F*** [%]	**Steel Area** [%]	**Concrete Area** [%]
25	0.13	0.12	-0.90	-9.52	1.50
30	0.00	0.00	-1.69	0.00	0.00
35	-1.60	-0.68	-1.25	-8.33	0.30
40	-2.24	-1.01	-1.76	-9.47	0.06
Avg.	**-0.93**	**-0.39**	**-1.40**	**-6.83**	**0.47**

6.4.2.3 Case Study of Halvors Länk

Finally, the guidelines were also evaluated in a case study of the road bridge, Halvors länk. An illustration of the geometry is shown in Figure 6.14 and the dimensions are presented in Table 6.11. The bridge is slightly curved as can be seen in Figure 6.15. Due to the curvature, the bridge deck has a horizontal inclination of 4.0%.

Similar to the other section with an extended slab, the road bridge also have a redefined geometry for the notional lanes as presented in Table 6.12 and Figure 6.16. The area of each strand has also been reduced from 193 to 150 mm^2 to be consistent with the actual bridge. In contrast to the other bridges in this study, the bridge has been designed as completely prestressed, meaning no tensile stresses were allowed.

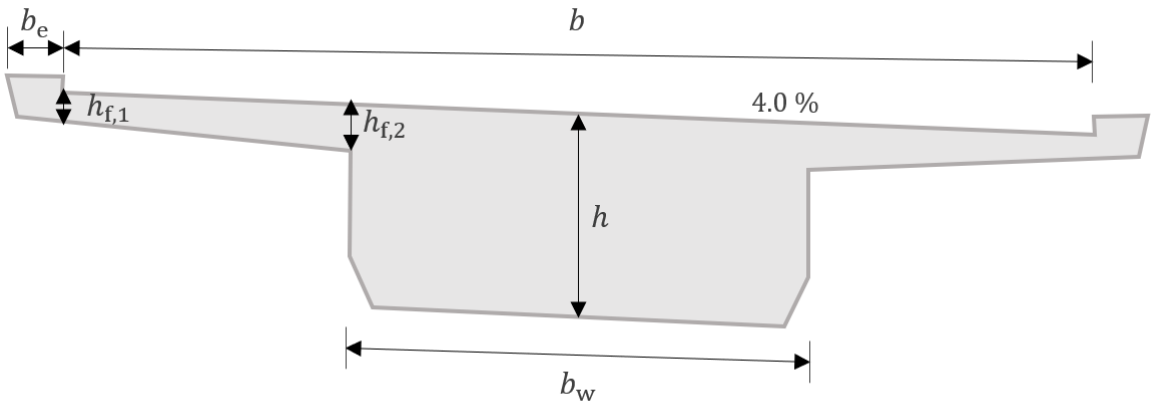

Figure 6.14: Cross-section geometry for the T-section of the road bridge, Halvors länk.

Table 6.11: Dimensions and cable configuration for Halvors länk road bridge.

Parameter	**Magnitude**	**Unit**
Length, L	35	m
Cross-section height, h	1,750	mm
Outer slab height, $h_{f,1}$	200	mm
Inner slab height, $h_{f,1}$	400	mm
Carriageway width, b	9,000	mm
Web width, b_w	4,000	mm
Edge width, b_e	500	mm
Perpendicular slab inclination	4	%
Bridge radius	430	m
No. of cables, n	18	-
No. of strands per cable, $n_{strands}$	19	-
Strand diameter, ϕ_{strand}	15.7	mm

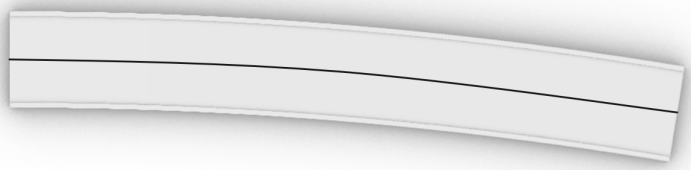

Figure 6.15: Top view showing the bridge deck curvature of Halvors länk.

Table 6.12: Carriageway geometry for Halvors länk.

Object	Position [m]
Left deck end	-4.5
Left curbstone	-4.0
Right curbstone	4.0
Right deck end	4.5

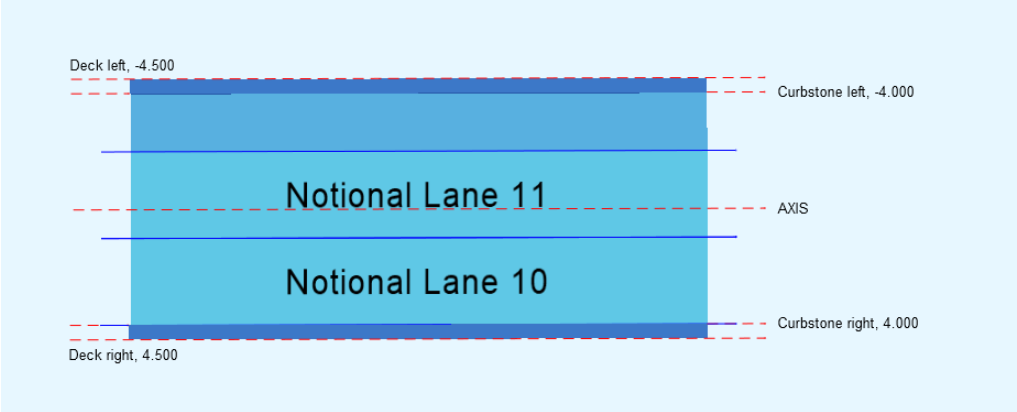

Figure 6.16: Right-aligned notional lanes for Halvors länk road bridge from SOFiSTiK based on Eurocode.

For this comparison, the cross-section has been kept constant even if the number of cables is changed. The cables were also restricted to only 19 strands to make the results more comparable to the original design. Using the conventional solution, based on load balancing, 18 cables had to be used to achieve complete prestressing. The actual bridge also used 18 cables, consistent with the model. The bridge designed with the guidelines only needed 16 cables, reducing the cost with 5.1% and the amount of prestressing steel with 11%. For a full comparison of the different optimization objectives between the guidelines and the conventional solution, see Table 6.13.

Table 6.13: Differences in utilization ratio for stresses and deflection as well as cost, GWP, and fitness compared to the conventional layout.

State	Objective	Conventional	Optimized		Difference [%]
	No. of cables*	18	16		**-11.1**
	Cost	2,039,500	1,936,200	SEK	**-5.06**
	GWP	270,000	266,600	CO_2e	**-1.27**
Construction	Tension[2]	-4.48	-1.99	MPa	55.6
SLS	Deflection[1]	18.7	17.6	mm	-2.44
	Compression[2]	11.2	11.3	MPa	0.89
	Compression[3]	14.4	13.4	MPa	-6.94
	Tension[3]	-0.30	-0.33	MPa	-10.0
	Fitness	1.32	1.27		**-3.17**

* Number of strands was set to 19 for both layouts.

Load combinations: [1] Frequent
[2] Quasi-permanent
[3] Characteristic

7

Discussion

The results show that the guidelines developed for the cable placement outperform the load balancing method with an improvement of nearly 7% in cost and 5% in GWP, for the beam cross-section geometry studied. In addition, varying improvements in cost and GWP were also observed for other cross-section geometries with span lengths ranging between 25 to 40 m. When examining the slightly wider bridge, no substantial difference in the result could be found between the guidelines and the conventional solution. This indicates that use of the proposed guidelines could be more suitable for bridges with smaller widths. However, this is somewhat contradicted by the case study of Halvors länk where the guidelines gave a 5% reduction in cost. It should be noted that the different cross-sections used in the study have been relatively constrained. As a consequence, the total concrete volume is consistent between different cable layouts which prevents any larger improvements in cost and GWP. The rather large reduction in steel area however, 11.6% for the original cross-section and 11.1% in the case study, show that the guidelines are using a more effective cable placement.

When comparing the normalized cable eccentricities from the guidelines with the average conventional layout, it was found that each node was placed on average 9 p.p. lower in the cross-section, see Table 6.5. This shift was responsible for the improved performance in that it not only allows for a larger field moment but also utilizes the secondary moment more efficiently.

When looking at some of the characteristics of the guidelines, the position of maximum eccentricity was placed at a length of 37% of the span length from the end support. This can be compared to the study performed by Utrilla and Samartin (1997) who found that the optimal position was around 40%. However, they also claimed that the eccentricity at this point should be as large as possible with regards to the cover thickness (Utrilla & Samartín, 1997). This does not align with the result of this study as the optimal position of the cable was found to be at a lower eccentricity. A possible explanation for this could be that, in their study, the prestressing force was calculated freely whereas the cables always were fully tensioned in this study (Utrilla & Samartín, 1997). This limited our model to only use discrete steps in prestressing force. Another factor could be the cross section of the bridge. Utrilla and Samartin (1997) investigated bridges with widths from 8-16 m and slendernesses of 18-30 compared with the width of 8 m and slenderness of 20 used in this study. Finally, the loads in this study were based on Eurocode while the code used by Utrilla and Samartins (1997) was not disclosed.

The suggested cable eccentricity in the guidelines crosses the neutral axis at almost

80% of the span length. Similarly, Aspegren and Möörk (2021) found that the optimal place for the zero eccentricity was at 85% although their range was set to 75-85% in their optimization. Aspegren and Möörk (2021) also concluded that the effects from the secondary moment should be minimized for smaller bridges, below 32 m, as the self-weight of the bridge would be too small to counteract the secondary moment. This conclusion was not consistent with what was found in this study, where instead the secondary moment had a positive effect in all bridges studied by increasing the capacity over the mid-support. A possible explanation to this discrepancy could be that the differences in cross-section geometry between the studies means that the bridges in Aspegren and Möörks (2021) study have a larger primary moment over the support and, thus, an increase in secondary moment could become unfavorable for smaller bridges.

It was also found that the eccentricities of all nodes were relatively constant with regards to the span length except for Node 1 and 2. These were instead found to be linearly dependent on the length of the span with the eccentricities decreasing for increasing span lengths. It is possible that, for smaller spans, the nodes had to be shifted downwards in order to increase the secondary moment or, as the curves are normalized, it could be that the relative difference between these nodes and the other field nodes increases.

Choosing a cable layout with the guidelines has been found to be comparable in effort to that of the conventional solution. To find a cable layout with the guidelines, the designer has to decide on a configuration of cables and strands. The position of the cable can then be found by using the guidelines in a process similar to that of the load balancing method. It should be noted that not all cable and strand combinations are valid and that the designer therefore still is required to choose reasonable solutions.

It was found that the guidelines performed similarly to the optimized solutions and on average even outperformed the optimized solutions. This indicates that the optimization sometimes either suffered from premature convergence or did not reach full convergence, resulting in a less fit solution. This is, however, one of the characteristics of GAs as they can find improved solution in a reasonable time but finding the global minimum could be difficult as it mostly depends on the smoothness and shape of the fitness landscape together with how accurate the initial guess is.

7.1 Limitations of the Guidelines

Although the guidelines are designed to be generally applicable, some factors have been neglected in order to not exceed the time-frame. Hence, not only potential loads such as earth pressure has been neglected, but also the mandatory verifications performed with horizontal loadings as well as the vehicle models presented by the Swedish Traffic Administration (2019a). In addition, the guidelines are also generated for incompletely prestressed bridges although the comparison with Halvors länk still showed a significant improvement in cost and fitness for complete prestressing. The choice of studying incomplete prestressing was based on the goal of optimizing the design by utilizing as much of the available capacity as possible. The

guidelines are also somewhat limited to bridges with similar cross-section geometry as the one used in the optimization, i.e., T-sections with cross-section heights of $L/20$. In the validation of the guidelines, the bridge with an extended slab width of 10 m seemed to be the least beneficial to optimize with virtually no improvements.

7.2 Optimization Parameters

Due to the relatively small scale of implementation approaches for GAs in structural engineering found during the study, some parameter choices have been purely evaluated from theoretical arguments and not based on any sufficiently large empirical study. The balance between convergence rate with respect to time and diversity in the GA have also been considered during the execution. While a wider population probably would have lead to a decrease of the former and an increase of the latter, parameters such as initial boost, inbreeding radius and remainder have a much more complex relation to these two. As the concept of inbreeding radius seems unique to the Galapagos solver, a lot of uncertainties regarding the parameter lead to the default value being used. In addition, the concepts of premature convergence and reaching convergence have not been handled during the study as it was deemed difficult to quantize and may require extensive testing. For the number of generations performed in each optimization process, the default measure of convergence in Galapagos, maximum stagnant, was deemed a poor choice and instead a 16 hour time limit was assumed to be sufficient for achieving convergence. For this problem, a time limit seemed to be more suitable. Due to the small number of generations in the optimization, maximum stagnant performed inconsistently in terms of the degree of achieved convergence as opposed to using a time limit.

Another aspect of uncertainty in the execution was the implementation of the fitness function. Despite the fitness function being formulated using common approaches, recommendations for the weights have not been presented in the studied research. Consequently, the fitness function have also been designed based on both testing and an intuitive assessment of each sub-objective's importance. Whereas different projects might favor priority of either the cost or the environmental impact, the guidelines were designed to give equal contribution to both objectives.

The data for cost and GWP were derived from a study by Aspegren and Möörk (2021). As of February 2022, the price of reinforcement steel had increased by 44% compared to the previous year as a consequence of current events (Statistiska centralbyrån, 2022). This causes two problems regarding the guidelines. Firstly, the data used for the optimization does not match current prices. Secondly, it may be of interest to the contractor to reevaluate the weighting between the cost and the environmental impact. A problem with the guidelines is thereby that the weights for cost and environmental impact cannot be updated.

To properly scale the different objectives with each other, some sort of normalization of the cost and GWP had to be performed. By choosing a cross-section geometry of a reference bridge, some weighting between the GWP and cost had already implicitly been included, not only making the matter more complicated but also somewhat subjective.

In order to find more effective layouts when cable and strand configuration or cross-sectional geometry remained unchanged, the requirements were implemented into the unpenalized fitness contribution. The argument for this choice was to encourage the algorithm to find solutions with more margin to the requirements. By design with more margin, the design may be more susceptible to further updates in number of cables and strands in a later design stage which otherwise may be problematic in optimized designs. The concept of desiring margins in the design does however disagree with the theory presented by Bäck et al. (Bäck et al., 2000), that the optimum design in practical applications commonly lies at the boundary of what is feasible and not.

The implementation of stresses in the fitness function may also provide the optimization process with a smoother transition to a more effective cable and strand configuration. As the step size in steel area is relatively steep, a change in cable and strand configuration very often seems to lead to an unfeasible design if the layout is not already effective in terms of material stresses. By encouraging decreased material stresses, the algorithm is promoted to find more optimal cable layouts before the cable and strand configuration is updated. As the decreases in stresses had a low weight in comparison to cost and GWP, the main objectives often became dominant.

In the results, one can occasionally see that the algorithm have been more inclined to optimize towards the requirements instead of the GWP. This can be seen when comparing bridges with 33 and 35 m long spans in Table 6.6 where the improvements in cost and GWP are almost identical while improvements in fitness differ slightly. This suggests that the design of the bridge with 35 m long spans may be more effective with respect to the requirements.

Although not presented for all bridge geometries, it was commonly the requirements in (3.23), (3.26), and (3.29) that resulted in a design being unfeasible. For reference, see Table 6.13. The other criterion always seemed to be fulfilled. It can therefore be reasonable to argue that an improved fitness function would only include the requirements in (3.23), (3.26), and (3.29) for the unpenalized contribution as the other criterion only steal focus from the two main objectives, reducing cost and GWP.

7.3 Application of Guidelines and Optimization

This study has also shown the differences between optimization through algorithms and by using guidelines. With the choice of FE software, each solution was fairly time-consuming and the GA took several hours to compute. Considering the simplicity of the studied problem, it can be concluded that this method of optimization is less suitable in common bridge design where time may be a critical issue and conventional solutions exists. The potential of GAs may be realized in problems with more complex geometries although the implementation of SOFiSTiK in Grasshopper is deficient for this purpose and a more time-efficient FE solver would be recommended.

Despite the time-consuming process the optimization was successful and solutions

that outperformed the conventional designs were found. By compiling the optimized solutions into guidelines, it was possible to make the discoveries found by the GA accessible without the need for hour-long computations. Normally, it would be expected that the guidelines would perform slightly worse than the optimized solutions as they are not computed for each specific case. However, in this case, better solutions were found using the guidelines as opposed to the solutions found using the GA. This was attributed to the flexibility of the guidelines to be able to easily test different cable and strand combinations as the GA is more rigid. For the same number of cables and strands, it is still expected that the optimized solution would perform better as it does minimize the stresses better than the guidelines.

Due to the simplicity of the guidelines, they or similarly derived guidelines could easily be implemented into a program or a plug-in to be used by bridge designers in order to give a different perspective on problems or provide possible starting points for designs.

7.4 Further Studies

To further validate the proposed guidelines, they should be used to design a wider range of cross-sections and more case studies would be beneficial. The guidelines could also be extended by studying cables tensioned between the end and mid-support as this is a common solution for longer spanning bridges. It could also be interesting to investigate how bridges with asymmetrical spans behave and if the proposed guidelines still are valid. In addition, some loads have for simplicity been excluded from the study, such as horizontal forces and earth pressure. To make the guidelines even more applicable in preliminary design, some of the aforementioned effects could also be included in further research. Another possible solution for improving the guidelines would be to use the current guidelines as the initial guess for the GA optimization in order to improve convergence.

Furthermore, the study shows the potential of developing general guidelines with the use of GAs for preliminary design that includes and optimizes the main and shear reinforcement. In addition, the guidelines created in this study could be complemented with guidelines for bridges with other sectional geometries when the proposed guidelines does not produce sufficient results. There is also reason to believe that GAs possibly could be applied more extensively to generate guidelines for other types of structures as well.

8

Conclusions

In this study, general guidelines for efficient cable placement in continuous post-tensioned concrete bridges were established with the goal of reducing cost and GWP. This was achieved by first optimizing the cable layout with the use of FE analyses combined with GA optimization for different span lengths and then compiling the results into guidelines. These were then compared to both the solution optimized with the GA as well as bridges designed with the conventional approach, load balancing. The results showed that bridges designed following the guidelines saw a reduction in cost and GWP compared to the conventional solution in the range of 1-7%. Due to the use of overly constrained cross-sections, further improvements were impossible. A significant reduction of 8-19% in prestressing steel could however be achieved, indicating a more optimal cable placement. This includes a bridge with wider bridge deck where the benefits of using the guidelines were smaller compared the section geometries. Still, when adopting the guidelines to a case study of the already constructed, similarly wide bridge, Halvor's länk, it was possible to reduce the cost by 5% and the prestressing steel area by 11%. This shows the possible benefits from using the guidelines in real applications.

The suggested guidelines are limited by the inability to change the weighting of the cost and GWP as the GA computations would have to be rerun. While different projects might favor cost-efficiency and others more sustainability, the guidelines were generated from optimizations that prioritized both objectives equally. If a more extensive set of guidelines would be developed in the future, different weightings between cost and environmental impact could be of interest as it is possible that a different layout would be preferable in those circumstances. Another factor that has influenced the results is the input parameters for the optimization solver. There are indications that the optimized solutions have not fully converged. This could be a result of the choice of the input parameters in the solver which often are case-specific and either have been set as the default values or based on general recommendation from available research. Another possible reason for the premature convergence of the optimization could be the quality of the initial guess that was based on a conventional solution. Therefore, to improve these guidelines, it could be possible to use the current guidelines as the initial guess instead of a conventional cable layout.

From this research, it has become apparent that implementing GAs in structural design can be beneficial to discover efficient solutions. As the computations necessary for finding these solutions can be very extensive, it cannot always be recommended to implement it into common structural designs. The potential rather seem to lie

within the context of creating general guidelines that easily and efficiently can be implemented. Although the study only covered optimization of post-tensioning cables in bridges, it is reasonable to assume that similar results can be achieved in other areas of structural design by creating guidelines using GA optimization.

Bibliography

Aalami, B. O., & Jurgens, J. D. (2003). Guidelines for the design of post-tensioned floors. *Concrete International*, *25*(3), 77–83.

Ahsan, R., Rana, S., & Ghani, S. N. (2011). Cost optimum design of posttensioned i-girder bridge using global optimization algorithm. *Journal of Structural Engineering*, *138*(2), 273–284. https://doi.org/https://doi.org/10.1061/(ASCE)ST.1943-541X.0000458

Al-Emrani, M., Engström, B., Johansson, M., & Johansson, P. (2013). *Bärande konstruktioner: Del 1*. Chalmers Tekniska Högskola.

Al-Emrani, M., Engström, B., Johansson, M., & Johansson, P. (2014). *Bärande konstruktioner: Del 2*. Chalmers Tekniska Högskola.

Amouzgar, K. (2012). *Multi-objective optimization using genetic algorithms* (Master's thesis). School of Engineering in Jönköping. ODR. http://www.diva-portal.org/smash/get/diva2:570751/FULLTEXT01.Pdf

Aspegren, D., & Möörk, E. (2021). *Early estimations of dimensions for prestressed concrete bridges: Optimization by set-based parametric design of cross-section and prestressing force in a preliminary stage* (Master's thesis). Chalmers University. ODR. https://hdl.handle.net/20.500.12380/304088

Bäck, T., Fogel, D. B., & Michalewicz, Z. (2000). *Evolutionary computation 2: Advanced algorithms and operators*. IOP Publishing Ltd.

Bhatt, P. (2011). *Prestressed concrete design to eurocodes*. CRC Press. https://doi.org/10.1201/b12839

Dolan, C. W., & Hamilton, H. R. (2019). *Prestressed concrete*. Springer International Publishing. https://doi.org/10.1007/978-3-319-97882-6

DYWIDAG-Systems International. (n.d.). *Dywidag bonded post-tensioning systems using strands* (Manual).

DYWIDAG-Systems International. (2021). *Post-tensioning: Dywidag multistrand pt system for bonded application with 3 to 55 strands eta-13/0815* (Manual). http://assets.ctfassets.net/wz1xpzqb46pe/2lU00FYUnS6oLUkNL1yEhh/9fccf11dd176e5ff311756a87fe90462/Online_ETA-13_0815_EN.pdf

Engström, B. (2011). *Design and analysis of prestressed concrete structures.* Chalmers University of Technology.

Engström, B. (2015). *Design and analysis of continuous beams and columns*. Chalmers University of Technology.

Eshani, M. R., & Blewitt, J. R. (1986). Design curves for tendon profile in prestressed concrete beams. *PCI Journal*, *32*(3), 114–135. https://doi.org/https://doi.org/10.15554/pcij.05011986.114.135

Gilbert, R. I., Mickleborough, N. C., & Ranzi, G. (2017). *Design of prestressed concrete to eurocode 2*. CRC Press. https://doi.org/10.1201/9781315389523

Johansson, C., & Evertsson, G. (2003). *Optimizing genetic algorithms for time critical problems* (Master's thesis). Bleking Institute of Technology. ODR. https://www.diva-portal.org/smash/get/diva2:832349/FULLTEXT01.pdf

Khan, A. A., Pathak, K. K., & Dindorkar, N. (2010). Cable layout design of one way prestressed concrete slabs using fem. *Journal of Engineering, Science and Management Education*, *2*(3), 34–41.

Krishnamurthy, N. (1983). Magnel diagrams for prestressed concrete. *Journal of Structural Engineering*, *109*(12), 2761–2769. https://doi.org/https://doi.org/10.1061/(ASCE)0733-9445(1983)109:12(2761)

Kuyucular, A. (1991). Prestressing optimization of concrete slabs. *Journal of Structural Engineering*, *117*(1), 235–254. https://doi.org/https://doi.org/10.1061/(ASCE)0733-9445(1991)117:1(235)

Libby, J. (2012). *Modern prestressed concrete: Design principles and construction methods*. Springer US. https://books.google.se/books?id=sI7uBwAAQBAJ

Lounis, Z., & Cohn, M. Z. (1993). Optimization of precast prestressed concrete bridge girder systems. *PCI Journal*, *38*(4), 60–78. https://doi.org/https://doi.org/10.15554/pcij.07011993.60.78

Marler, R., & Arora, J. (2004). Survey of multi-objective optimization methods for engineering. *Structural and Multidisciplinary Optimization*, *26*(6), 369–395. https://doi.org/http://dx.doi.org/10.1007/s00158-003-0368-6

Mirjalili, S. (2019). *Evolutionary algorithms and neural networks*. Springer International Publishing. https://doi.org/10.1007/978-3-319-93025-1

Nusrath, F. R., Satheesh, V. S., Manigandan, M., & Suresh, B. S. (2015). An overview on tendon layout for prestressed concrete beams. *International Journal of Innovative Science, Engineering & Technology*, *2*(9), 944–949.

PTC Inc. (2022). *Ptc mathcad features*. Retrieved March 11, 2022, from https://www.mathcad.com/en/capabilities

Robert McNeel & Associates. (n.d.-a). *Galapagos* [Optimization software].

Robert McNeel & Associates. (n.d.-b). *Grasshopper 3d* [Visual programming language]. Retrieved January 31, 2022, from https://www.rhino3d.com/6/new/grasshopper/

Rombach, G. A. (2011). *Finite-element design of concrete structures: Practical problems and their solutions* (2nd ed.). ICE Publishing.

Rutten, D. (2010a). Evolutionary principles applied to problem solving. Retrieved March 28, 2022, from https://www.grasshopper3d.com/profiles/blogs/evolutionary-principles

Rutten, D. (2010b). Hi Sangsu, I'm not quite certain in what category Galapagos falls in terms of Genetic Algorithms. In a way [Comment on the online forum post *References about Galapagos?*]. Grasshopper 3D. Retrieved April 24, 2022, from https://www.grasshopper3d.com/forum/topics/references-about-galapagos?overrideMobileRedirect=1

Rutten, D. (2013). Galapagos: On the logic and limitations of generic solvers. *Architectural Design*, *83*(2), 132–135. https://doi.org/10.1002/ad.1568

SIS. (2002a). *Eurocode - basis of structural design* (Standard).

SIS. (2002b). *Eurocode 1: Actions on structures - part 1-1: General actions - densities, self-weight, imposed loads for buildings* (Standard).

SIS. (2003). *Eurocode 1: Actions on structures - part 1-5: General actions - thermal actions* (Standard).

SIS. (2005). *Eurocode 2: Design of concrete structures – part 2: Concrete bridges – design and detailing rules* (Standard).

SIS. (2008). *Eurocode 2: Design of concrete structures – part 1-1: General rules and rules for buildings* (Standard).

SIS. (2010). *Eurocode 1: Actions on structures – part 2: Traffic loads on bridges* (Standard).

Smith, A. E., & Coit, D. W. (1996). *Handbook of evolutionary computation*. Oxford University Press Institute of Physics Publishing.

SOFiSTiK AG. (n.d.-a). *Axis variable points*. Retrieved February 28, 2022, from https://www.sofistik.de/documentation/2020/en/rhino_interface/grasshopper/components/AxisVariablePoints.html

SOFiSTiK AG. (n.d.-b). *General explanations for the use of maxima - action combinations in order to get design forces or load case combinations*. Retrieved March 15, 2022, from https://www.sofistik.de/documentation/2020/en/tutorials/superpositions/general-maxima/superposition_general-maxima.html

SOFiSTiK AG. (n.d.-c). *Grasshopper*. Retrieved May 2, 2022, from https://www.sofistik.de/documentation/2020/en/rhino_interface/grasshopper/index.html

SOFiSTiK AG. (n.d.-d). *Prestressing system*. Retrieved March 10, 2022, from https://www.sofistik.de/documentation/2020/en/tutorials/listoftutorials/general-workflows/prestressing-system.html

SOFiSTiK AG. (n.d.-e). *Sofistik* [Finite element program]. Retrieved January 31, 2022, from https://www.sofistik.com

SOFiSTiK AG. (n.d.-f). *Tendon geometry standard*. Retrieved February 15, 2022, from https://www.sofistik.de/documentation/2020/en/rhino_interface/grasshopper/components/TendonGeometryStandard.html

SOFiSTiK AG. (n.d.-g). *Traffic loader*. Retrieved March 10, 2022, from https://www.sofistik.de/documentation/2020/en/tutorials/listoftutorials/general-workflows/traffic_loader.htmll

SOFiSTiK AG. (2020a). *Aqb: Design of cross sections* (Manual) [Service Pack 2020-13, Build 412].

SOFiSTiK AG. (2020b). *Aqua: Materials and cross sections* (Manual) [Service Pack 2020-13, Build 412].

SOFiSTiK AG. (2020c). *Ase: General static analysis of fe structures* (Manual) [Service Pack 2020-13, Build 412].

SOFiSTiK AG. (2020d). *Csm: Construction stage manager* (Manual) [Service Pack 2020-13, Build 412].

Statistiska centralbyrån. (2022). *Construction costs rose by 0.9 percent in february*. Retrieved April 26, 2022, from https://www.scb.se/en/finding-statistics/statistics-by-subject-area/prices-and-consumption/building-price-index-and-construction-cost-index-for-bu/construction-cost-index-for-buildings-cci-input-price-index/pong/statistical-news/construction-cost-index-for-buildings-february-2022/

Trafikverket. (2019a). *Krav brobyggande* (Standard) [3.0]. https://www.trafikverket.se/contentassets/5e3d8c0eb4e94efd9738cca74b912bf5/krav-brobyggande.pdf

Trafikverket. (2019b). *Råd brobyggande* (Råd) [3.0]. https://trvdokument.trafikverket.se/Versioner.aspx?spid=4053&dokumentId=TDOK%5C%202016%5C%3A0203

Trafikverket. (2020). *Kodförteckning och beskrivning av brotyper*. Retrieved February 8, 2022, from https://batmanhandbok.trafikverket.se/dokument/Bro_konstruktionstyper

Trafikverket. (2022). *Krav - VGU, vägars och gators utformning* (Krav) [1.0]. http://trafikverket.diva-portal.org/smash/get/diva2:1621114/FULLTEXT02.pdf

Transportstyrelsen. (2018). *Transportstyrelsens föreskrifter och allmänna råd om tillämpning av eurokoder* (Standard). https://www.transportstyrelsen.se/TSFS/TSFS%202018_57.pdf

Utrilla, M., & Samartín, A. (1997). Optimized design of the prestress in continuous bridge decks [Computational Structures Technology]. *Computers & Structures*, *64*(1), 719–728. https://doi.org/https://doi.org/10.1016/S0045-7949(96)00434-8

Vägverket. (1996). *Broprojektering - en handbok* (Krav).

A

Analytical Verification

A.1 Calculations

Load Case

Include the following contributions with factors corresponding to the boolean values 0 and 1:

- **Self-weight** $include.selfweight := 1$
- **Thermal load** $include.thermal := 1$
- **Prestressing** $include.prestressing := 1$

Geometry

Bridge Beam

Span length:

$l := 30\ \text{m}$

Cross-section dimensions:

$b := 8000\ \text{mm}$

$h := \frac{l}{20} = 1500\ \text{mm}$

$h_f := 300\ \text{mm}$

$b_{wt} := 2990\ \text{mm}$

$b_{wb} := 1990\ \text{mm}$

$h_w := h - h_f = 1200\ \text{mm}$

Effective flange width:

$b_{ef} := b - 200\ \text{mm}$

Cross-section area:

$A := b \cdot h_f + \text{mean}\left(b_{wt}, b_{wb}\right) \cdot h_w = 5.388\ \text{m}^2$

Reinforcement Steel

Bar diameter:

$\phi_s := 20\ \text{mm}$

Cover thickness for reinforcement bars:

$c_{1st} := 55\ \text{mm}$

Presstressing Steel

Number of cables

$n := 10$

Number of strands per cable

$n_s := 19$

Strand diameter:

$\phi_{strand} := 15.7\ \text{mm}$

Duct diameter:

$\phi_{duct} := 100\ \text{mm}$

Area per cable:

$A_{pi} := n_s \cdot \pi \cdot \frac{\phi_{strand}^2}{4} = 3678.263\ \text{mm}^2$

Total area:

$A_p := n \cdot A_{pi} = 36782.631\ \text{mm}^2$

Vertical Spacing:

$a_{pv} := \phi_{duct} = 100\ \text{mm}$

Cover spacing:

$c_{1pt} := c_{1st} + 2\ \phi_s + a_{pv} = 195\ \text{mm}$

Material Properties

Concrete, C40/50 (Cement class N)

Characteristic stregnth
$f_{ck} := 40\ \text{MPa}$

Mean strength:
$f_{cm} := 48\ \text{MPa}$

Young's modulus:
$E_{cm} := 35220\ \text{MPa}$

Thermal coefficient:
$\alpha_c := 10 \cdot 10^{-6}\ \text{K}^{-1}$

Initial drying shrinkage:
$\varepsilon_{cdi} := 0.315 \cdot 10^{-3}$

Final autogenous shrinkage
$\varepsilon_{cafin} := 0.075 \cdot 10^{-3}$

Strength-dependent factor for creep behavior
$\beta_{fcm} := 2.43$

Prestressing Steel, Y1860

Characteristic strength
$f_{puk} := 1860\ \text{MPa}$

Characteristic strength:
$f_{p0.1k} := 1600\ \text{MPa}$

Young's modulus:
$E_p := 195\ \text{GPa}$

Neutral Axis of Concrete-Section

For the flange and the web:

$x_{NAf} := \frac{h_f}{2} = ?$ $\quad A_{fef} := b_{ef} \cdot h_f = ?$

$x_{NAw1} := h - \frac{h_w}{2} = \left(900 \cdot 10^{-3}\right)\ \text{m}$ $\quad A_{w1} := b_{wb} \cdot h_w = 2.388\ \text{m}^2$

$x_{NAw2} := h - \frac{2}{3}\ h_w = \left(700 \cdot 10^{-3}\right)\ \text{m}$ $\quad A_{w2} := \frac{1}{2}\ \left(b_{wt} - b_{wb}\right) \cdot h_w = \left(600 \cdot 10^{-3}\right)\ \text{m}^2$

For the whole cross-section:

$A_{ef} := A_{fef} + A_{w1} + A_{w2} = 5.328\ \text{m}^2$

$x_{NA} := \frac{x_{NAf} \cdot A_{fef} + x_{NAw1} \cdot A_{w1} + x_{NAw2} \cdot A_{w2}}{A_{ef}} = 0.548\ \text{m}$

Flexural Stiffness

Since a fully prestressed remains uncracked, the analysis can be performed in State I. By assuming that the steel have a neglagable contribution the stiffnesses presented below can be used.

Local Moment of Inertias

$I_{flocef} := \frac{b_{ef} \cdot h_f^{\,3}}{12} = ?$

$I_{wloc} := \frac{\text{mean}\left(b_{wt}, b_{wb}\right) \cdot h_w^{\,3}}{12} = \left(358.56 \cdot 10^{-3}\right)\ \text{m}^4$

Global Moment of Inertias

Steiner's theorem is used in order to calculate the global moment of inertia.

$I := I_{flocef} + A_{fef} \cdot \left(x_{NA} - \frac{h_f}{2}\right)^2 + I_{wloc} + A_{w1} \cdot \left(h - \frac{h_w}{2} - x_{NA}\right)^2 + A_{w2} \cdot \left(h - \frac{2}{3}\ h_w - x_{NA}\right)^2 = 1.057\ \text{m}^4$

Flexural Stiffness

$EI := E_{cm} \cdot I = 37.211\ \text{GN} \cdot \text{m}^2$

Cable Profile

Maximum eccentricity location (as percentage of the span length):

$\eta_{max} := 37\%$

Cable eccentricities defined with respect to the top of the beam:

$e_1 := 0.544\ \text{m}$
$e_2 := 0.580\ \text{m}$
$e_3 := 0.662\ \text{m}$
$e_4 := 0.734\ \text{m}$
$e_5 := 0.761\ \text{m}$
$e_6 := 0.700\ \text{m}$
$e_7 := 0.503\ \text{m}$

$e_8 := c_{1pt} + \frac{\phi_{duct}}{2} = 0.245\ \text{m}$

Predefined x-coordinates for cable defintion points:

$x_1 := 0$
$x_2 := 1\ \text{m}$
$x_5 := \eta_{max} \cdot l = 11.1\ \text{m}$
$x_8 := l = 30\ \text{m}$

x-coordinates for intermediate cable defintion points:

$x_3 := x_2 + (x_5 - x_2) \cdot \frac{1}{3} = 4.367\ \text{m}$
$x_4 := x_2 + (x_5 - x_2) \cdot \frac{2}{3} = 7.733\ \text{m}$
$x_6 := x_5 + (x_8 - x_5) \cdot \frac{1}{3} = 17.4\ \text{m}$
$x_7 := x_5 + (x_8 - x_5) \cdot \frac{2}{3} = 23.7\ \text{m}$

Create vectors for e (with respect to the neutral axis) and x:

$$E := \begin{bmatrix} e_1 \\ e_2 \\ e_3 \\ e_4 \\ e_5 \\ e_6 \\ e_7 \\ e_8 \end{bmatrix} - x_{NA} = \begin{bmatrix} -0.004 \\ 0.032 \\ 0.114 \\ 0.186 \\ 0.213 \\ 0.152 \\ -0.045 \\ -0.303 \end{bmatrix} \text{ m} \qquad X := \begin{bmatrix} x_1 \\ x_2 \\ x_3 \\ x_4 \\ x_5 \\ x_6 \\ x_7 \\ x_8 \end{bmatrix} = ?$$

Cable profile:

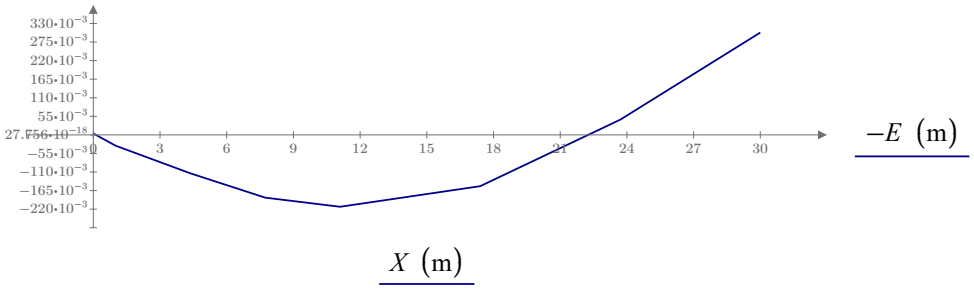

Actions

Self-Weight

Self-weight of concrete:

$$\rho_{ck} := 25 \frac{\text{kN}}{\text{m}^3} \qquad g_{ck} := \rho_{ck} \cdot A = 134.7 \frac{\text{kN}}{\text{m}}$$

Self-weight of pavement and layer thickness

$$\rho_{pk} := 24 \frac{\text{kN}}{\text{m}^3}$$

$$t_p := 100 \text{ mm} \qquad g_{pk} := \rho_{pk} \cdot t_p \cdot b = 19.2 \frac{\text{kN}}{\text{m}}$$

Self-weight of the barriers

$g_{bki} := 0.5\ \frac{\text{kN}}{\text{m}}$ $g_{bk} := 2\ g_{bki} = 1\ \frac{\text{kN}}{\text{m}}$

Thermal Loading

Temperature gradient

$\Delta T := -8\ \text{K}$

Prestressing Force

Average cable force per cable after anchorage:

$P_{0mi} := min\left(0.85\ f_{p0.1k}, 0.75\ f_{puk}\right) \cdot A_{pi} = 5002.4\ \text{kN}$

Total average presstressing force

$P_{0m} := P_{0mi} \cdot n = 50024.378\ \text{kN}$

Design Loads

Permanent

$g_d := \text{if } include.selfweight \quad g_{ck} + g_{pk} + g_{bk} \quad \text{else} \quad 0 = 154.9\ \frac{\text{kN}}{\text{m}}$

Prestressing

$\gamma_p := \text{if } include.selfweight \vee include.thermal \quad 0.9 \quad \text{else} \quad 1.0 = ?$

$P_{0d} := \text{if } include.prestressing \quad \gamma_p \cdot P_{0m} \quad \text{else} \quad 0\ \text{kN} = 45021.9\ \text{kN}$

Thermal Strain

$$\varepsilon_d := \begin{cases} \alpha_c \cdot \Delta T & \text{if } include.thermal \\ 0 & \text{else} \end{cases} = -0.008\%$$

Support Moment

Due to continuety and symmetry when neglecting the traffic load, the support rotation should be equal on both sides, i.e., $\theta_{B1} = \theta_{B2}$. In order to simplify the calculations, a constant flexural stiffness EI have been assumed.

Support Rotations

The contributions to the support rotation are each handled seperately.

1. Permanent Uniform Load (Parabolic Curvature)

Includes the self-weight of:

- The bridge beam
- The pavement
- The traffic barriers

$$\theta_g := \frac{g_d \cdot l^3}{24\ EI} = 4.683 \cdot 10^{-3}$$

2. Support Moment (Triangular Curvature)

Includes the counteracting moment from:

- The permanent load
- The prestressing

$$\theta_M := \frac{M_1 \cdot l}{3\ EI}$$

3. Thermal Load (Constant Curvature)

If the sign of the temperature gradient is defined to be positive for a decreasing temperature downwards in the cross-section, the thermal contribution becomes

$$\theta_T := -\frac{\varepsilon_d \cdot l}{2\ h} = 800 \cdot 10^{-6}$$

4. Prestressing (Case-Specific)

The curvature from prestressing is given by

$$\kappa_{pi}(x) := -\frac{P_{0d}}{EI} \cdot \text{linterp}(X, E, x) \qquad \theta_{pi} := \frac{1}{l} \int_0^l \kappa_{pi}(x) \cdot x \, dx = -94.473 \cdot 10^{-6}$$

Moment Contributions

Primary Prestressing Moment

$$M_{pi} := \kappa_{pi}(l) \cdot EI = 13.646 \text{ MN} \cdot \text{m}$$

Restraint Moment

Restraint moment for $\theta_{B1} = 0$

$$M_{ri} := \theta_g + \frac{M_{ri} \cdot l}{3\ EI} + \theta_{pi} + \theta_T \xrightarrow{solve, M_{ri}} \frac{-0.020051563080827334 3826 \cdot \text{GN} \cdot \text{m}^2}{m}$$

$$M_{ri} = -20.052 \text{ MN} \cdot \text{m}$$

Support Moment

$$M_{si} := M_{ri} + M_{pi} = -6.406 \text{ MN} \cdot \text{m}$$

A.2 Support Moments

Short term support moment from the analytical model.

Actions	**Moment [kNm]**		
	Fundamental	**Restraint**	**Total**
Self-weight, $g_{\mathrm{d}} = 25$ kN/m	0	-17,426	-17,426
Thermal loading, $\Delta T = -8°\mathrm{C}$	0	-2,977	-2,977
Prestressing, $P_{0\mathrm{m}}$	15,162	391	15,522
Characteristic combination, $\gamma_{\mathrm{p}} = 0.9$	13,646	-20,052	-6,406

B

Model Implementation into SOFiSTiK

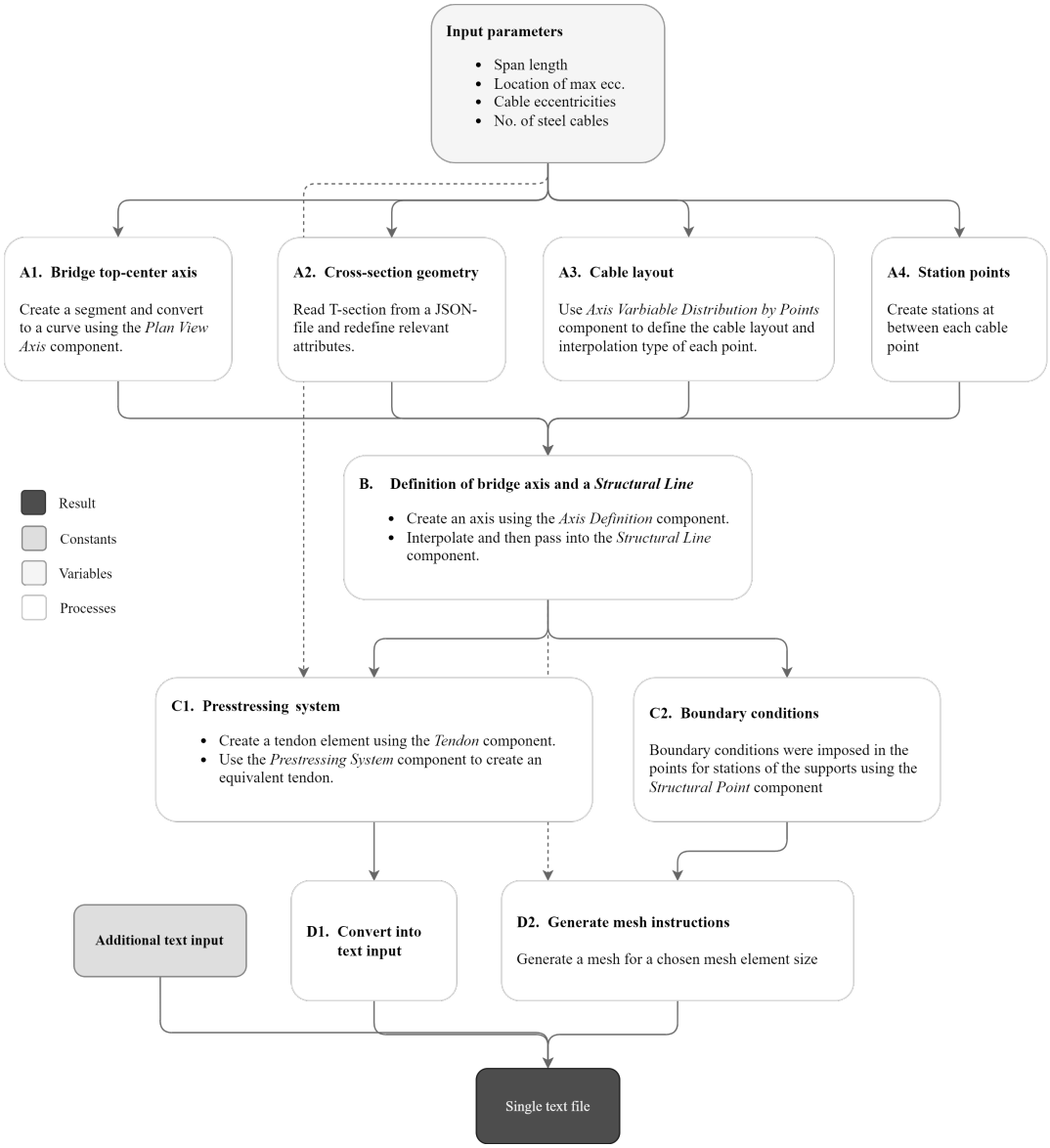

Figure B.1: Flowchart of the parameterization of the model in Grasshopper. The model was built using the SOFiSTiK plugins in Grasshopper.

C

Results

C.1 Conventional Layout

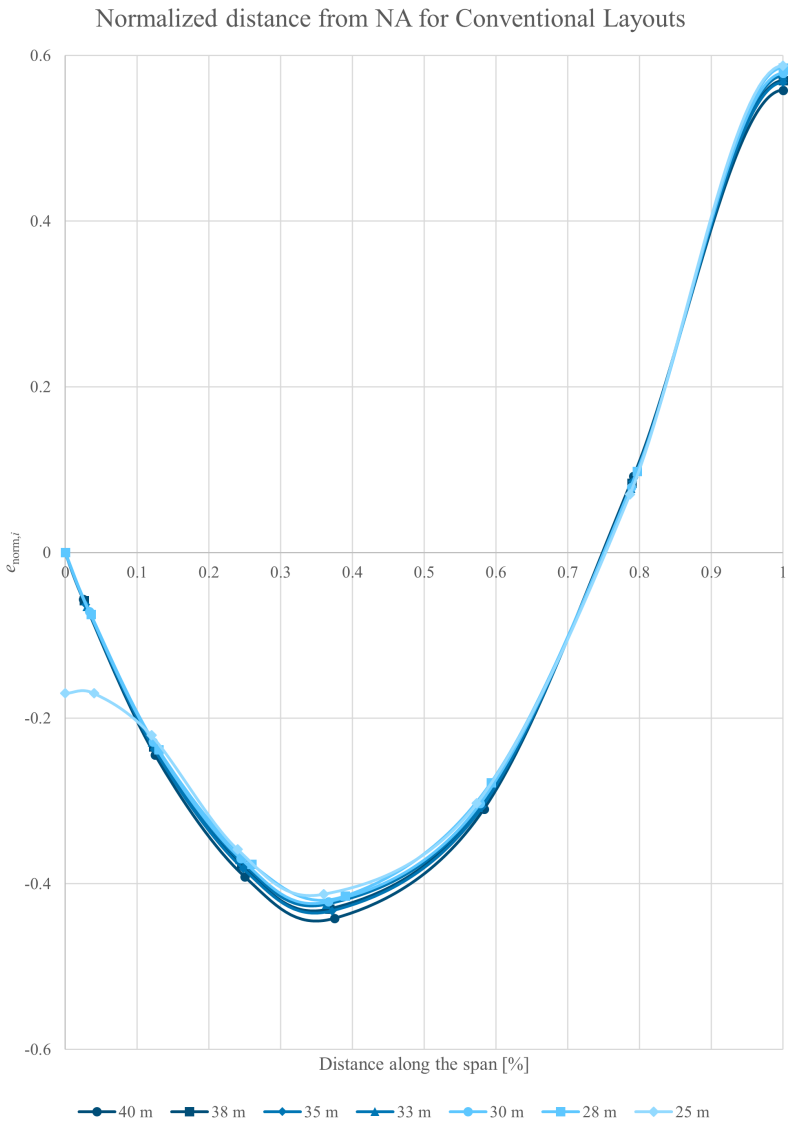

Figure C.1: Detailed graph of the normalized cable eccentricities for conventional layouts with respect to both span length and distance between maximum and minimum eccentricity.

Table C.1: Cable eccentricities from the bottom of the cross-section for multiple span lengths with conventional layouts.

Span length	**Height**	**Eccentricities**							
L	h	e_1	e_2	e_3	e_4	e_5	e_6	e_7	e_8
25	1,250	760	760	744	701	684	718	835	998
30	1,500	956	920	838	766	739	800	997	1,255
35	1,750	1,117	1,077	966	874	841	921	1,172	1,480
40	2,000	1,239	1,187	1,016	882	836	956	1,322	1,748
m	**mm**	**mm**							

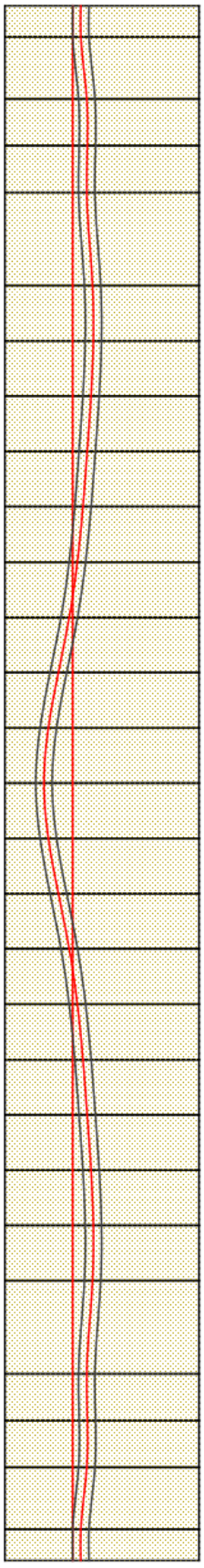

Figure C.2: Duct and cable eccentricity in SOFiSTiK for the bridge with 25 m long spans when using the conventional layout.

C.2 Optimized Layout

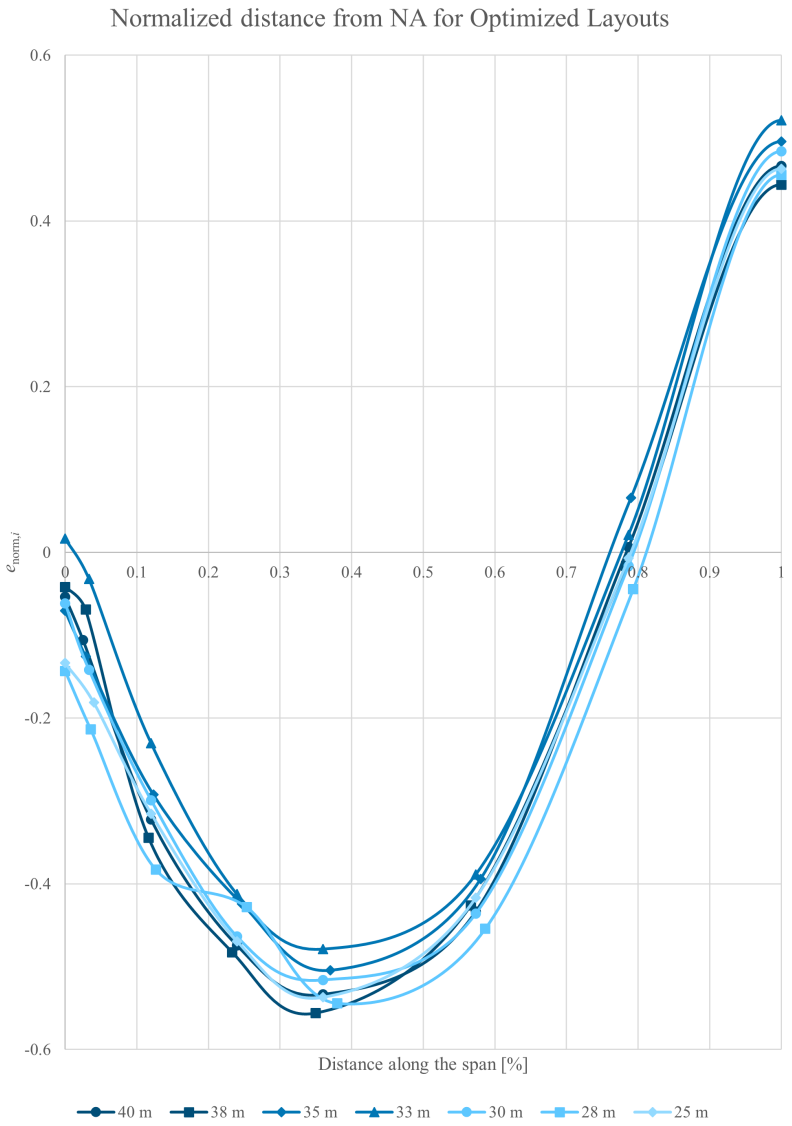

Figure C.3: Detailed graph of the normalized cable eccentricities for conventional layouts with respect to both span length and distance between maximum and minimum eccentricity.

Table C.2: Cable eccentricities from the bottom of the cross-section for multiple span lengths with optimized layouts.

Span length	**Height**	**Eccentricities**							
L	h	e_1	e_2	e_3	e_4	e_5	e_6	e_7	e_8
25	1,250	766	747	693	631	604	652	816	1,005
30	1,500	937	890	799	703	672	719	964	1,255
35	1,750	1,060	1,017	888	787	725	810	1,165	1,498
40	2,000	1,204	1,150	923	765	703	808	1,267	1,748
m	**mm**	**mm**							

C.3 Comparison

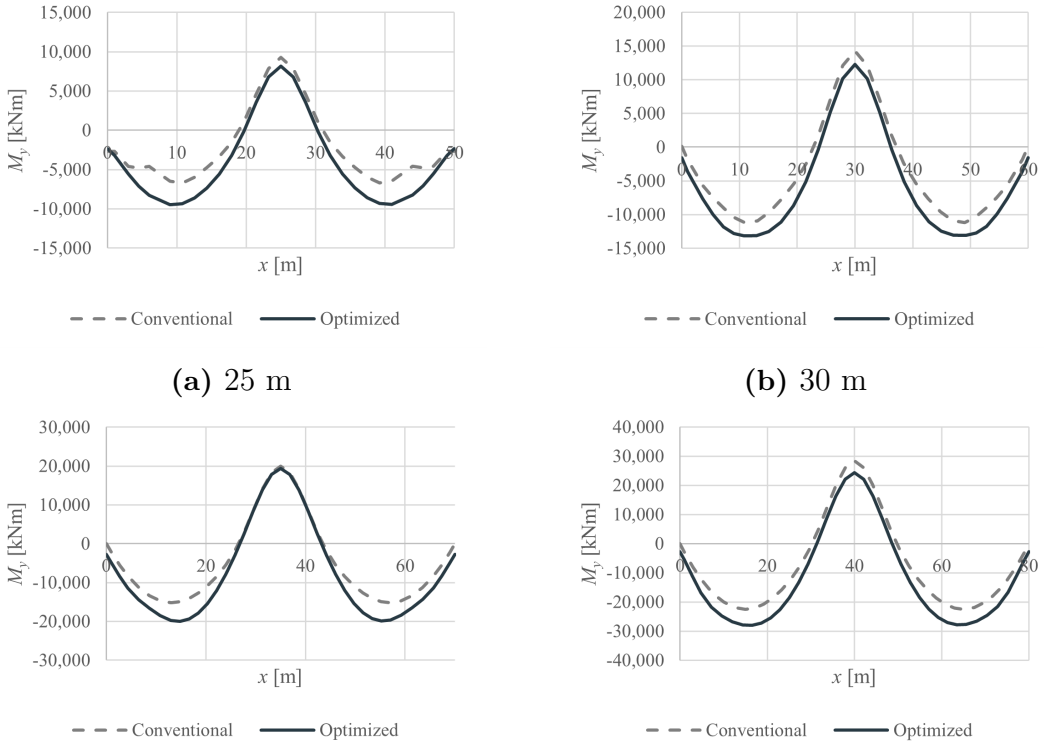

(a) 25 m

(b) 30 m

(c) 35 m

(d) 40 m

Figure C.4: Primary prestressing moment for optimized and conventional layouts for span lengths between 25-40 m in (a)-(d).